UC San Diego

UC San Diego Electronic Theses and Dissertations

Title

Multi-Scale Cardiac Electrophysiology: Bridging the Scales to Decipher Arrhythmia Mechanisms

Permalink

https://escholarship.org/uc/item/7nm4d38r

Author

Vincent, Kevin Patrick

Publication Date

2016

Peer reviewed|Thesis/dissertation

eScholarship.org Powered by the California Digital Library
University of California

UNIVERSITY OF CALIFORNIA, SAN DIEGO

MULTI-SCALE CARDIAC ELECTROPHYSIOLOGY: BRIDGING THE SCALES TO DECIPHER ARRHYTHMIA MECHANISMS

A Dissertation submitted in partial satisfaction of the
requirements for the degree
Doctor of Philosophy

in

Bioengineering with a Specialization in Multi-Scale Biology

by

Kevin Patrick Vincent

Committee in charge:

Professor Andrew McCulloch, Chair
Professor Jeffery Omens, Co-Chair
Professor Pedro Cabrales
Professor Ju Chen
Professor David Krummen
Professor Hemal Patel

2016

Copyright
Kevin Patrick Vincent, 2016
All rights reserved.

The Dissertation of Kevin Patrick Vincent is approved, and it is acceptable in quality and form for publication on microfilm and electronically:

_____

_____

_____

_____

_____
Co-Chair

_____
Chair

University of California, San Diego

2016

DEDICATION

To my wonderful wife, Victoria.

EPIGRAPH

Non multa, Sed multum

— Plinius Caecilius Secundus

TABLE OF CONTENTS

Signature Page iii

Dedication iv

Epigraph v

Table of Contents vi

List of Figures viii

Acknowledgements x

Vita xiii

Abstract of the Dissertation xiv

Chapter 1 Introduction 1
1.1 Fundamentals of cardiac electrophysiology 2
1.2 Cardiac arrhythmias 8
1.3 Methods for studying arrhythmia mechanisms 12
1.4 Scope of the dissertation 18

Chapter 2 Using cellular action potential models to understand caveolin-3 mediation of action potential duration 21
2.1 Introduction 21
2.2 Electrophysiology and metabolism of caveolin-3-overexpressing mice 22
2.3 Long QT Syndrome Associated F97C and S141R Caveolin-3 Mutations Differentially Modulate K_V4 and $Ca_V1.2$ Channels Contributing to Action Potential Prolongation 37
2.4 Acknowledgements 49

Chapter 3 High-order finite element methods for cardiac monodomain simulations 50
3.1 Introduction 50
3.2 Methods and Models 52
3.3 Results 57
3.4 Discussion 63
3.5 Conclusions 69
3.6 Acknowledgements 69
3.7 Appendix I 70

Chapter 4 Structural contributions to fibrillatory rotors in a patient-derived computational model of the atria . . . 72
4.1 Introduction . . . 72
4.2 Methods . . . 73
4.3 Results . . . 76
4.4 Discussion . . . 81
4.5 Limitations . . . 88
4.6 Conclusion . . . 90
4.7 Acknowledgements . . . 90

Chapter 5 Toward a hierarchy of mechanisms in CaMKII-mediated arrhythmia 91
5.1 Introduction . . . 91
5.2 Cellular Mechanisms of CaMKII-Mediated Arrhythmia . . 94
5.3 Arrhythmogenic Influence of CaMKII in Congenital Heart Disease . . . 95
5.4 Arrhythmogenic Influence of CaMKII in Acquired Heart Disease . . . 105
5.5 Summary and Conclusion . . . 113
5.6 Caveats and Important Future Directions . . . 115
5.7 Acknowledgments . . . 116

Chapter 6 Experimental Techniques and Analytical Methods for Cardiac Optical Mapping . . . 118
6.1 The Langendorff Perfused Isolated Heart . . . 119
6.2 Optical Mapping of Cardiac Action Potentials . . . 124

References . . . 128

LIST OF FIGURES

Figure 2.1: ECG features in Cav-3 OE mice recorded with telemetry 28
Figure 2.2: Ion channel protein expression in Cav-3 OE mice 29
Figure 2.3: Action potential shortening in a cellular model of Cav-3 OE mice 32
Figure 2.4: Reparameterization of the O'Hara-Rudy model for the Cav3-F97C mutation 44
Figure 2.5: Reparameterization of the O'Hara-Rudy model for the Cav3-S141R mutation 46
Figure 2.6: Cav-3 mutant action potential models prolong the action potential 47

Figure 3.1: A comparison of the electrophysiology solvers presented in the Niederer benchmark paper 58
Figure 3.2: Cubic Hermite-style serendipity elements converge better per degree of freedom than conventional cubic Hermite or linear Lagrange elements 59
Figure 3.3: The relationship between cell Thiele modulus and conduction velocity error is nearly constant for each basis function type. 60
Figure 3.4: Non-physiological oscillations were seen in unconverged solutions 62
Figure 3.5: Convergence results on a physiological mesh 64

Figure 4.1: Example of focal impulse and rotor mapping 74
Figure 4.2: Action potential duration, effective refractory period, and conduction anisotropy all protect normal atrial tissue from sustaining a rotor from a broken wave on the lateral wall of the right atrium . 78
Figure 4.3: Fiber discontinuities help to stabilize a meandering rotor 79
Figure 4.4: Fiber discontinuities can trap a meandering rotor 80
Figure 4.5: Structural remodeling (fibrosis, scar) simulated by placing an inexcitable region near the rotor core trapped the meandering rotor from Figure 4.3 and converted it to stable macro-reentry 82
Figure 4.6: Structural remodeling (fibrosis) near the crista terminalis altered reentry dynamics and resulted in the rotor being displaced 83

Figure 5.1: CaMKII regulation of cardiomyocyte electrophysiology and Ca^{2+} handling 93
Figure 5.2: CaMKII positive feedback mechanisms involved in cardiac disease 95
Figure 5.3: Mechanisms of CaMKII-mediated afterdepolarizations 96

ACKNOWLEDGEMENTS

First, I would like to thank Dr. Andrew McCulloch and Dr. Jeffery Omens for their support and guidance during my time in the Cardiac Mechanics Research Group. I owe my success at UCSD to their mentorship. I would also like thank Dr. Pedro Cabrales, Dr. Ju Chen, Dr. David Krummen, and Dr. Hemal Patel, for their service on my doctoral committee.

I owe a debt of gratitude to all of my CMRG labmates. Their help and friendship eased the inevitable struggles of graduate school. Thanks especially to Matt Gonzales, Andy Edwards, Jeff Van Dorn, and Jen Stowe. They were each generous with their time and expertise, and I learned a tremendous amount from them.

I had the good fortune to work on many collaborative projects during my PhD. I owe a special thanks to Simone Pezzuto, Pedro Gonzalez-Cabrera, Matt Klos, and Jianlin Zhang. My time as a PhD student was much richer for working with and learning from each of them. Thank you also to the people at Simula Research Laboratory who helped arrange and support my research visit to Oslo including Andy Edwards, Molly Maleckar, Aslak Tveito, and Johan Hake, and to the NSF GROW program and the Research Council of Norway for providing the funding. It was rich academic and cultural experience that I will always remember fondly.

I would like to thank my friends and family for their support, perspective, and companionship. To my parents, thank you for the wonderful education you provided me and your encouragement along the way. Finally, I offer an inadequate thank you to my wife, Victoria. Your boundless support and encouragement have made this possible.

Chapters 1 and 6 are original documents. The content of Chapter 2 contains

excerpts from two manuscripts. Section 2.2 is a reprint of a excerpts previously published manuscript with minor edits to fit the format of this dissertation. The citation is Schilling JM, Horikawa YT, Zemljic-Harpf A, Vincent KP, Tyan L, Yu JK, McCulloch AD, Balijepalli RC, Patel HH, Roth DM,"Electrophysiology and metabolism of caveolin-3 over expressing mice", *Bas Res Cardiol* 111:29, 2016. This work is republished with the permission of Springer Publishing. Section 2.3 contains unpublished material being prepared for publication under the title "Long QT Syndrome Associated F97C and S141R Caveolin-3 Mutations Differentially Modulate Kv4 and Cav1.2 Channels Contributing to Action Potential Prolongation" with authors Tyan L, Vincent KP, McCulloch AD, Kamp T, and Balijepalli RC.

The content of Chapter 3 is, in full, a reprint of a previously published manuscript with minor edits to fit the format of this dissertation. The citation is Vincent KP, Gonzales MJ, Gillette AK, Villongco CT, Pezzuto S, Omens JH, Holst MJ, McCulloch AD, "High-order finite element methods for cardiac monodomain simulations", *Front Physiol*, 6:217, 2015. This paper was published with a Creative Commons Attribution License.

The content of Chapter 4 is, in full, a reprint of a previously published manuscript with minor edits to fit the format of this dissertation. The citation is Gonzales MJ, Vincent KP, Rappel W-J, Narayan SM, McCulloch AD, "Structural contributions to fibrillatory rotors in a patient-derived computational model of the atria", *Europace*, 16:iv3-iv10, 2014. This work is republished with permission of Oxford University Press.

The content of Chapter 5 is, in full, a reprint of a previously published manuscript with minor edits to fit the format of this dissertation. The citation

is Vincent KP, Gonzales MJ, Gillette AK, Villongco CT, Pezzuto S, Omens JH, Holst MJ, McCulloch AD, "High-order finite element methods for cardiac monodomain simulations", *Front Physiol*, 6:217, 2015. This paper was published with a Creative Commons Attribution License.

VITA

1986	Born, St. Louis, Missouri
2009	B. S. in Biomedical Engineering *Summa Cum Laude*, Marquette University
2012	M. S. in Bioengingeering, University of California, San Diego
2016	Ph. D. in Bioengingeering, University of California, San Diego

PUBLICATIONS

Howard EJ, Kerckhoffs RCP, **Vincent KP**, Krishnamurthy A, Villongco CT, Mulligan LJ, McCulloch AD, Omens JH, "Myofiber prestretch magnitude determines regional systolic function during ectopic activation in the tachycardia-induced failing canine heart", *Am J Physiol Heart Circ Physiol*, 305:H192-202, 2013.

Gonzales MJ, **Vincent KP**, Rappel W-J, Narayan SM, McCulloch AD, "Structural contributions to fibrillatory rotors in a patient-derived computational model of the atria", *Europace*, 16:iv3-iv10, 2014

Vincent KP, McCulloch AD, Edwards AG "Toward a hierarchy of mechanisms in CaMKII-mediated arrhythmia" *Front Pharmacol*, 5:110, 2014

Vincent KP, Gonzales MJ, Gillette AK, Villongco CT, Pezzuto S, Omens JH, Holst MJ, McCulloch AD, "High-order finite element methods for cardiac monodomain simulations", *Front Physiol*, 6:217, 2015

Sanna MG*, **Vincent KP***, Repetto E*, Nhan N, Brown SJ, Abgaryan L, Riley SW, Leaf NB, Cahalan SM, Kiosses WB, Kohno Y, Brown JH, McCulloch AD, Rosen H, Gonzalez-Cabrera PK, "Bitopic $S1P_3$ Antagonist Rescue from Complete Heart Block: Pharmacological and Genetic Evidence for Direct $S1P_3$ Regulation of Mouse Cardiac Conduction", *Mol Pharmacol* 89:176-186, 2016

Schilling JM, Horikawa YT, Zemljic-Harpf A, **Vincent KP**, Tyan L, Yu JK, McCulloch AD, Balijepalli RC, Patel HH, Roth DM,"Electrophysiology and metabolism of caveolin-3 over expressing mice", *Bas Res Cardiol* 111:29, 2016

ABSTRACT OF THE DISSERTATION

MULTI-SCALE CARDIAC ELECTROPHYSIOLOGY: BRIDGING THE SCALES TO DECIPHER ARRHYTHMIA MECHANISMS

by

Kevin Patrick Vincent

Doctor of Philosophy in Bioengineering with a Specialization in Multi-Scale Biology

University of California, San Diego, 2016

Professor Andrew McCulloch, Chair
Professor Jeffery Omens, Co-Chair

Cardiac arrhythmias are a major source of morbidity, mortality, and healthcare cost in the United States. Arrhythmias are inherently multi-scale phenomena where cellular and subcellular abnormalities result in pathological impulse propagation. The failure of clinical therapies to sufficiently prevent or terminate arrhythmias is due, in part, to a lack of understanding of the underlying mechanisms. Integrating experimental results across spatial and temporal scales using computation modeling presents an important paradigm for investigating arrhythmia mechanisms. In this

dissertation, computational modeling and experimental data at the subcellular, cellular, and tissue scales are used together to gain insight in to mechanisms of arrhythmias for clinically relevant cardiac diseases.

On the cellular and subcellular scale, the ability of caveolin-3 to modulate action potential duration through ion channel regulation was investigated using action potential models to interpreting ion channel data. Two examples are presented in Chapter 2. In the first example, a mouse ventricular action potential model is able to link changes in $K_V4.3$ channel expression to observed QT shortening from the electrocardiogram of caveolin-3-overexpressing mice. The second example parameterizes ionic currents in a human ventricular action potential model with patch clamp data from ion channels co-expressed with Long QT Syndrome causing mutations in caveolin-3. The results identify slowed calcium-dependent inactivation of the L-type calcium channel as an potentially arrhythmogenic mechanisms.

Integrating the subcellular, cellular, and tissue scales for multi-scale cardiac electrophysiology modeling presents numerical, computational, and physiological challenges. Chapter 3 examines these numerical challenges and presents a new high order finite element method to potentially reduce computational expense. This multi-scale electrophysiology solver is used to investigate the behavior of electrical rotors in the human atria in Chapter 4. Specifically, discontinuities in the fiber architecture of the right atria are shown to anchor rotors.

Transgenic mouse models present a unique ability investigate genome effects on the tissue scale. The final two chapters provide literature reviews aimed towards future work investigating triggered arrhythmia mechanisms. Chapter 5 reviews the mechanisms of CaMKII mediated afterdepolarization in cardiac disease. Finally,

Chapter 6 provides a detailed methodological review of Langendorff perfusion and optical mapping of ex-vivo transgenic mouse hearts.

Chapter 1

Introduction

The heart is a pump tasked with supplying oxygenated blood throughout the body to meet metabolic demand. The highly coordinated pumping motion required to efficiently eject blood necessitates a sophisticated control system. Analogous to many modern mechanical pumps, control of the heart's pumping function is accomplished electrically. The electrical activity of the heart emerges from the excitability of cardiomyocytes and the connections between adjoining myocytes at low resistant gap junctions to form a functional syncytium.

Abnormal electrical activity in the heart, a medical condition called cardiac arrhythmia, is a major source of morbidity, mortality, and healthcare cost. Sudden cardiac death, frequently attributed to lethal ventricular arrhythmias, is responsible for approximately 300,000 deaths per year in the United States [KFP+11]. The most prevalent clinical arrhythmia, atrial fibrillation, affects over 3 million patients in the United States predisposing them to stroke and costing the healthcare system approximately $6 billion [KJC+11]. The burden of cardiac arrhythmias falls not only on elderly patient with predictive co-morbidities (e.g., heart failure and/or myocardial

infarction) but also on younger patients with congenital arrhythmogenic diseases (e.g., long QT syndrome, catecholaminergic polymorphic ventricular tachycardia, and Brugada syndrome). Current therapies to control or terminate arrhythmias, including pharmacological, medical device, and surgical interventions, have failed to adequately reduce morbidity and mortality. This is due to a combination of ineffective therapies and poor patient identification. A better understanding of the mechanisms underlying cardiac arrhythmias could help in the development of new therapies to reduce patient suffering and lower healthcare costs.

1.1 Fundamentals of cardiac electrophysiology

Cardiac electrophysiology is a complex physiological process that spans orders of magnitude in spatial and temporal scale. Cardiomyoctes are excitable cells, and the cardiac action potential forms the basis for the electrical activation of the heart. Excitability emerges from the nonlinear interactions of subcellular processes, and action potential propagation on the tissue scale is a result of current flow between neighboring myocytes. Understanding this hierarchy of spatial scales (i.e., subcellular, cellular, and tissue) and how the scales are interdependent is necessary for a better understanding of arrhythmia mechanisms.

Cardiac ion channels

Ion channels are membrane-bound pore-forming proteins that are highly selective for specific ionic species. The opening and closing of channels to allow ions to pass across the membrane is known as channel gating. Many important cardiac ion channels (e.g., the fast sodium current, the L-type calcium channel, and nu-

merous potassium channels) are voltage-gated meaning they activate, deactivate, or inactivate based on the transmembrane potential. Ligand-gated channels open in response to a chemical binding event. Examples of ligand-gated channels include inwardly rectifying potassium currents that require the binding of ATP ($I_{K(ATP)}$) or acetylcholine ($I_{K(ACh)}$). The ionic species specific to a channel can self regulate and serve as the ligand providing feedback to channel gating as with calcium-dependent inactivation of the L-type calcium channel. Finally, mechanical stretch can open certain mechanosensitive channels.

Further regulation of cardiac ion channel function is achieved through protein-protein interactions and subcellular signaling networks. One important regulatory mechanism is controlling the density of channel protein on the cell membrane. This is achieved by altering the balance between gene expression, protein trafficking to the membrane, and degradation via ubiquitination. In addition to the primary pore-forming protein (known as the α-subunit), many ion channels have important accessory proteins (known as β-subunits) that alter channel function or localization. Finally, post-translational modifications, primarily phosphorylation by protein kinase A (PKA) or Ca2+/calmodulin-dependent protein kinase II (CaMKII) but also nitrosylation or glycosylation, can also alter ionic currents.

The cardiac action potential

Ion channel function integrates to the cell scale by generating and maintaining electrochemical gradients in important ionic species (e.g., K^+, Na^+, Ca^{2+}, and Cl^-). These electrochemical gradients and the respective ionic permeabilities define the transmembrane electrical potential difference. Resting membrane potential in a

cardiomyocyte is typically around −85 mV due to the high permeability and large gradient in potassium ions (∼140 mM intracellular vs ∼5 mM extracellular). Provided a sufficient stimulus, currents through ion channels will cause the membrane potential to rapidly depolarize. followed by a slow repolarization back to the resting potential. This sequence is known as the cardiac action potential.

The cardiac action potential has five distinct phases, each a result of the activation and deactivation of specific ion channels. Phase 0 commences with sodium channel activation by a supra-threshold stimulus resulting in a rapid influx of sodium ions and depolarization of the membrane potential. As sodium channels inactivate and the peak membrane potential is reached, the rapid repolarization of Phase 1 begins. Transient outward potassium currents (I_{to}) are the dominant driver of rapid repolarization. Voltage-dependent channels with slower activation kinetics are dominant during Phase 2 — the action potential plateau. Most important among these is the L-type calcium current (I_{CaL}). Ca^{2+} influx through the L-type calcium channel initiates the release of large calcium stores from the sarcoplasmic reticulum (SR) through the ryanodine receptor in a process known as calcium-induced-calcium-release. This large increase in intracellular calcium drives cross-bridge cycling which is responsible for the mechanical contraction of the myocyte. The increase in calcium also sustains depolarization during the plateau phase. Potassium extrusion dominates once the calcium channels have inactivated resulting in repolarization during Phase 3. Phase 4 is the maintenance of the resting membrane potential during the diastolic interval primarily by the inward-rectifying potassium current (I_{K1}).

Cardiac impulse propagation

Low resistance gap junctions located at intercalated disks allow current to passively spread between cells and create propagating waves of depolarization on the tissue scale. Gap junctions are ion channels formed by hexameric connexin proteins that directly connect the cytoplasm of adjoining cells. In a depolarized myocyte, current passively flows through the cytoplasm and across the gap junction to the surrounding cells. Intracellular and intercellular passive conduction is primarily carried by K^+ ions, whereas passive extracellular currents are carried by Na^+ and Cl^-. If the passive current is sufficient in magnitude, the adjoining quiescent cells will reach threshold potential and the wave of depolarization propagates. Passive current in and around flow in myocytes is a function of membrane capacitance, membrane resistance, intracellular resistance (cytoplasmic resistance), intercellular resistance (gap junction resistance), and extracellular resistance. Of these, membrane resistance and gap junction resistance are the largest and therefore determine the cardiac electrical space constant. The space constant for cardiac tissue (i.e., the distance where the depolarization will have passively decayed to 37% of its peak value) is approximately 1-2 mm [Wei52, HCCS90, ARR01].

An alternative theory of impulse propagation, known as ephaptic coupling, posits that extracellular microdomains and not intercellular connections at gap junctions are required for conduction. Ephaptic, or field effect, coupling, is dependent on regions rich in sodium channels located near small extracellular clefts between cells; an arrangement that has recently been observed at the intercalated disk with super-resolution microscopy [VLH$^+$15]. When one cell depolarizes, efflux through sodium channels depletes the sodium ions in the shared extracellular space. This

decreases the extracellular potential. Transmembrane voltage is relative, so reducing the extracellular potential depolarizes the opposing cell membrane which can lead to local activation of sodium channels and trigger an action potential [SM02, CK08]. Recent experimental observations have demonstrated shortcomings in the gap junction theory of conduction. For example, genetic ablation of connexin 43, the primary gap junction forming protein in ventricular myocytes, only reduces the conduction velocity by 50% despite elimination of 90% of gap junctions [GMT$^+$01, DRL$^+$08]. Additionally, a 50% reduction of connexin 43 has yielded conduction velocity results demonstrating no change [MVS$^+$99] or a significant reduction [ELY$^+$01] even when using the same genetic mouse line. Recent experimental and computational studies probing these inconsistencies have lent support to the presence of ephaptic coupling [GSL$^+$15, GBZ$^+$16]. It is possible that gap junction coupling and ephaptic coupling co-exist and are complementary.

Cardiac tissue architecture determines the behavior of impulse propagation. Cardiomyocytes are rod-shaped cells with a dominant axis along which sarcomeres align and mechanical contraction primarily occurs. Ventricular myocytes are electrically coupled at intercalated disks to about 11 other cells with the connections roughly evenly divided between the long axis ends and short axis sides [SKG$^+$94]. Due to the anisotropy of cell shape, the density of cell-to-cell electrical connections is much higher at the long axis ends. Therefore, the anisotropy of conductance is primarily dictated by the cell's length-to-width ratio of approximately 7:1 [CGS87, GKM$^+$92]. Conduction velocity scales as the square-root of conductance [KS98], and indeed the observed anisotropy ratio of ventricular conduction velocity, 3:1 [Cle76, RHS79], is near that predicted by the length-to-width ratio. The end-to-end connections on

the long axis of myocytes determine the dominant fiber direction and primary axis of propagation in cardiac tissue. Importantly, myocytes are not the only cell type in cardiac tissue. Fibroblasts, abundant in healthy cardiac tissue and more so in many disease states, can modulate cardiac conduction directly through cell-to-cell coupling [KCBS05] or indirectly by regulating fibrotic extracellular matrix proteins composition[LCWT01, BF11].

Anisotropic propagation of electrical activity within the cardiac tissue architecture is insufficient for highly coordinated contraction. A specialized conduction system is needed to provide pathways for rapid propagation to ensure synchronous contraction. Cells in the conducting system express different ion channels and have a higher density of gap junctions at their long axis ends. These adaptations allow more rapid conduction along their fiber axis without leaking current into the surrounding tissue.

The activation sequence of the heart initiates in the right atrium at the sino-atrial (SA) node where leaky potassium currents and leaky intracellular calcium stores contribute to periodic depolarization [LD09, GCJ$^+$10]. This depolarizing wave spreads across the right atrium and a high conductance pathway known as the Bachmann's bundle depolarizes the left atrium nearly simultaneously. The propagating wave slows as it conducts through the narrow atrio-ventricular (AV) node causing roughly a 120 milliseconds delay to permit the atria to contract and prime the ventricles for ejecting blood. After exiting the AV node, the depolarization enters a network of highly coupled and rapidly conducting cells. The propagation first passes through the His bundle which bifurcates into the right and left bundle branches. These pathways then repeatedly branch into the Purkinje cell pathways which finally electrically couple

to the bulk of the ventricular myocardium. The resulting rapid depolarization allows the ventricles to activate synchronously and efficiently pump blood.

1.2 Cardiac arrhythmias

Cardiac arrhythmias are inherently multi-scale problems where cellular and subcellular abnormalities manifest themselves on the tissue scale. The term cardiac arrhythmia encompasses a wide range of clinical conditions. Abnormal electrical activation can be due to a heart rate that is too slow (bradycardia) or too fast (tachycardia). Other types arrhythmias occur when propagation through the specialized conduction system is abnormal (e.g., AV block or bundle branch block). This section will focus on mechanisms underlying tachycardias as these can degrade into atrial or ventricular fibrillation, the most prevalent and lethal arrhythmias, respectively. Tachyarrhythmias can be broadly categorized as either triggered or reentrant.

Triggered arrhythmias and afterdepolarizations

Triggered arrhythmias occur when aberrations in membrane potential, known as afterdepolarizations, overcome the electrotonic loading from surrounding tissue to generate an ectopic propagating wave. Isolated cardiomyocytes routinely exhibit afterdepolarizations initiating either during repolarization, known as early afterdepolarizations (EADs), or during the diastolic interval, known as delayed afterdepolarizations (DADs). Afterdepolarizations occurring during different phases of the action potential have different underlying mechanisms.

EADs occur under conditions that reduce repolarization reserve. This reduction in net outward current can be due to reduced outward currents or increased inward

currents. Reduced repolarization reserve can potentiate cells, but specific aberrant currents are required in initiate an EAD [QXO$^+$13]. I_{CaL} is the current primarily responsible for Phase 2 EADs. At membrane voltages of between 0 mV and −30 mV, L-type calcium channels can produce a steady state "window current" due to overlapping activation and availability of the channels, and this current can initiate EAD formation [MNA94, WGK$^+$10]. The electrogenic sodium-calcium exchanger (I_{NCX}) can also drive an EAD generating inward current [SSRL94]. I_{NCX} can act synergistically with I_{CaL} and help facilitate EADs, or I_{NCX} can be activated independent of I_{CaL} due to spontaneous calcium release from the SR similar to the DAD mechanism described below [WGK$^+$10]. The mechanisms underlying Phase 3 EADs are less clear, but a recent study in isolated murine cells demonstrated non-equilibrium reactivation of I_{Na} driving afterdepolarizations with take off potentials near −47 mV [EGH$^+$14]. Triangularization of the action potential leading to calcium extrusion via I_{NCX} has also been shown to reactivate I_{Na} and trigger a Phase 3 EAD [TJO$^+$12]. DADs are caused by spontaneous Ca^{2+} release from the SR during the diastolic interval [TKB07]. This Ca^{2+} release triggers calcium waves that drive inward I_{NCX} and can reach the threshold for I_{Na} activation.

Cellular afterdepolarization are infrequent events, but the probability for EADs and DADs can be increased under certain conditions. Sensitizing conditions for EADs include slow rate, reduced repolarizing currents, and action potential prolongation. DADs are potentiated by any conditions leading to calcium overload such as rapid rate or Na^+ overload. Genetic channelopathies can increase the propensity for afterdepolarizations [NBMP12]. Congenital long QT syndromes have been shown to promote EADs through mutations in the channel and accessory proteins that

underly I_{Ks}, I_{Kr}, and I_{Na} [BPR$^+$17]. Mutations in SR Ca^{2+} release and Ca^{2+} buffering proteins, specifically the ryanodine receptor [PNT$^+$01] and calsequestrin [LPO$^+$01], can increase the probability for spontaneous Ca^{2+} release and therefore DAD generation. LQT3 mutations in SCN5A that result in a persistent component to I_{Na} ($I_{Na,L}$) have also been shown to promote DADs [LHM$^+$09]. Additionally, subcellular signaling networks, especially PKA and CaMKII signaling, are potent afterdepolarization promoters. A detailed description of afterdepolarization mechanisms arising from CaMKII hyperactivity and dysregulation in different disease states is included in Chapter 5

Afterdepolarizations occur in isolated cells, but evidence of the ectopic activity that defines triggered arrhythmias is rare on the tissue scale even in diseased hearts. This is due to the functional connections between cardiomyocytes at gap junctions. When one cell experiences abnormal increase in membrane potential due to an afterdepolarization, current is drawn away from this cell and dissipated by the surrounding cells. This is known as the source-sink effect. Due to this electrotonic loading, many cells must simultaneously exhibit afterdepolarizations to overcome the source-sink mismatch. Regions with fewer connection between cells, such as purkinje fibers and tissue boundaries, require drastically fewer cells to generate ectopic activity [XSG$^+$10]. Stochasticity [CSP$^+$15] and regional chaos synchronization [SXS$^+$09, dXQ12] have been proposed to explain how large groups of cells simultaneously experience afterdepolarizations with the latter being the dominant theory.

Reentrant arrhythmias

Reentrant arrhythmias occur when circulating waves of depolarization repeatedly activate cardiac tissue. When the rotation is around a physical obstacle, it is called anatomical reentry. For example, an inexcitable ischemic scar or a narrow accessory pathway near the AV node could serves as the obstacle for anatomical reentry. To establish reentry, the time it takes for the wave to rotate around the obstacle must be greater than the tissue's refractory time. If this were not the case, the wave would collide with its refractory tail and extinguish. This concept, known as a vulnerable window, is fundamental to reentry, and it was proposed alongside the first description of anatomical reentry in 1914 by George Mines [Min14, DeS97]. More formally, the path length around the obstacle must be longer than the excitation wavelength. Wavelength is approximated by the product of conduction velocity and refractory period, and the spatial region between the depolarizing wavefront and its non-refractory tail is known as the excitable gap [KR04].

Functional reentry occurs when rotating electrical waves are sustained without an obstacle. This electrical activity is known as a spiral wave in 2-D contexts or a scroll wave in 3-D. An excitable gap is not needed for functional reentry, and when the excitation wave front and wave back meet to form a phase singularity, the self-organizing source is called a rotor [VCJ08, PJ13]. As discussed in Chapter 4, Rotors can be stable, possibly due to anatomical features such as fiber architecture or tissue curvature, or they can meander. Meandering rotors are more fibrillatory and therefore more dangerous than stable rotors.

Reentrant arrhythmias are fundamentally tissue-scale, but they require cellular and subcellular phenomena to provide a vulnerable tissue substrate and initiating trig-

ger. Spatial heterogeneities in refractoriness combined with slowed conduction velocity provide a cardiac substrate that can sustain reentry. Pathological action potential duration (APD) dynamics are one mechanism underlying gradients in refractoriness. When beat-to-beat alternations in APD become out of phase across adjoining regions, known as spatially discordant alternans, it creates a substrate susceptible to reentry [WNGQ11, WKS$^+$06]. Afterdepolarization driven ectopic activity in the region with a repolarization gradient provides the initiating trigger for reentry. Unidirectional block occurs when the ectopic wave collides with the refractory region on one side but is able to propagate into the non-refractory region. Finally, afterdepolarizations serve not only as potential reentry triggers, but sub-threshold afterdepolarizations can also contribute to an arrhythmogenic substrate [LdG$^+$15].

1.3 Methods for studying arrhythmia mechanisms

Experimental methods

Experimental models have provided much of our understanding of arrhythmia mechanisms. However, they typically focus on a single scale of cardiac electrophysiology, and integrating information across scales remains a challenge. The patch clamp technique allows for the measurement of the current through ion channels, and dynamic patch clamping protocols can help obtain results under more relevant physiological conditions [Wil06, ANC09]. On the cellular level, action potentials and calcium transients can be measured in isolated myocytes, but these preparations lack information regarding specific channels or cell-to-cell coupling. Cultured monolayers of myocytes provide some conduction information, but are still meaningfully

different from intact tissue. One important emerging technique on the cell and monolayer level is the use of cardiomyoctes derived from human induced pluripotent stem cells [YVSO$^+$07, MZN$^+$12]. These cells reproduce some of the important electrophysiological characteristics of native myocytes including genetics channelopathies [MBW$^+$10, IMH$^+$11], and are therefore able to provide more information across scales. On the tissue scale, Langendorff perfusions has long been used to study the electrophysiology in intact ex-vivo hearts with electrodes or optical dyes allowing tissue scale electrical activity to be measured. Chapter 6 provides a detailed review of Langendorff perfusion and optical mapping of membrane potential. Catheter based electrode systems can measure electrical activity in anesthetized large animals. These data are more clinically relevant, but lack specific channel or cell level information.

Inadequate understanding of the interdependency across spatial scales in cardiac electrophysiology can be dangerous and result in flawed arrhythmia therapies. Studies in isolated myocytes indicated that Class Ic sodium channel blockers may be effective antiarrhythmic agents in post-myocardial infarction patients by increasing threshold potential, abolishing DADs, and prolonging the refractory period [BM70, RH73]. However, in a large placebo-controlled randomized clinical trial, two antiarrhythmic drugs, flecainide and encainide, failed catastrophically with almost three times the rate of arrhythmia deaths in the treatment arm [MI89, ELM$^+$91]. The single cell studies failed to consider the tissue-scale effects of the drug. The desirable cell-scale effect, decreased excitability, also slowed the conduction velocity. The prolonged refractoriness did not outweigh the slowed conduction, and the vulnerable window and potential for conduction block were actually increased.

Following the failure of Class Ic antiarrhythmic drugs, it was hypothesized that

blocking the rapid delayed-rectifier potassium current (I_{Kr}) and prolonging the APD with d-sotalol would be antiarrhythmic [VHA+95]. Again, a large placebo-controlled randomized trial was stopped early due to increased rate of arrhythmic deaths in the treatment group [WCd+96]. The most likely arrhythmia mechanism underlying the failure of this trial was spatially inhomogeneous APD lengthening which increased gradients in refractoriness and increased the propensity for EADS resulting in a lethal arrhythmia known as *torsades de pointes* [SH05]. HERG channel block (the channel protein responsible for the I_{Kr} current) is now commonly screened during drug development to identify drugs that may be proarrhythmic.

Computational methods

Computational modeling of cardiac electrophysiology can integrate information across scales to study emergent phenomena not obvious from experimental results. The use of computational models is particularly important for complex, nonlinear systems where common intuition, even of experienced practitioners, can be misleading [Nob02]. Hodgkin and Huxley developed the first computational model of an action potential with experimental data from a giant squid axon [HH52]. A decade later Nobel modified their work to describe the electrical behavior of Purkinje cells [Nob62]. These cell level models are circuit analogs described by a system of ordinary differential equations. They have intracellular and extracellular pools of electrolytes with the cell membrane modeled as a capacitor and ion channels as time- and voltage-dependent resistors. Cardiac cell models have grown much more complex by incorporating additional ion channels, subcellular compartmentation, regulatory networks and complex Markov State models of channel gating [RS06]. The most detailed cell models today can have

over one hundred coupled differential equations to describe the cellular processes. Using cellular action potential models to interpret patch clamp data from ion channels is the topic of Chapter 2.

Tissue-scale models combine cellular action potential models with the flow of current across a geometry. In models of electrical wave propagation, cardiac tissue can be treated either as a continuum or as a network of discrete cells. Continuum models assume the length scale of the constitutive parts (i.e., individual myocytes) is small enough to ignore, and thus, conduction can be considered continuous. Mathematically, continuum models take the form of reaction-diffusion partial differential equations where the reaction portion is described by the cellular action potential model and the diffusion accounts for the passive spread of current. These complex nonlinear equations are commonly solved using finite element methods [RM94a, Sun06]. Tung formalized the continuum approach by deriving the bidomain model in 1978 using a homogenization technique [Tun78]. The bidomain equations define an extracellular and intracellular potential at every point, and tensors describe the extracellular and intracellular conductivity along the primary axes of the tissue architecture. If the conductivity anisotropy is assumed to be the same in the both domains, the model can be simplified to the monodomain equation. Numerical considerations for solving the monodomain equation is the topic of Chapter 3. The alternate to continuum modeling is to consider each discrete cell in cardiac tissue as part of a resistively coupled network. Discrete cardiac models become particularly important under conditions where the continuum assumptions begin to break down such as reduced gap junction coupling [Kee90, BPW14], ephaptic coupling [LK14], or afterdepolarizations being opposed by electrotonic loading [XSG$^+$10].

Multi-scale computational modeling has made many important contributions to understanding arrhythmia mechanisms. Incredibly, within a year of the failed Class Ic antiarrhythmic drug trial, the nascent field of computational cardiac modeling was able to demonstrate a proarrhythmic mechanisms. In this rudimentary model, Starmer et al. demonstrated that flecainide would increase the vulnerable window and identified accumulating unavailable sodium channels at high rate, known as use-dependent block, as a key factor [SLNG91]. A recent, mechanistically detailed study supported that conclusion using cable, sheet, and biventricular models of cardiac tissue [MZY$^+$11]. The ability for multi-scale electrophysiology modeling to weigh the proarrhythmic and antiarrhythmic affects of a potential therapy can also identify valuable therapies that might otherwise be neglected. Moreno et al. computationally predicted that the antiarrhythmic inhibition of the late sodium current with ranolazine outweighs the mild sodium channel block and QT prolongation using 1-,2-, and 3-dimensional models of cardiac tissue [MYB$^+$13]. Preliminary clinical results have supported this conclusion, but large scale clinical trials have not been completed [SMERC16]. Tissue-scale electrophysiology models have also had demonstrable success in identifying cellular and tissue-scale mechanisms underlying the initiation and maintenance of anatomical reentry and rotors [PK95, BJ98, FK98, XQG98, QWG99].

Transgenic mice as a model multi-scale system

Transgenic mice present a unique paradigm that combines experimental and computational methods to bridge from the genetic scale to the tissue scale. The malleability of the mouse genome allows the function of specific genes to be probed by knocking them out or over expressing them. Tamoxifen inducible Cre combined with an

α-myosin heavy chain promoter allows for for conditional, tissue-specific genome editing [SNC$^+$01]. Isolation of adult murine cardiomyoctes is a well established technique [LSW11]. Electrophysiological studies at the subcellular and cell scales is also routine. Patch clap and optical imaging allow ion channel, calcium spark, transmembrane potential, and calcium transients all to be measured. On the tissue scale, voltage and calcium optical mapping of Langendorff perfused hearts allows measurement of tissue properties (e.g., conduction velocity and restitution time) and the direct observation of arrhythmia behavior [HLJ12, MWK$^+$12, KNLS15]. Computational methods for mouse electrophysiology are also well developed. Recently, a new action potential model was published with detailed cellular electrophysiology and calcium handling [MEM$^+$14]. Tissue scale measurements of conduction velocity can be used to parameterize existing continuum models of propagation. This ability to measure and simulate electrophysiology across all relevant scales is not available in any other model system.

However, the electrophysiology of the mouse is substantially different from that of humans and care must be taken when extending conclusions [KHG98]. The most apparent difference between mouse and human hearts is the size. It has long been hypothesized that mouse hearts were too small to sustain reentry and fibrillation [Gar14, Win94], but careful experimental studies in ex-vivo hearts have observed them with optical mapping [VMSJ99]. Basal heart rate in mice is around 600 bpm compared to 60-70 bpm for humans. This impacts many aspects of the electrophysiology including recovery from inactivation of certain ion channels. Perhaps most importantly, murine ventricular myocytes express different ion channels than human ventricular myocytes resulting in a much shorter and more triangular action potential[Ner04]. The balance

between calcium re-uptake into the SR and extrusion from the cell during diastole is also much different between mouse and human with SR re-uptake being much more dominant in mouse (∼90% vs ∼50%, respectively) [Ber01]. Combined, these differences may make mouse hearts susceptible to different arrhythmia mechanisms from those in humans [KV12]. Again, computational modeling can be used to overcome some of these challenges by anthropomorphizing, with caution, results from transgenic mice.

1.4 Scope of the dissertation

The synthesis of experimental and computational techniques in cardiac electrophysiology is a powerful tool for probing arrhythmia mechanisms. This dissertation demonstrates the utility of this approach by using computational modeling across different scales to interpret and extend experimental results.

On the cellular and subcellular scale, the ability of caveolin-3 to modulate action potential duration through direct and indirect ion channel regulation was investigated using mathematical action potential models to interpret ion channel data. Chapter 2 looks at this regulatory function in two contexts. In the first, a mouse ventricular action potential model is able to link changes in $K_V4.3$ channel expression to observed QT shortening from the electrocardiogram of caveolin-3-overexpressing mice. The second example parameterizes ionic currents in a human ventricular action potential model with patch clamp data from ion channels co-expressed with Long QT Syndrome causing mutations in caveolin-3. The results identify slowed calcium-dependent inactivation of the L-type calcium channel as an potentially arrhythmogenic mechanisms.

Integrating the subcellular, cellular, and tissue scales for multi-scale cardiac electrophysiology modeling presents numerical, computational, and physiological challenges. The verification of an electrophysiology solver using high-order elements is presented in Chapter 3. Cubic Hermite elements are demonstrated to have a convergence advantage over linear methods. A novel high-order element scheme is also presented as a way to lessen the computational demand of the problem. These cubic Hermite-style serendipity interpolations methods have the same convergence order as traditional cubic Hermite methods with half of the degrees of freedom in a 3-dimensional hexahedral element. A dimensionless number to quantify stability and convergence of tissue-scale electrophysiology problems is derived and tested to help ensure that spurious numerical artifacts do not misinform conclusions about arrhythmia mechanisms.

A multi-scale model of cardiac electrophysiology is used to investigate the behavior of electrical rotors in the human atria in Chapter 4. The pulmonary veins are important structural features known to help maintain atrial fibrillation (AF) in the left atrium by providing a favorable conditions for focal beats and a substrate for reentry. Recent clinical data have demonstrated that rotors in the right atrium may also play a role in maintaining AF in as many as a quarter of all patients. The multi-scale model is used to demonstrate that right atrial fiber discontinuities can transiently and permanently anchor rotors in a patient derived model of the human atria.

The final two chapters provide literature reviews aimed towards future work. Transgenic mouse models of CaMKII hyperactivity and deletion provide an opportunity to study the initiation of triggered arrhythmias in a physiologically important setting.

Chapter 5 is a detailed review of CaMKII mediated afterdepolarization mechanisms for difference cardiac diseases. Finally, Chapter 6 provides a detailed methodological review of Langendorff perfusion and optical mapping.

Chapter 2

Using cellular action potential models to understand caveolin-3 mediation of action potential duration

2.1 Introduction

Since they were first developed, mathematical models of cellular electrophysiology have been essential to understanding ion channel function, excitability, and electrical propagation. From their careful voltage-clamp measurements, Hodgkin and Huxley quantitatively described the membrane potential across a giant squid axon using four currents (capacitive, Na^+, K^+, and leak) with voltage- and time-dependent gating equations for K^+ activation (n), Na^+ activation (m), and Na^+ inactivation (h) [HH52]. Somewhat incredibly, Andrew Huxley made the first calculations of an

action potential model using a manual calculating machine over the a period of three weeks 1951. [Hod94]. Mathematical models of cellular electrophysiology have grown increasingly complex (and computational methods exponentially more efficient), and they remain an indispensable tool for interpreting ion channel data at the cellular scale.

This chapter presents two examples of using cellular action potential models to interpret ion data. Both look at the ability of structural protein caveolin-3 (Cav-3) to mediate action potential duration through direct and indirect regulation of ion channels. The first example uses channel expression data to help explain electrocardiogram observations in caveolin-3-overexpressing mice. This work was published in *Basic Research in Cardiology* in 2016. In the second example, the mechanisms underlying two long WT syndrome 9 mutations (Cav-3 F97C and Cav-3 S141R) are examined by incorporating changes in $I_{Ca,L}$, I_{to}, and I_{Na} into a human ventricular action potential model. This work is being prepared for submission, and only figures corresponding to the modeling work performed by the dissertation author are included here.

2.2 Electrophysiology and metabolism of caveolin-3-overexpressing mice

Caveolae are small flask-like invaginations of the sarcolemmal membrane discovered over six decades ago [Pal53, Yam55]. Recent work has identified caveolae as signaling epicenters made up of essential scaffolding proteins called caveolins. Caveolae and caveolins are necessary for the precise temporal and spatial localization and organization of cellular signaling molecules [HTPR14, PMI08] involved in cardiac

protection [HPT$^+$08] [SHST$^+$14] [THJ$^+$08] [TTH$^+$14b, TTH$^+$14b, TTH$^+$14a] and cardiac remodeling [HPK$^+$11]. There are three distinct caveolin (Cav) isoforms including Cav-1 and Cav-2, which are ubiquitous in all cell types, and Cav-3 which is found predominantly in skeletal and cardiac myocytes [CHSL04, RWL02, SST$^+$96]. Cav-3, via its scaffolding domain, has been shown to interact with numerous signaling molecules including G-protein-coupled receptors (GPCRs), ion channels, and receptor tyrosine kinases[HTPR14, PMI08, SB01]. Mice with cardiac-specific overexpression of caveolin-3 (Cav-3 OE) demonstrate tolerance to myocardial ischemia and left ventricular pressure overload suggesting stress adaptation of the heart [HPK$^+$11, THJ$^+$08].

Cav-3 plays an integral role in organizing signaling molecules that are essential for the generation of heart rate, rhythm, and cardiac chronotropy [CVV$^+$13, MFP$^+$11, VAY$^+$06, YBF$^+$08]. Cav-3 mutations have been implicated in cardiac arrhythmias, particularly prolonged QT syndrome, given their association with adrenergic receptors and ion channels. Furthermore, specific chronotropic ion channels have been localized within caveolae including SCN5A-encoded voltage-gated Na^+ channels [YLLS02b], voltage-dependent K^+ channel [BDB$^+$07], sodium calcium exchangers [BTJKH02a, BTJKH02b], and L-Type Ca^{2+} channels [BFH$^+$06a, LFS$^+$00].

Despite these provocative findings regarding Cav-3 expression and cardiac conduction, there are no data regarding the effect of Cav-3 overexpression in the heart on basic electrophysiology and metabolism. In the current study, we describe baseline cardiac conduction and metabolism in Cav-3 OE mice as a means to add mechanistic insight into the alterations in stress adaption previously observed in Cav-3 OE mice.

Methods

Animals

All mice were treated in compliance with the Guide for the Care and Use of Laboratory Animals (National Academy of Science) and the protocols were approved by the VA San Diego Healthcare System Institutional Animal Care and Use Committee. Animals were kept on a 12-h lightdark cycle (with light on from 6:00 to 18:00 hours) in a temperature-controlled room with ad libitum access to food and water. Transgenic mice were generated in our laboratory using the α-myosin heavy chain promoter to produce cardiac myocyte-specific overexpression of Cav-3 (Cav-3 OE) in a C57BL/6 background. Full-length Cav-3 cDNA (455 bp) was cloned into a vector containing the α-myosin heavy chain promoter and was used for microinjection by the UCSD Transgenic Core. Cav-3 OE mice have a $\sim$1.8-fold increase in caveolin-3 protein in whole heart homogenates [THJ^{+}08] . Transgene-negative littermates were used as control mice. All experiments were performed on male mice.

Telemetry

4- to 5-month-old male Cav-3 OE (N = 7/group) and control mice (N = 8/group) were anesthetized with 1.4% isoflurane. A small peritoneal incision was made and the transmitter [ETA-F10, Data Sciences International (DSI), Inc, St. Paul, MN, USA] was inserted into the peritoneal cavity. The leads were secured in the right thorax and lower abdominal regions according to the manufacturers protocol. Continuous signals were transmitted wirelessly to the receivers located below the cage. Animals were given analgesia (buprenorphine) and allowed to recover for 72 h. Mice

were then acclimated for 10 days without analgesia. All mice were housed in ventilated cages with ad libitum food and water. Light and dark cycles were maintained using automatic timers. Continuous telemetry recordings were monitored for 72 h using Dataquest ART software (Data Sciences International, Inc., St. Paul, MN, USA) and analyzed with the programs default mouse parameters. QTc was measured using previously published derived equations for conscious mice, QTc = QT/SQRT(RR/100) [MJK98, ZWK$^+$14].

Immunoblotting

Immunoblotting was performed on adult mouse ventricular homogenates prepared from either control or Cav-3 OE mice (N = 57/group). Homogenates were solubilized using ice-cold 11 mmol/L TrisHCl, pH 7.4, 1.1 mmol/L EDTA, 0.2% SDS, 11% glycerol, and protease inhibitors (2 mM phenylmethylsulfonyl fluoride, 12 μg/ml aprotinin, 1 mM benzamidine, 10 μM leupeptin, 5 μM pepstatin A). The lysate was centrifuged at 5000g for 10 min to remove insoluble debris. The protein content was estimated in the soluble supernatant and an equal amount of each sample was analyzed by SDS/PAGE (415% gradient gels, Bio-Rad) and Western blot by probing with antibodies to Cav-3, connexin 43 (Cx43) and GAPDH (Millipore), $K_V1.4$, $K_V4.2$, and $K_V4.3$ antibodies (NeuroMab, UC Davis, CA), $Ca_V1.2$ antibody (Alomone labs, Jerusalem, Israel), and $Na_V1.5$ antibody (Millipore Corporation). Protein signals for Cav-3 and channel subunits were quantified by normalizing the signal to GAPDH.

Computational modeling

A recently published murine ventricular action potential model [MEM$^+$14] was used to investigate the observed changes in ion channel expression in the Cav-3 OE mice. This computational model consists of a system of 158 ordinary differential equations describing the myocyte ion channels and Ca^{2+} handling as well as PKA and CaMKII signaling networks. The model source code was obtained from the authors website (https://somapp.ucdmc.ucdavis.edu/Pharmacology/bers/) [MEM$^+$14], and all simulations were executed using the ode15s algorithm in MATLAB (The MathWorks, Inc., Natick, MA, USA). In the absence of functional ion channel data, previous studies have meaningfully incorporated differences in ion channel transcript levels into an action potential model by scaling the whole-cell ion channel conductance based on relative differences [BSD$^+$11, CGT$^+$09]. Similarly, we created a Cav-3 OE version of the action potential model by scaling the ion channel conductance by statistically significant changes in ion channel protein expression measured by Western blot. The action potential duration (APD) was measured with respect to the control repolarization levels, so that changes in action potential amplitude alone would not alter the APD results.

Statistics

Investigators were blinded to the genetic background of mice in all study protocols. Statistical analysis was performed with GraphPad Prism Software v6.0 (La Jolla, CA, USA). All values are presented as mean ± standard deviation [M (SD)]. Two-way or two-way repeated measure (RM) ANOVA followed by post hoc Tukeys correction for multiple comparisons and unpaired Students t test were utilized. An

α-level of $p < 0.05$ for all statistical tests was used.

Results

Cav-3 OE mice have prolonged PR intervals as well as shortened QT intervals

ECG data from Cav-3 OE and control mice (N = 78/group) were analyzed for a 24-h period. Cav-3 OE mice (M = 38.51 ms, SD = 2.04) had significantly longer PR interval times compared to control mice [Figure 2.1.B ; M = 35.09 ms, SD = 1.10; $t(13) = 4.12$, $p = 0.001$]. No significant difference was observed in the QRS interval times when Cav-3 OE mice (M = 12.97 ms, SD = 0.63) were compared to control mice [Figure 2.1.C; M = 13.10 ms, SD = 0.63; $t(13) = 0.40$, $p = 0.70$]. Furthermore, Cav-3 OE mice (M = 46.82 ms, SD = 3.45) had significantly shorter QTc interval times compared to control mice [Figure 2.1.D; M = 53.95 ms, SD = 4.15; $t(13) = 3.59$, $p = 0.003$].

Cav-3 OE mice show increased $K_V1.4$ and $K_V4.3$ potassium channels, $Na_V1.5$ sodium channels, and Cx43 expression

As changes in conduction, rate, and rhythm may be linked to changes in ion channel expression, we determined the expression of the major ion channels involved in the cardiac action potential in the left ventricles by immunoblot analysis. As shown in Figure 2.1, the protein expression of $K_V1.4$ [Figure 2.1.A; N = 5/group; Cav-3 OE M = 2.76, SD = 0.85 versus control M = 1.41, SD = 0.67; $t(8) = 2.78$, $p = 0.02$] and $K_V4.3$ [Figure 2.1.C; N = 5/group; Cav-3 OE M = 1.71, SD = 0.56 versus control M

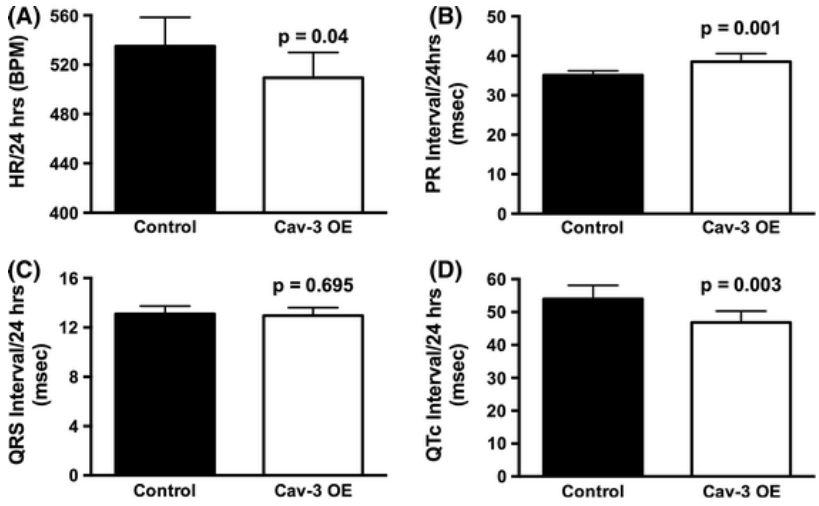

Figure 2.1: **ECG features in Cav-3 OE mice recorded with telemetry.** Cav-3 OE mice show (a) lower 24-h heart rates, (b) prolonged PR intervals, (c) no significant difference in overall QRS complex length, and (d) shortened QT intervals. p is assumed to be significant when <0.05. Data are presented as mean ± SD; N = 78/group

= 0.79, SD = 0.33; t(8) = 3.18, p = 0.01] was significantly increased in the Cav-3 OE mice compared to control mice, respectively. However, the protein expression of the $K_V4.2$ [Figure 2.1.B; N = 5/group; Cav-3 OE M = 1.71, SD = 1.58 versus control M = 1.59, SD = 0.33; t(8) = 0.16, p = 0.87] and $Ca_V1.2$ was unchanged between groups [Figure 2.1.D; N = 56/group; Cav-3 OE M = 1.35, SD = 0.39 versus control M = 0.98, SD = 0.32; t(9) = 1.72, p = 0.12]. Additionally, $Na_V1.5$ protein expression [Figure 2.1.E; N = 56/group; Cav-3 OE M = 1.31, SD = 0.26 versus control M = 0.76, SD = 0.48; t(9) = 2.41, p = 0.04] and Cx43 expression [Figure 2.1.F; N = 56/group; Cav-3 OE M = 1.28, SD = 0.37 versus control M = 0.85, SD = 0.24; t(9) = 2.21, p = 0.05] were significantly increased in Cav-3 OE mice. We performed a confirmatory immunoblot to show that Cav-3 was significantly increased in Cav-3 OE mice [Figure 2.1.G; N = 57/group; Cav-3 OE M = 1.31, SD = 0.34 versus control M = 0.70, SD = 0.42; t(10) = 2.78, p = 0.02].

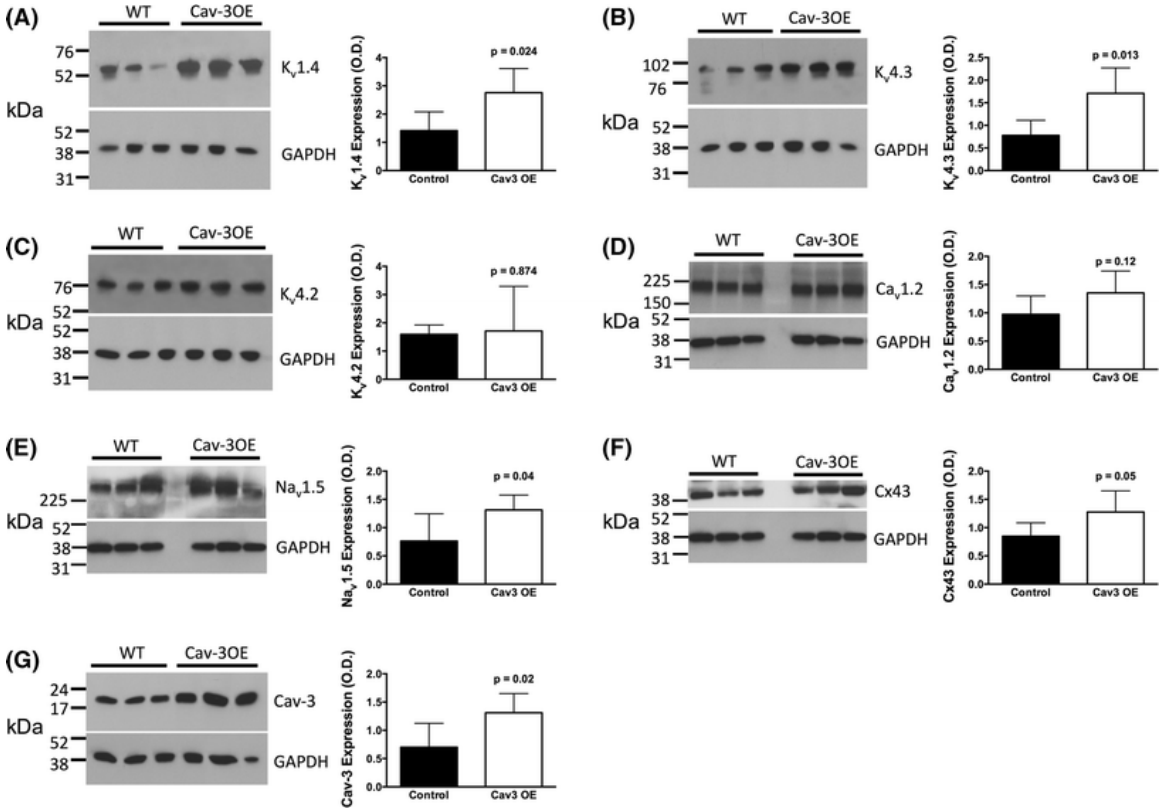

Figure 2.2: **Ion channel protein expression in Cav-3 OE mice.** Left ventricular tissue from Cav-3 OE mice showed increased protein expression of $K_V1.4$ (a), and $K_V4.3$ (b), no change in $K_V4.2$ (c) and $Ca_V1.2$ (d), but increased protein levels of in $Na_V1.5$ (e) and Cx43 (f). Elevated Cav-3 protein expression was confirmed in Cav-3 OE hearts (g). p is assumed to be significant when <0.05; Data are presented as mean $\pm$ SD; N = 57/group

A computation model of ventricular myocytes from Cav-3 OE mice predicted shortened action potential duration

To better understand the effects of altered ion channel expression on the observed electrophysiology phenotype, significant changes in protein expression from Figure 2.2 were incorporated into a computation model of a mouse ventricular myocyte action potential. The conductance of the fast component of the transient outward potassium current ($G_{to,f}$), carried by the $K_V4.3$ channel protein, was increased 2.2-fold from 0.44 to 0.97 mS/μF, and the conductance of the fast sodium channel (G_{Na}), carried by the $Na_V1.5$ channel protein, was increased 1.7-fold from 10 to 17 mS/μF. The slow component of the transient outward potassium current ($I_{to,s}$), carried by the $K_V1.4$ channel protein, was not included in the original model [MEM+14] as its expression was typically limited to septal myocytes in the mouse [XGN99].

The resulting Cav-3 action potential model has shortened action potential duration (APD) compared to the control model (Figure 2.3.A). The maximum decrease in APD occurred at 50% repolarization (APD_{50}; 55% reduction at 6-Hz pacing) with a substantial decrease still present at 90% repolarization (APD_{90}; 12% at 6-Hz pacing) (Figure 2.3.B). This change in APD is consistent across a range of heart rates (Figure 2.3.C). Since the largest suppression in APD occurred in the voltage range important for calcium influx, intracellular calcium transients (CaT) were also evaluated in the model. There was a slight reduction in CaT amplitude at 1-Hz pacing (15%) that decreased near physiological rates (9% at 6-Hz pacing) (Figure 2.3.D). The relative contributions of each conductance change were dissected by implementing them independently. The increased $G_{to,f}$ was wholly responsible for the decrease in action potential duration (Figure 2.3.E). Increasing $G_{to,f}$ and G_{Na} individually had opposing effects on CaT

amplitude, resulting in the minimal resultant change in the Cav-3 OE model (Figure 2.3.F).

Discussion

Cav-3 has been implicated in playing a role in cardiac rhythm, chronotropy [BGR$^+$04, CVV$^+$13, MFP$^+$11, VAY$^+$06, YBF$^+$08], and stress adaptation [HPK$^+$11, THJ$^+$08]; however, the effects of cardiac overexpression of Cav-3 on baseline cardiac conduction and metabolism have never been investigated. We have shown for the first time that cardiac-specific overexpression of Cav-3 results in significant lower heart rates at rest, prolonged PR interval, shortened QTc intervals, and alterations in ion channel expression, while baseline whole organism metabolism remains unchanged.

The normal healthy heart relies on efficient electrical conduction via the sinoatrial node, the atrioventricular node, and the Purkinje fibers to optimize cardiac contraction [DSS$^+$14]. The rate at which the heart contracts is modified by various intrinsic and extrinsic signaling mechanisms [CO06]. Intrinsically, various ion channels regulate depolarization and repolarization of each individual myocyte. Interestingly, caveolins and caveolae have been associated with many of these ion channels as well as many G proteins that are known to interact with ion channels [BKov]. Mutations in Cav-3 can lead to congenital long-QT syndrome by affecting sodium ion channel regulation [VAY$^+$06]. Furthermore, recent studies show that Cav-3 and caveolae are essential for stretch-dependent conduction slowing [PWE$^+$14]. Finally, Cav-3 can form macromolecular complexes with one of the major subunits within the cardiac pacemaker channels, affecting cardiac conduction [BGR$^+$04, YBF$^+$08]. These previous findings and our novel data suggest a critical role for Cav-3 in regulating cardiac

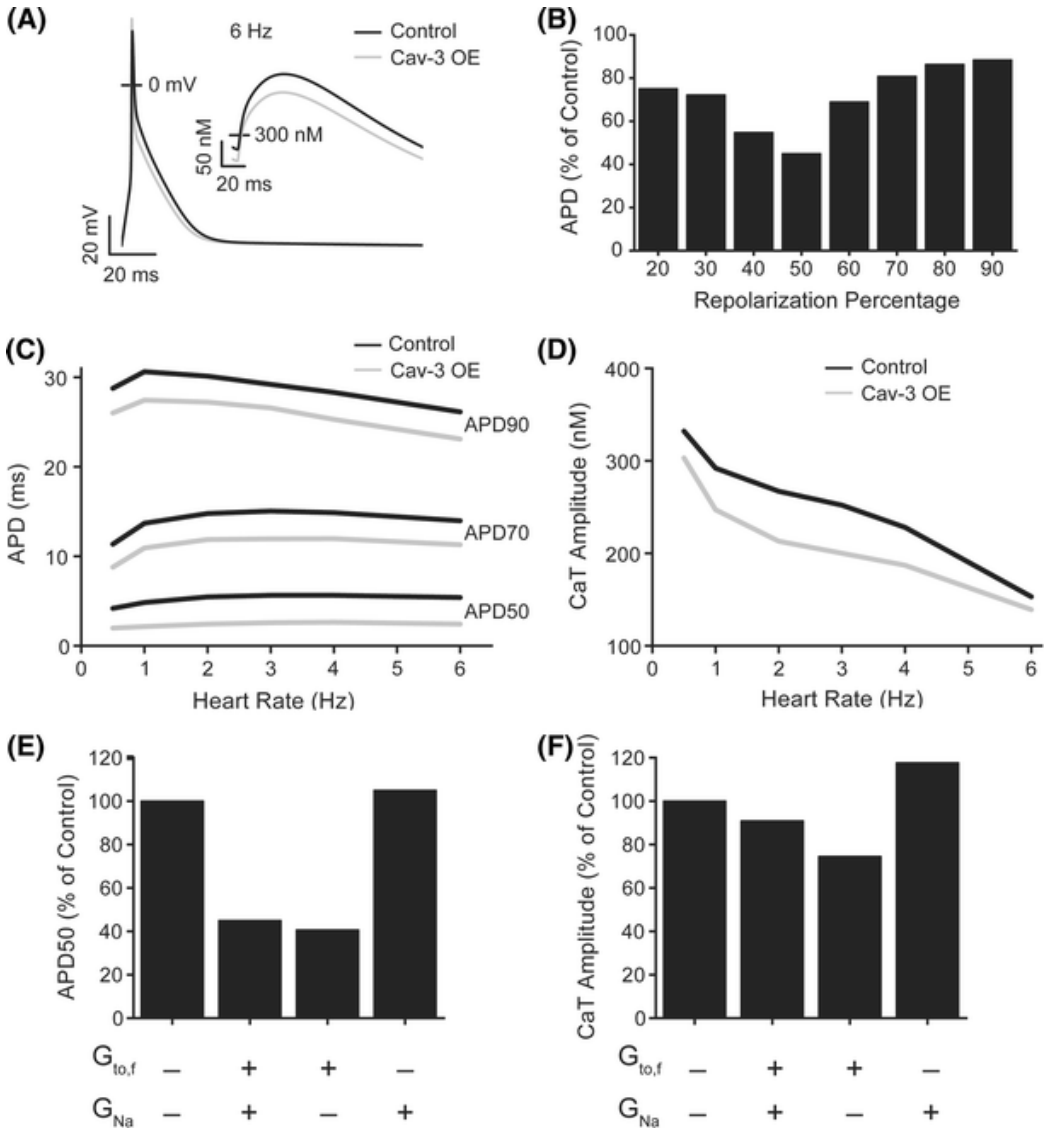

Figure 2.3: **Action potential shortening in a cellular model of Cav-3 OE mice.** (A) Action potential and intracellular Ca2+ (inset) from simulated 6 Hz pacing for control (black line) and Cav-3 OE (grey line) model parameters. (B) APD was decreased in the Cav-3 OE model compared to control. (C) This decrease was consistent across a range of pacing rates. (D) Intracellular calcium transient amplitude was slightly decreased in the Cav-3 OE model with the effect diminishing near physiological rates. (E) The increase in Gto,f was responsible for the decrease in APD. (F) Increasing $G_{to,f}$ and G_{Na} had opposing effects on the CaT amplitude when applied individually.

conduction and chronotropy.

We show that $K_V1.4$ and $K_V4.3$ channel protein expression levels are significantly increased in Cav-3 OE mice. K_V channels via effects on Ito currents are essential to cardiac repolarization. Indeed, when the channel protein expression differences measured in Cav-3 OE mice were used to scale whole-cell ion channel conductances in a mouse ventricular myocyte mode, the APD was shortened. APD_{90} and QTc are closely related [ZWK$^+$14], and the reduction in APD_{90} from the model (12% at 6-Hz pacing) was similar to the reduction in QTc measured with telemetry (13%). These results suggest that the increase in K_V channel expression is sufficient to explain the QTc decrease in Cav-3 OE mice. Although a severely shortened QT interval has been associated with congenital heart disorders that may cause cardiomyopathy and arrhythmias [SBW08], our mice do not exhibit any characteristics of cardiomyopathy even at old age (unpublished data) and have no increase in mortality when compared to littermate control mice. In contrast, Cav-3 OE mice have been shown to be resistant to myocardial ischemia and demonstrate increased survival in response to chronic pressure overload hypertrophy [HPK$^+$11, THJ$^+$08], with decreased hypertrophic response, suggesting a phenotype of stress adaptation. Many different signaling pathways are involved in cardioprotection [Heu15], and Cav-3 may serve as a molecular integrator of these various pathways.

Sinus bradycardia and prolonged PR interval are well documented in the trained athlete and are thought to be secondary to unknown intrinsic factors and modified by increased vagal tone on the sinoatrial pacemaker [Lam12][MP06]. Our data suggest that caveolins may be an intrinsic factor involved in the cardiac response to exercise via their multiple interactions with ion channels and other cell signaling molecules.

Previous investigations have shown that Cav-3 mRNA is upregulated in trained animal hearts by approximately twofold [GMR$^+$09]. Interestingly, our Cav-3 OE mice have an approximate twofold elevation of Cav-3 protein at baseline [THJ$^+$08]. Short- and long-QT syndromes are both uncommon in trained athletes [SLK13]. However, changes within the QT interval are observed during exercise and recovery and are known as QT hysteresis [42]. This shortening in the QT interval is exaggerated in long-QT syndrome and hysteresis has been suggested as a possible marker of long QT [KKY97]. Interestingly, beta-blockade can normalize this exaggerated response as well as lower cardiac risk seen with long-QT syndrome [KYC$^+$02, MZH$^+$00]. Furthermore, early repolarization and not terminal repolarization appears to be the major contributor to these changes [KHN$^+$08]. The outward potassium current, Ito, activates transiently in the sub-threshold range of membrane potential to initiate rapid repolarization following the action potential and helps to set the plateau membrane potential and subsequently the length of the QT interval and action potential duration [NK05]. In the heart, I_{to} is formed from the heteromeric assembly of three primary alpha subunits (K_V1.4, K_V4.2, and K_V4.3), which are differentially expressed and associated with K_V channel-interacting proteins (KChIPs) or the β subunits. The K_V4.2 and K_V4.3 α subunits contribute to the rapidly recovering ($I_{to,f}$) components, whereas K_V1.4 α subunits contributes to the slowly recovering ($I_{to,s}$) components in the ventricular myocytes [NN10, PC05]. The K_V4.2 and K_V4.3 channels are shown to partition into caveolae by interacting with the A-kinase anchoring protein, AKAP100, and Cav-3 to form a macromolecular signaling complex [AUGC10]. These findings correlate with our results where K_V1.4 and K_V4.3 channels are overexpressed resulting in faster cardiac repolarization and possibly minimizing exaggerated QT hysteresis.

Cav-3 has also been implicated in voltage-gated sodium channel function. Cav-3 has been shown to co-immunoprecipitate with $Na_V1.5$ [VAY$^+$06, WPBJ15, YLLS02b] (the α-subunit responsible for the inward sodium current resulting in phase 0 of the action potential). Disruption of this channel has been implicated in long-QT syndrome type 3 [SGA13, WSS$^+$95, WPBJ15] and Brugada syndrome [SBEB$^+$03, SEP$^+$02, SW02]. Most recently, in vitro, co-expression of mutant Cav-3 and $Na_V1.5$ resulted in prolonged action potential duration leading to a long-QT type 9-like phenotype [CYK$^+$07]. Our results further support the relationship between Cav-3 and $Na_V1.5$, as $Na_V1.5$ is significantly increased in Cav-3 OE mice. However, the effect of increased $Na_V1.5$ expression on the phenotype is uncertain. The action potential model did not support a role for $Na_V1.5$ in the observed QTc decrease. This is consistent with the lack of APD or QTc changes in cardiac-specific SCN5A-overexpressing mice [ZYTW07]. The increased $Na_V1.5$ expression may provide a compensatory effect to offset the Ito-mediated decrease in CaT amplitude predicted by the computational model.

Previous studies have suggested a key role for Cx43 in electrical coupling and action potential propagation [Fvdv12, KR04]. We show that Cx43, a vital component in gap junction formation, is increased in Cav-3 OE hearts. An interaction between caveolins and Cx43 has been described [YRM$^+$14]. A specific role for Cav-3 in S-nitrosylation of Cx43 in cardiac mitochondria has been suggested [FHH$^+$14, SNM$^+$14, SNA$^+$15]. Others have shown that reduction of Cx43 and $Na_V1.5$ results in polymorphic ventricular arrhythmias in cardiac hypertrophy [FRv$^+$14]. Interestingly, Cav-3 overexpression has been shown to protect against cardiac hypertrophic remodeling [HPK$^+$11, MPW$^+$15].

The current manuscript has potential limitations. Our data extrapolate ion channel expression to physiological changes and potential computational models. Patch clamp experiments to confirm these data are currently being performed by the laboratory. Similarly, data regarding Cav-3 KO animals that would support our conclusion are currently being performed as well. In addition, the pharmacological experiments were performed with IP injections rather than IV. It is possible that IV administration could result in altered pharmacological responses compared to those we report in this manuscript.

In conclusion, our data suggest that cardiac-specific overexpression of Cav-3 results in alterations in baseline cardiac conduction, heart rate, and expression levels of certain cardiac ion channels. Although further investigations are necessary to elucidate the full physiological and clinical implications of Cav-3 overexpression on heart rate control, our novel data support a critical role for Cav-3 in cardiac conduction. The changes observed in baseline cardiac conduction and ion channel expression in our study may provide further mechanistic insight into the phenotype of ischemic tolerance and resistance to pressure overload-induced stress that have been observed previously in Cav3- OE mice.

2.3 Long QT Syndrome Associated F97C and S141R Caveolin-3 Mutations Differentially Modulate K_V4 and $Ca_V1.2$ Channels Contributing to Action Potential Prolongation

Caveolin-3 (Cav3) is one of three types of caveolins, scaffolding proteins required for forming caveolae. Cav3 is expressed in cardiac muscle, in skeletal and smooth muscles [SST+96]. Caveolae are membrane microdomains enriched in cholesterol and sphingolipids, present in cardiomyocytes and other cells, and localize a number of different ion channels and signaling proteins [BKov]. It has been shown that in caveolae localized potassium channels [MSS+01], [SHSD04] including channels forming transient outward potassium current ($K_V1.4$, $K_V4.2$, and $K_V4.3$), L-type Ca2+ channels (Cav1.2) [BFH+06a], Na+ channels ($Na_V1.5$) [YLLS02b], Na+/Ca2+ exchanger (NCX1) [BTJKH02a] and others. Caveolae play a role in cell signaling, ion channels regulation, participating in lipid regulation[BKov]. Also, they can serve as mechanosensors in various cell types [NWH+13].

Mutations in Cav3 lead to a variety of pathological conditions impacting primarily cardiac muscle and skeletal muscle. The F97C and S141R mutations in Cav3 have been linked with the congenital long QT syndrome (LQT9) [VAY+06]. LQT9 is characterized prolongation of the QT interval on the electrocardiogram, and predisposing individuals with LQT9 to ventricular tachycardia, syncope, and sudden death [SCI12]. It has been shown, that F97C mutation leads to decreased Kir2.1 current density [VVS+13]. Also, Cav3 F97C and S141R prolong the duration of action

potential (AP) by increasing sodium channel late current [CVV$^+$13].

The reason of prolonged QT interval is prolongation of cardiac AP duration (APD). Transient outward potassium current (Ito) is responsible for the early repolarization phase of cardiac AP. L-type Ca2+ current is responsible for plateau the second phase of cardiac AP. Together this two currents have impact on the length of the QT interval. Ito consisted from 2 parts, with different recovery from inactivation time constants, fast and slow Ito [GXLN99, PC05]. Kv1.4 channel mediates the slow (Ito,s) component of Ito. Kv4.2 and Kv4.3 channels generate the fast (Ito,f) component of Ito [NK05, OKS$^+$01]. Reduced Ito,f densities are observed in failing human hearts [BNE93], as well as canine animal model [KNC$^+$96]. Dysregulations in Ito plays a role in the Brugada syndrome [Ant06]. Moreover, the activity of Ito channels influences the activation of voltage-gated Ca2+ channels and the balance of inward and outward current during the plateau [GCKN00]. The Cav1.2 channel is a candidate for modulation by LQT9 Cav3 mutations because a subpopulation of the channels associate with Cav3 and are localized to caveolae [BFH$^+$06a]. Furthermore, studies have indicated that caveolae serve as calcium signaling domains which could be impacted by alterations in Cav1.2 function [PDZI74, Gab71, LLS$^+$00]. Studies have also shown that mutations in Cav1.2 can cause a form of LQTS called Timothy syndrome which has been associated with delayed voltage-dependent inactivation of ICa,L [STS$^+$04, APC$^+$07].

The purpose of the present study was to determine the impact of LQT9 Cav3 mutations F97C and S141R on the function of Kv4.2, Kv4.3 and Cav1.2 channels expressed in HEK 293 cells. Our results demonstrate that these Cav3 mutations down regulate Ito,fast channels functions and impact differentially Cav1.2 channels in a

calcium-dependent fashion by increasing current density and channel gating in the case of S141R and delaying calcium-dependent inactivation for F97C.

Methods

Chemical reagents and Plasmid construction

All chemicals, reagents, and antibodies were procured from Sigma unless otherwise stated. The cDNA for Kv4.2 (human KCND2, Genbank accession no. BC110449), Kv4.3 (human KCND3, Genbank accession no. BC113475), were obtained from Open Biosystems, (GE Healthcare) and subcloned into pcDNA3.1 plasmid vector (Invitrogen, Carlsbad, California), as previously described [VAY$^+$06]. Plasmids encoding the human pore-forming 1C,77 (Cav1.2), auxiliary 2cN4 LTCC and hemagglutinin (HA)-Cav1.2 subunits have been previously described [BFB$^+$11, FBD$^+$04, SBR95]. Preparation and subcloning of wild type human Cav3 (GenBank accession no. NM_033337), Cav3-F97C and Cav3-S141R mutations were previously reported [VAY$^+$06].

HEK-293 cell maintenance and transfections

HEK-293 cells were grown and maintained in DMEM supplemented with 10% fetal bovine serum (GIBCO), 100 U/ml penicillin, 100 g/ml streptomycin, and 2 mM L-glutamine. The Cav3-WT, Cav3-F97C, and Cav3-S141R (1 μg each) were transiently cotransfected with expression vectors containing Cav1.2 and Cavβ2cN4 L-type Ca2+ channel subunits or Kv4.2 or Kv4.3 at a ratio of 1:1 respectively into HEK-293 cells plated on 35-mm plastic dishes at densities between 2 and 2.5 104 cells/dish using Lipofectamine 2000 (Invitrogen) according to manufacturers instructions. In all cases,

0.15 μg of plasmid DNA encoding the green fluorescent protein (GFP) was included to identify transfected cells. Two days after transfection, GFP-positive HEK-293 cells were selected for functional studies.

Whole cell patch clamp electrophysiology

Electrophysiological experiments were carried in the whole cell configuration of the patch clamp technique at room temperature using Axopatch 200B amplifier (Axon Instruments, Foster City, CA) with pCLAMP 10.2, software. Recording pipettes were pulled from thin walled borosilicate glass capillaries (World Precision Instruments, Inc., Sarasota FL) with pipette resistance of 1.52.5Mω. The data were filtered at 5 kHz and digitized at 50 kHz. All solutions and buffers are indicated in mmoles/L. For Ito current measurements external bath solution contained 136 NaCl, 4 KCl, 2 MgCl2, 1 CaCl2, 5 CoCl2, 10 glucose, and 10 HEPES, pH 7.4 (NaOH). Intracellular pipette solution contained 137 KCl, 1 MgCl2, 4 Mg-ATP, 1 Li-GTP, 10 EGTA, and 10 HEPES, pH 7.2 (KOH). Ionic currents were recorded in the ruptured whole-cell configuration using 2.5 s voltage steps from - 40 to 60 mV from a holding potential of -60 mV. Recovery from the inactivation was investigated using a conventional two-depolarizing pulse protocol: an inactivating pulse depolarizing to 40 mV for 2 s (P1) followed by a variable recovery interval steps of 50 ms (0.05 3 s) and subsequent 40 mV test pulse (P2). The interpulse potential was set at 60 mV. The ratio of test pulse current/inactivating pulse current amplitudes (P2/P1) was used to evaluate Ito recovery from inactivation, which was best fit with a single exponential equation (y=A1*exp(-x/t1)+y0).

For currents measurements through L-type Ca^{2+} channels external bath solution

contained 142 NaCl, 5.4 KCl, 1.8 CaCl2, 1 MgCl2, 0.33 Na2HPO4, 5 HEPES, 5 glucose (pH 7.4) and the following pipette solution: 100 CsOH-H2O, 100 Glutamic acid, 40 CsCl, 10 HEPES, 0.5 CaCl2, 240 mg/ml Amphotericin B (pH 7.2). Recordings were performed using amphotericin perforated whole cell patch configuration in three different solutions. 5 Ca^{2+} (mM): 65 NaCl, 70 TEACl, 10 HEPES, 1 MgCl2, 10 glucose, 5 CaCl2, 10 M tetrodotoxin (pH 7.4); 10 Ba2+ (mM): 10 BaCl2, 133 CsCl, and 10 HEPES (pH 7.4); 10 Ca^{2+} (mM): 10 CaCl2, 133 CsCl, and 10 HEPES (pH 7.4). The holding potential was -80 mV. The inactivation curves were fit to a Boltzmann distribution with the V1/2 is the voltage midpoint for the distributions. Data were analyzed using Microcal Origin software (Origin Lab Corporation Northampton, MA USA).

Computational modeling

A mathematical model of the human ventricular action potential [OVVR11] was used to further investigate the observed effects of Cav3 mutations on $I_{Ca,L}$, I_{to}, and I_{Na}. This model consists of a coupled system of 41 ordinary differential equations that together describe ionic currents and intracellular Ca2+ cycling. The model source code was obtained from the original author's website (http://rudylab.wustl.edu), and all simulations were executed using the ode15s algorithm in MATLAB (The MathWorks, Inc., Natick, MA, USA). The Cav3-WT version of the model corresponds to the O'Hara-Rudy model as originally published. To simulate the effect of the Cav3-F97C and Cav3-S141R mutations, currents were adjusted to match the whole cell patch clamp data. Significant differences in channel gating (i.e., time constants) or current density were incorporated into the Cav3 mutant models. When there were

discrepancies between measured values and the baseline model parameters, relative changes were applied. For the Cav3-F97C model, changes were made to $I_{Ca,L}$, I_{to}, and $I_{Na,L}$. For the Cav3-S141R model, changes were made to $I_{Ca,L}$ and $I_{Na,L}$. Virtual knock-out of the individual effect for each channel was performed to identify their overall contribution to the changes in action potential duration. All simulations were paced to steady state (1000 beats). Finally, simulations used the epicardial parameterization of the O'Hara-Rudy model unless otherwise stated.

Statistical analysis

Data are reported as mean standard error of mean (SEM). Determinations of statistical significance were performed using a Student t-test for comparisons of two means or using analysis of variance (ANOVA) for comparisons of multiple groups. Statistical significance was determined by a value of $P < 0.05$. Statistical analysis was performed using Origin 7.5 (OriginLab Corporation, Northampton, MA).

Results

Only a summary of the ion channel patch clamp results in HEK-293 cells co-expressed with mutant or WT Cav3 is provided here to motivate the modeling studies. Full results will be included when the manuscript is submitted for publication.

WT and mutant Cav3 co-localized well with $K_V4.2$ and $K_V4.3$ channels in the HEK-293 cells. $I_{Kv4.2}$ was significantly reduced in cells transfected with Cav3-F97C compared to those transfected with Cav3-WT. Furthermore, analysis of channel kinetics showed a significant slowing of the activation and inactivation time constants with Cav3-F97C co-expression. $I_{Kv4.2}$ recovery from inactivation was also slowed

with the Cav3-F97C transfection. When the Cav3-S141R mutation was transfected together with $I_{Kv4.2}$, similar results were seen with a significant reduction in peak current, slowed activation, and prolonged recovery from inactivation. However, no significant differences in inactivation kinetics were seen.

Cells co-expressing $K_V4.3$ and Cav3-F97C also showed a significant reduction in peak $I_{Kv4.3}$. The activation time constants and recovery from inactivation were slowed with Cav3-F97C similar to the results with $K_V4.2$, but no significant differences were seen between the inactivation time constants. Interestingly, no significant differences in $I_{Kv4.3}$ peak current or kinetic when comparing $K_V4.3$ coexpressed with the Cav3-S141R versus Cav3-WT.

WT and mutant Cav3 also co-localized well with $Ca_V1.2$ + $Ca_V\beta_{2cN4}$ proteins co-expressed in the HEK-293 cells. Neither the Cav3-F97C nor the Cav3-S141R mutations altered voltage-dependent inactivation (VDI)when Ba^{2+} was the charge carrier ($I_{Ba,L}$). The Cav3-F97C and Cav3-S141R mutations differentially regulated the calcium current with its physiological charge carrier. Co-expression with Cav3-F97C did not increase $I_{Ca,L}$ density compared to Cav3-WT, but it did slow Ca^{2+}-dependent inactivation (CDI). Whereas, co-expression with Cav3-S141R significantly increased $I_{Ca,L}$ density but did not alter CDI.

These changes in channel density and kinetics described above were combined with previously published data on $I_{Na,L}$ [VAY$^+$06, CVV$^+$13] to create action potential models meant to reproduce the electrophysiology of a Cav3 mutation. Importantly, $K_V4.3$ is expressed much more abundantly in human ventricular tissue compared to $K_V4.2$ [DSW$^+$96, GLBS$^+$07], and therefore, only the significant changes seen in $I_{Kv4.3}$ were incorporated into the models.

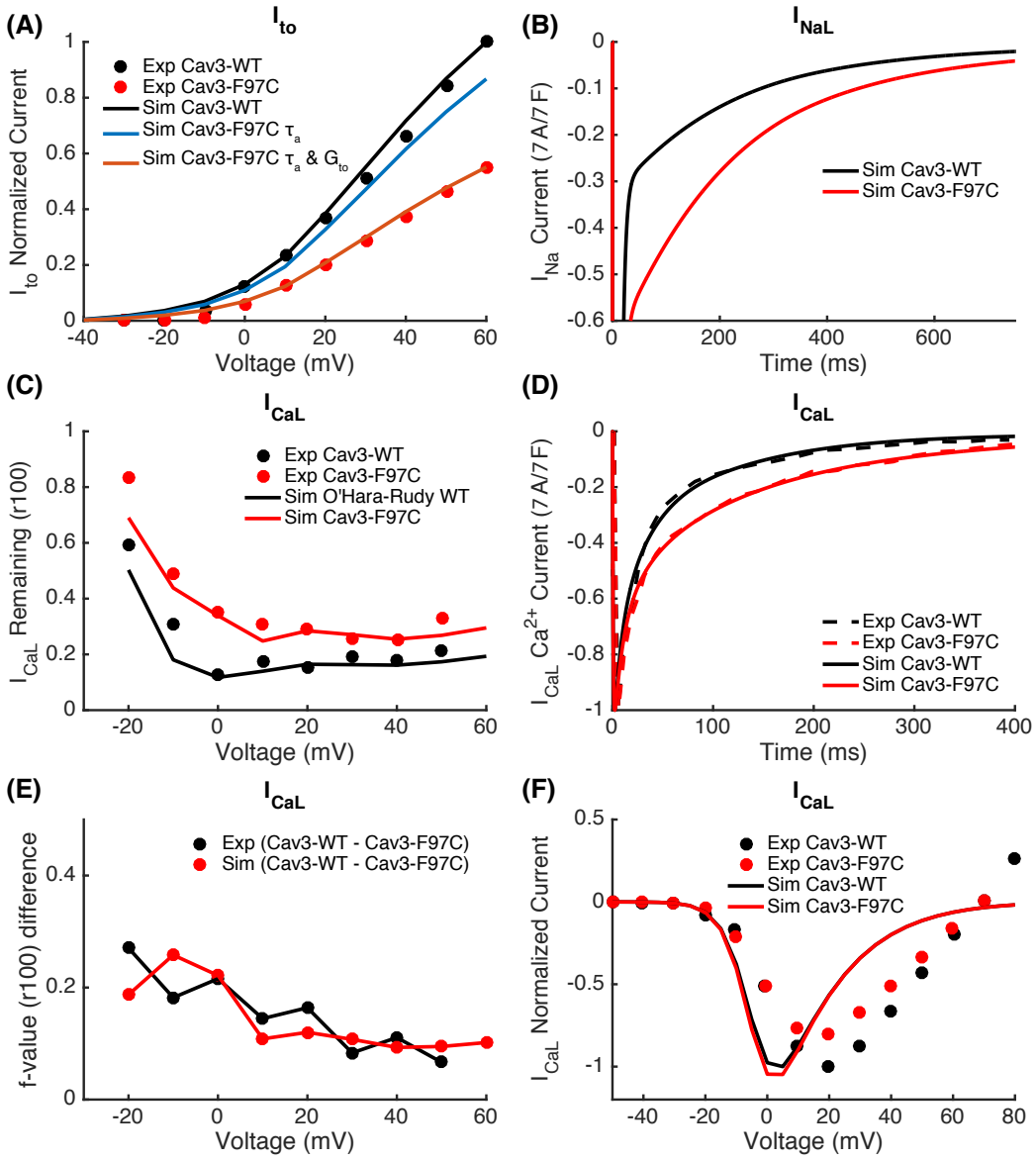

Figure 2.4: **Reparameterization of the O'Hara-Rudy model for the Cav3-F97C mutation.** (A) Slowing the I_{to} activation time constant (τ_a) resulted in a small decrease in current density. Current density was further reduced by scaling the conductance. (B) $I_{Na,L}$ conductance was doubled in the Cav3-F97C model. (C) Experimental and simulation results compare favorably for the fraction of $I_{Ca,L}$ still active at 100 ms (r100). (D) CDI time constants were fit to experimental data. (E) The relative difference in $I_{Ca,L}$ remaining between Cav3-WT and Cav3-F97C was similar for the experimental and simulation data. (F) Peak $I_{Ca,L}$ was not impacted by the slowed CDI.

.

Figure 2.4 includes the changes to fit the Cav3-F97C mutation. First, I_{to} was altered to account for the slowed activation and reduced peak density observed with $K_V4.3$ expression with Cav3-F97C. The activation time constant was scaled by 41% to account for the slowing observed experimentally. However, this effect alone was insufficient to account for the large decrease in current density (Figure 2.4.A). The channel conductance was reduced by 36.5% to fully account for the decease in channel density. The density of the late sodium current ($I_{Na,L}$) was doubled to account for previously published effects of Cav3-F97C (Figure 2.4.B). Next, slowed CDI was incorporated into the model of $I_{Ca,L}$. The parameterization of $I_{Ca,L}$ in the O-Hara-Rudy model compared favorably to the experimental results gathered here (Figure 2.4.C; Black). The time constants governing CDI were adjusted to match those observed with Cav3-F97C co-expression (Figure 2.4.D). I result on CDI matched the experimental observations well (Figure 2.4.C; Red). Notably, the neither model reproduced the very slow CDI seen at the most negative holding potentials (Figure 2.4.C; -20 mV). However, the relative differences measured by the f-value (difference in $I_{Ca,L}$ remaining 100 ms past the peak between Cav3-WT and Cav3-F97C) were similar between the model and experiments across a range of potentials (Figure 2.4.D). Finally, the above changes caused only minor effects on the density of $I_{Ca,L}$ (Figure 2.4.F).

The reparameterization of the O'Hara-Rudy model for the Cav3-S141R mutation is portrayed in Figure 2.5. To account for changes in $I_{Ca,L}$, the Cav3-S141R model increased the current density by 27% and shifted the steady state activation curve -6 mV (Figure 2.5.A). The density of the $I_{Na,L}$ was doubled to account for previously published effects of Cav3-S141R (Figure 2.5.B).

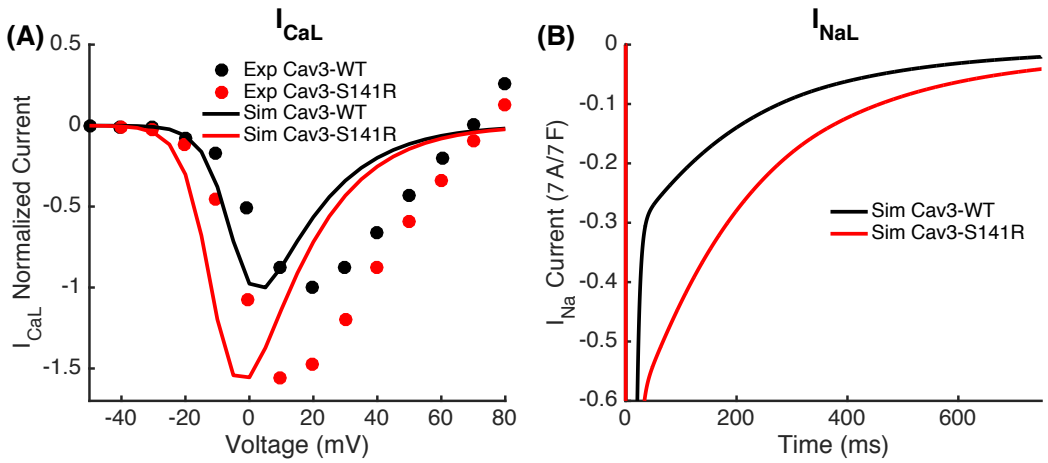

Figure 2.5: **Reparameterization of the O'Hara-Rudy model for the Cav3-S141R mutation.** (A) The O'Hara-Rudy $I_{Ca,L}$ model was adjusted to match the Cav3-S141R experimental data by increasing the peak current and shifting the steady state inactivation cure more negative. (B) $I_{Na,L}$ conductance was doubled in the Cav3-S141R model.

In Figure 2.6 the results from the reparameterized action potential models demonstrate that both mutations prolong the APD. APD prolongation at 1000 ms cycle length was greater for the Cav3-F97C mutation (2.6.A) compared to the Cav3-S141R mutation (Figure 2.6.B). For the Cav3-F97C mutation, these APD effects were consistent across pacing rates and similar for endocardial and epicardial paramterizations of the O'Hara-Rudy model (Figure 2.6.C). For the Cav3-S141R mutation, there appear to be a increase in the APD prolongation in the endocardial version of the cell model at slow rates (Figure 2.6.D).

Virtually ablating the effect of one of the currents while leaving the others intact can allows the relative contributions to APD prolongation to be identified. The action potential prolongation in the Cav3-F97C model was dominated by the $I_{Ca,L}$ effect and the decrease in I_{to} density had very minimal impact (Figure **??**.E). For the Cav3-S141R model, however, the $I_{Ca,L}$ and $I_{Na,L}$ contributed more equally (Figure 2.6.E).

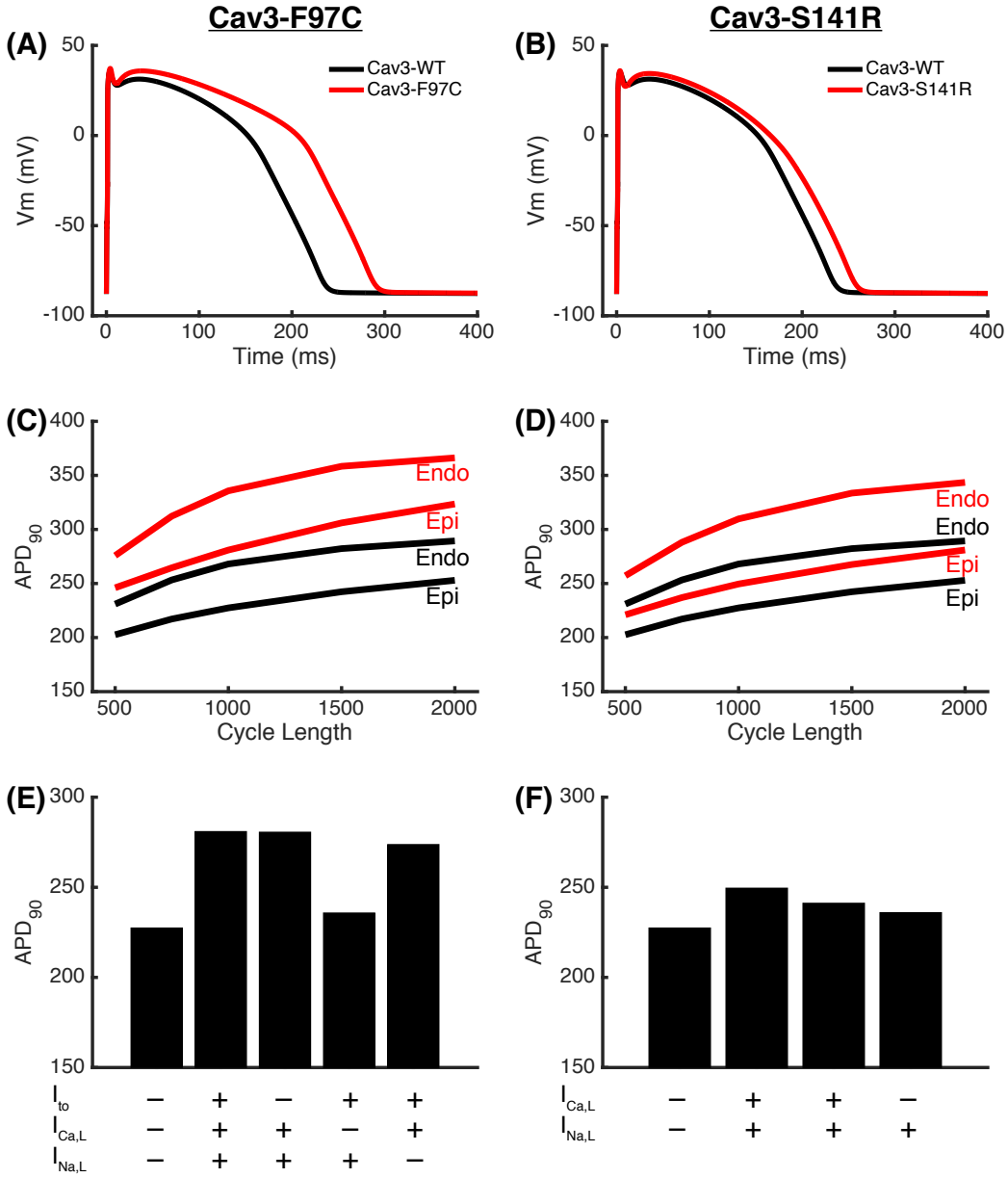

Figure 2.6: **Cav-3 mutant action potential models prolong the action potential.**Both the Cav3-F97C (A) and Cav3-S141R (B) action potential models prolong APD. Tracings shown are for 1000 ms cycle length pacing after 1000 beats (steady-state). The effect of rate and on APD is shown for endocardial and epicardial parameterizations of the O'Hara-Rudy model for Cav3-F97C (C) and Cav3-S141R (D). The presence (+) or absence (-) of different current effects are shown for the Cav3-F97C model (E) and the Cav3-S141R model (F). Selectively removing the effect of one current demonstrates the relative contribution of that current to the change in APD

Discussion

The identification of ion channels that localize to caveolae has brought attention to the role of this microdomain in cardiac excitability [BFH$^+$06b, YLLS02a, BFW$^+$08]. Initial experiments with the LQT9 Cav3 mutations, Cav3-F97C and Cav3-S141R, demonstrated an increase in sodium channel late current ($I_{Na,L}$) [CVV$^+$13]. Increased late I_{Na} can leads to calcium overload through reverse mode Na/Ca exchanger, diastolic dysfunction due to hyperactivated myofilaments, and electrophysiological instability due to prolongation of APD with early after depolarizations (EAD) and delayed after depolarizations (DAD) [GKK$^+$15]. Also, F97C prolongs repolarization by decreasing Kir2.1 current density. Kir2.1 loss of function is additive to the increase described in late I_{Na} [VVS$^+$13]. However, it was unclear whether these LQT9 mutations affect other caveolar ion channels. Our study showed the new effect of Cav3 on potassium channels generating $I_{to,f}$ and L-type Ca+ channels and confirmed the previous data on the role of F97C and S141R mutations of Cav3 on regulation of cardiac APD.

Results from the computational models of both mutations demonstrated action potential prolongation. This is consistent with the expected effects of the mutations and the clinical observation of long QT interval in patients carrying the mutation. The Cav3-F97C mutation model had a stronger effect on APD than the modeled Cav3-S141R mutation. Interestingly, Cav3-F97C mutation effect on $I_{Ca,L}$ was primarily responsible for the action potential effects, and the large decrease in I_{to} had minimal effect. In rodents such as the mouse with strong repolarization currents and short, triangular action potentials, strengthening the I_{to} current shortens the action potential and decreasing I_{to} prolongs action potential. However, in large mammals with an action potential plateau and longer action potential, the interaction of I_{to} with APD

is more complex. Ito plays a critical role in determining the plateau potential, and strengthening I_{to} can strengthen $I_{Ca,L}$ and actually prolong the action potential duration [ZXW$^+$12]. These types of complex, non-linear interaction are a reminder for why mathematical modeling is useful when interpreting results from ion channels.

2.4 Acknowledgements

The content of this chapter contains excerpts from two manuscripts. Section 2.2 is a reprint of a excerpts previously published manuscript with minor edits to fit the format of this dissertation. The citation is Schilling JM, Horikawa YT, Zemljic-Harpf A, Vincent KP, Tyan L, Yu JK, McCulloch AD, Balijepalli RC, Patel HH, Roth DM,"Electrophysiology and metabolism of caveolin-3 over expressing mice", *Bas Res Cardiol* 111:29, 2016. This work is republished with the permission of Springer Publishing. Section 2.3 contains unpublished material being prepared for publication under the title "Long QT Syndrome Associated F97C and S141R Caveolin-3 Mutations Differentially Modulate Kv4 and Cav1.2 Channels Contributing to Action Potential Prolongation" with authors Tyan L, Vincent KP, McCulloch AD, Kamp T, and Balijepalli RC.

Chapter 3

High-order finite element methods for cardiac monodomain simulations

3.1 Introduction

Detailed tissue-scale cardiac electrophysiology simulations are commonly used to investigate the dynamics and mechanisms of arrhythmias [SXS+09, MZY+11, Tra14] and drive electromechanical simulations [CHAS+09] [ASKV+11, NPC+11, Tra11]. Beyond the inherent physiological complexity, these models pose numerous numerical and computational challenges. For example, insufficient spatial resolution can lead to spurious behavior including artifactual breakup of reentrant waves [KSK13], a lack of wavebreak [BOCF08], or pinning of reentrant rotors to the computational grid [FCHE02]. Thus, independent verification of electrophysiology solvers is essential, particularly as models move closer to clinical applications.

Niederer et al. [NKB+11] provided a benchmark model for cardiac monodomain electrophysiology solvers that included anisotropic propagation and realistic human ventricular action potential kinetics. Previous studies had suggested that discretization to a spatial scale of 0.25 mm was sufficient for converged action potential propagation [CF04, XQY+04, CP08]. However, in the community benchmark exercise, none of the solution schemes were converged to within 5% of the consensus total activation time with element edge lengths of 0.2 mm, and many methods, including all solvers using hexahedral element meshes, deviated from the consensus solution by more than 10% at a spatial discretization of 0.1 mm [NKB+11]. This important report suggested that reliable electrophysiology simulations may require more highly refined spatial discretizations than previously thought.

The benchmark exercise also provided insight into the convergence behavior of different numerical schemes. A subsequent investigation identified mass lumping as the primary culprit for underestimated propagation speeds with larger spatial steps or element sizes in several solvers [PBN+12]. Another study identified combinations of lumping schemes and quadrature rules that provided somewhat more accurately converged results with increased computational efficiency [KSK13]. High-order methods have been proposed to take advantage of their potential convergence benefits [ABK12, ABK13, CYK+14]. However, these reports did not evaluate cubic Hermite finite element schemes, which have long been popular for modeling cardiac geometry [NLGSH91], electrophysiology [RM94a] and biomechanics [CHW+96].

Here we use the 2011 benchmark problem and a biventricular model to examine the convergence of a Galerkin finite element formulation of the monodomain problem using three types of elements on hexahedra: tri-linear Lagrange, tri-cubic Hermite,

and new cubic order Hermite-style serendipity elements. The serendipity element has significantly fewer basis functions than the tri-cubic element but still conforms to recent mathematical theory regarding cubic order convergence [AA11, AA14, Gil14].

The convergence of numerical electrophysiology solutions depends not only on element size but also on other properties including the conductivity [PBS93, RM94a] and ion channel kinetics [BVP02]. These intuitive relationships are commonly used to tune conduction velocity [CHR+13] and have been leveraged to reduce computational expense [BVP02]. However, the relationship between these parameters and convergence is not commonly reported. Therefore, we sought a dimensionless parameter that combines these properties into a more appropriate determinate of convergence than line length alone. We found that a version of the Thiele modulus, well known in transport theory as the ratio between the characteristic rates of reaction and diffusion [Thi39, HR14], is a more complete metric to describe discretization error and solution stability in monodomain simulations. Finally, we used this dimensionless number to better define the convergence criteria and compare the relative performance of each basis type for a modeling application where the activation pattern is required and strict numerical convergence is not essential.

3.2 Methods and Models

Governing Equation – the Monodomain Equation

Electrical impulse propagation in the heart is commonly modeled using either the bidomain equation [Tun78] or the monodomain equationn[KS98]. Here, as in Niederer et al. [NKB+11], we consider the monodomain equation. This reaction-

diffusion type parabolic partial differential equation (PDE) is derived from the cable equation and states the conservation of charge. The "reaction" portion of the monodomain equation is a system of ordinary differential equations (ODEs) that represent the flux of ions across the myocyte membrane, and the "diffusion" portion of the monodomain equation is a PDE that represents the spread of current through gap junctions and across cardiac tissue. The monodomain equation is as follows:

$$\chi \left(C_m \frac{\partial u}{\partial t} + I_{ionic}(u) \right) = \nabla \cdot \sigma \nabla u \tag{3.1}$$

where u is the transmembrane potential, σ is the conductivity tensor, I_{ionic} is the current due to the flow of ions through channels in the cell membrane, C_m is the specific capacitance of the cell membrane, and χ is the surface area to volume ratio. I_{ionic} is described by a system of ODEs where the current is a function of the voltage u, channel gating states, and other state variables.

Basis Functions

A Galerking finite element method was used for spatial discretization of the monodomain equation. The convergence of this numerical method with three types of finite element interpolation functions were evaluated: C_0 continuous linear Lagrange interpolation in trilinear hexahedral elements with 8 nodes and 8 degrees of freedom; C_1 continuous cubic Hermite interpolation in tricubic hexahedral elements with 8 nodes and 64 degrees of freedom; and newly derived C_0 continuous cubic Hermite-style "serendipity" interpolation in tricubic Hermite elements that preserve agreement of the partial derivatives along mesh edges with 8 nodes and 32 degrees of freedom.

Serendipity spaces allow for a reduction in the number of degrees of freedom in a finite element problem while retaining the maximum order of convergence under appropriate regularity of the solution. Arnold et al. recently demonstrated that only *superlinear monomials* up to and including the degree p are sufficient conditions for p-order convergence [AA11, AA14]. The superlinear degree of a monomial is its total degree, but ignoring any variables that appear with linear order. More recently, cubic Hermite-style serendipity basis functions were derived [Gil14], which are employed in the current work. The two-dimensional and three-dimensional cubic Hermite-style serendipity basis functions are provided in Supplementary Material. For the quadrilateral element, the number of degrees of freedom is reduced from 16 for bicubic Hermite interpolation to 12 for the bicubic Hermite-style serendipity interpolation; for the hexahedral element, the number is reduced from 64 to 32. For brevity, we will hereafter refer to cubic Hermite-style serendipity basis functions as "serendipity Hermite".

Cell Thiele Modulus

For reaction-diffusion problems, the Thiele modulus, used in chemical engineering, describes the ratio of the rate of reaction to the rate of diffusion [Thi39, HR14]. Analogous to the local or cell Péclet number for advection diffusion problems [BH82, PTH02, Qua09], we define the dimensionless cell Thiele modulus (ϕ_c) as the ratio of the discretization length to the characteristic length of the monodomain equation with the form:

$$\phi_c \equiv h\sqrt{\frac{k}{D}} \tag{3.2}$$

where k is the reaction rate (normalized $\mathrm{dV/dt}_{max}$, defined as $\mathrm{dV/dt}_{max}$ of the single cell ionic model divided the action potential amplitude), h is the mean element edge length, and D is the diffusivity along an eigenaxes of the conductivity tensor. A derivation of the cell Thiele modulus from the non-dimensionalization of the monodomain equation is provided in Supplementary Material .

Solution Scheme

Operator splitting [SLT05] was employed to separate the reaction (ODE) and diffusion (PDE) components of the monodomain equation and solve them in series. The system of ODEs representing the cell ionic model was first updated using a single-iteration backwards Euler solver [Lio10] with a fixed sub-stepping time step of 0.001 ms. The ODEs were evaluated at each Gauss-Legendre quadrature point in the computational mesh, and these calculations were accelerated by solving them on an NVIDIA GPU. The voltages at the quadrature points were then projected onto the basis functions. Thereafter, the coefficients defining the updated nodal voltages and their spatial derivatives were determined by solving the global linear system. A backwards Euler scheme with a fixed time step of 0.01 ms was employed for the PDE, and the linear solver was a conjugate gradient method implemented in PyTrilinos [SSH08] using incomplete LU factorization for the preconditioner. Finally, the updated voltage solution was evaluated at the quadrature points before the next time step. The solver was implemented in the publicly available *Continuity 6*[1] software package, which previously used a collocation finite element method to solve the monodomain equation [RM94a].

[1] www.continuity.ucsd.edu

Meshes and Simulations

Numerical experiments were performed on three test problems. All simulations used the 2006 ten Tusscher cell ionic model [tP06] as described in the benchmark study [NKB+11], except as noted.

The first test problem was the benchmark problem defined by Niederer et al. [NKB+11]. The mesh comprised a 20.0 × 7.0 × 3.0 mm cuboid of simulated cardiac tissue. The conductivity was transversely anisotropic with a conductivity of 0.133 mS/mm in the fiber direction (parallel to the long axis) and 0.0176 mS/mm along the other axes. A stimulus (2 ms at 50,000 μAcm^{-3}) was applied to a 1.5 mm cube in one corner of the mesh. The error in the total activation time was computed from the midpoint of the consensus solution presented by Niederer et al. (42.75 ms).

The second test problem was a simplified version of the 2011 benchmark that produced a planar propagating wavefront. A uniform stimulus (2 ms at 50,000 μAcm^{-3}) was applied to one end of the mesh, and average conduction velocity was measured using the activation times at 20 and 80% along the long axis of the mesh to avoid boundary effects. A series of nested cuboid meshes of the same aspect ratio was used to compare solutions across a large range of element edge lengths (0.05–8.0 mm) and nearly five orders of magnitude in degrees of freedom. This range was not possible by simple refinement of a single mesh. The conduction velocity measured using 0.05 mm cubic Hermite solution was used as the reference solution (0.62 m/s).

Finally, simulations were also performed in a three-dimensional anatomic model of the human ventricles using a previously published human biventricular geometry generated using clinical computed tomography data from a patient with left bundle branch block and dyssynchronous heart failure [VKS+14] . The transversely isotropic

conductivity was 0.0346 mS/mm in the fiber direction and 0.00494 mS/mm in the cross-fiber and sheet directions. A stimulus (2 ms at 50,000 μAcm^{-3}) was applied to a small region on the endocardium of the right ventricular free wall to simulate endocardial pacing.

3.3 Results

Verification of our electrophysiology solver was performed using the benchmark problem. As the mesh was refined and the element edge length decreased, the solutions computed using linear Lagrange, serendipity Hermite, and cubic Hermite basis functions all converged to the consensus solution presented in the benchmark paper (Figure 3.1). At an element edge length of 0.2 mm, the error in the total activation times were 11.5, 4.7, and 1.5% using linear Lagrange, serendipity Hermite, and cubic Hermite elements, respectively. With a 0.1 mm element edge length, the linear Lagrange solver had an error in total activation time of 1.1% and both the serendipity Hermite and cubic Hermite solutions had errors of 0.1% and were within the uncertainty of the consensus solution. All three schemes converged from propagation speeds that were too fast.

Next, the convergence behavior of the three basis types was examined in more detail using the second test problem with planar wavefront propagation. Here, the serendipity Hermite solutions converged with fewer total degrees of freedom than the cubic and linear solutions (Figure 3.2). Solutions using the same number of cubic Hermite and serendipity Hermite elements were almost identical for this test problem.

Since numerical solutions of the monodomain model depend on membrane kinetics and monodomain conductivity as well as spatial discretization, we compared

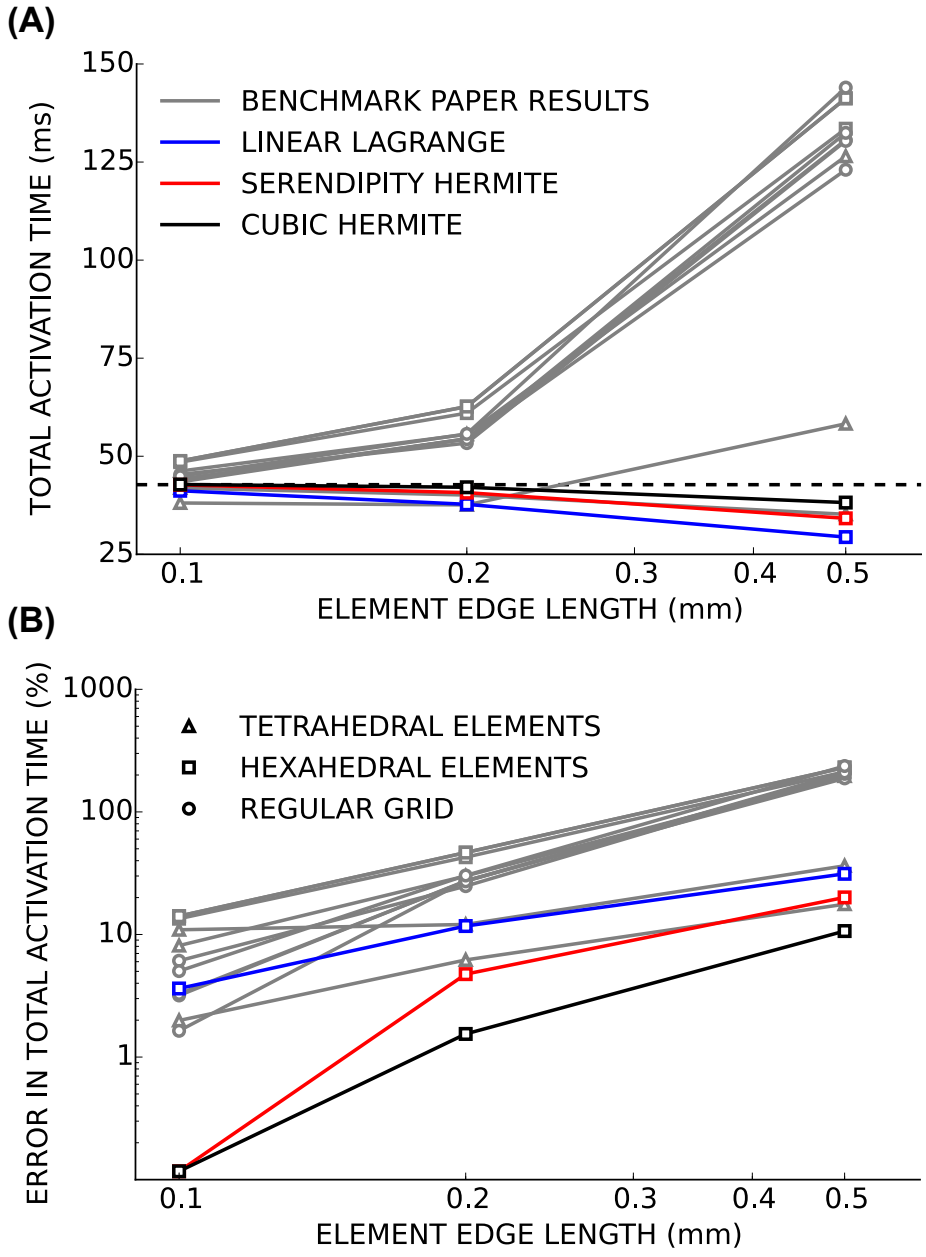

Figure 3.1: **A comparison of the electrophysiology solvers presented in the Niederer benchmark paper.** (A) Total activation time for simulations using cubic Hermite (black), cubic Hermite-style serendipity (red), and linear Lagrange (blue) elements all converge to the consensus total activation time (broken black line) for the cardiac electrophysiology benchmark problem. Gray lines represent solutions from the other solvers presented in Niederer et al. [NKB+11]. Hexahedral (box), tetrahedral (triangle), or regular grid (circle) meshes are indicated by the marker style. In (B) the results are presented as the percent error in the total activation time.

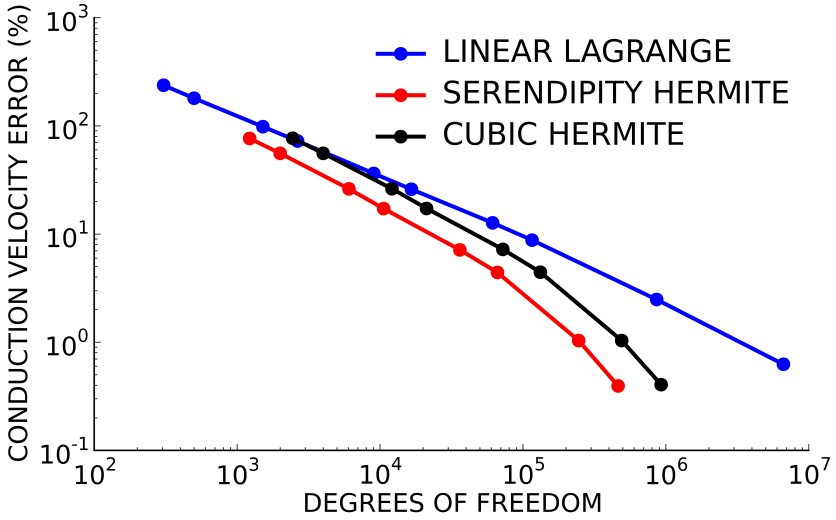

Figure 3.2: **Cubic Hermite-style serendipity elements (red) converge better per degree of freedom than conventional cubic Hermite (black) or linear Lagrange (blue) elements.**

solutions to the second test problem using eight element sizes, three diffusivities (D = 0.0126, 0.0953, and 0.953 mm^2/ms), two ionic models with different membrane kinetics (the ten Tusscher and Panfilov 2006 human ventricular myocyte model [tP06] with a normalized dV/dt_{max} of 2.47 ms^{-1} and the Beeler and Reuter [BR77] ventricular myocyte model with a normalized dV/dt_{max} of 1.38 ms^{-1}). Figure 3.3 demonstrates that the convergence error for these simulations is an almost unique function of cell Thiele modulus for each element type. A cell Thiele Modulus of 1.0 resulted in an error in the conduction velocity of approximately 0.1% with Hermite basis functions compared with 4% with linear Lagrange basis functions.

Non-physiological oscillations were observed in unconverged solutions (Figure 3.4.A). The amplitude of these oscillations, measured as the maximum negative deviation from resting membrane potential before the action potential upstroke, was a function of the cell Thiele modulus (Figure 3.4.B). However, this relationship was

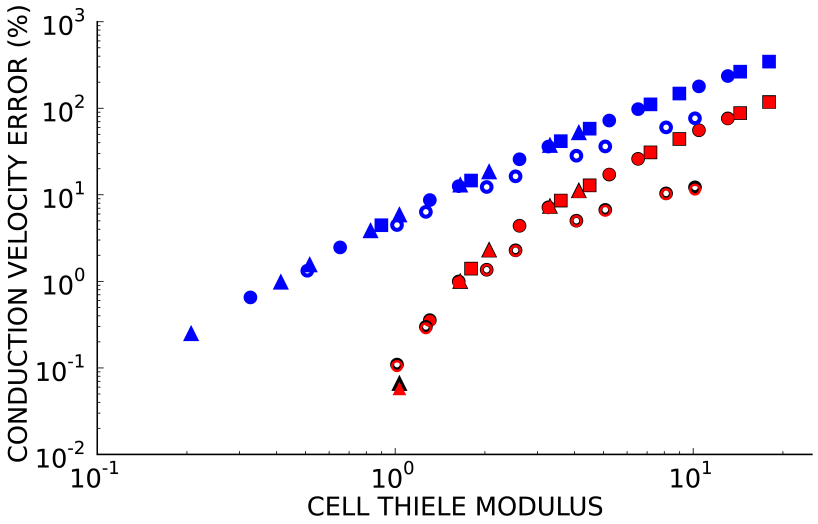

Figure 3.3: **The relationship between cell Thiele modulus and conduction velocity error is nearly constant for each basis function type.** Symbol color indicates interpolation type:cubic Hermite (black), cubic Hermite serendipity (red), and linear Lagrange (blue). Filled symbols represent solutions using the ten Tusscher [tP06] cellular ionic model and open symbols represent solutions using the Beeler-Reuter cellular ionic model [BR77]. Diffusivity is represent by symbol shape: D = 0.0126 mm^2/msec (boxes), D = 0.0953mm^2/msec (circles), D = 0.953mm^2/msec (triangles). Element lengths ranged from 0.05 to 4.0 mm.

much more non-linear than the relationship between conduction velocity error and cell Thiele modulus. The oscillation amplitude decreased sharply to zero around $\phi_c = 4.0$ for the cubic Hermite and serendipity Hermite basis functions and were completely eliminated at $\phi_c \lesssim 1.0$.

Finally, we sought to determine convergence criteria for electrophysiology solutions when only activation patterns rather than absolute conduction times are needed. This need arises commonly in patient-specific modeling, where the total activation time is known (e.g., from a measured QRS duration or electrocardiological mapping), but the conductivity is unknown. Electrical propagation in a patient-derived human biventricular mesh was simulated at four levels of spatial refinement resulting in simulations with an average cell Thiele modulus in the primary direction of propagation of 1.0, 2.0, 4.0, and 8.0 for the four mesh refinements. For this exercise, the simulation using cubic Hermite elements with $\phi_c = 1.0$ was considered fully converged. Activation times in the three less-converged simulations were compared to the converged activation times at node locations from the coarsest mesh (Figure 3.5.A). Since propagation of the high cell Thiele modulus simulations was too fast, the total activation time for those simulations was scaled to give a regression line with a slope of 1.0. The Bland-Altman plot in Figure 3.5.B comparing the scaled activation times and the fully converged activation times identifies a pattern of outliers (> 2 standard deviations) that were too fast compared with the fully converged solution. These outliers were located in the basal right ventricular free wall. The root-mean-squared (RMS) error between fully converged activation pattern and the scaled unconverged activation patterns decreases as the cell Thiele modulus decreases toward 1.0 for all three interpolation methods (Figure 3.5.C). The RMS error was less than 5 ms for all

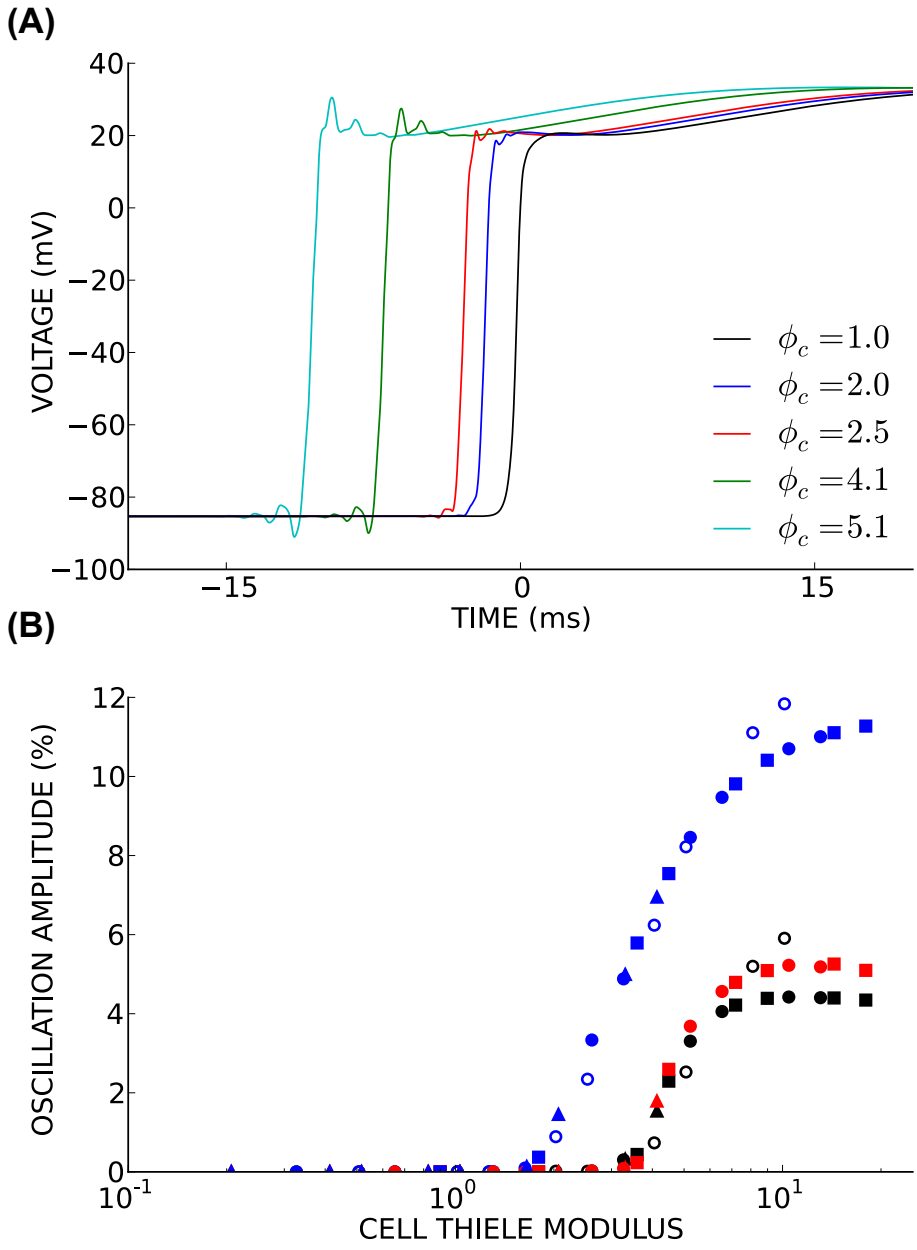

Figure 3.4: **Non-physiological oscillations were seen in unconverged solutions.** (A) Here t = 0ms is set to the activation time of the fully converged ($\phi_c = 1.0$) solution. (B) The amplitude of these oscillations is a function of the cell Thiele modulus. Symbol color indicates element type: cubic Hermite (black), cubic Hermite-style serendipity (red), and linear Lagrange (blue). Filled symbols represent solutions using the ten Tusscher [tP06] cellular ionic model and open symbols represent solutions using the Beeler-Reuter cellular ionic model [BR77]. Diffusivity is represent by symbol shape: D = 0.0126 mm^2/msec (boxes)), D = 0.0953mm^2/msec (circles), D = 0.953mm^2/msec (triangles). Element lengths ranged from 0.05 to 4.0 mm.

unconverged simulations and twice the RMS error was less than 5 ms for the $\phi_c = 2.0$ and $\phi_c = 4.0$ simulations with cubic Hermite elements, the $\phi_c = 2.0$ and $\phi_c = 1.0$ simulations with serendipity Hermite elements, and the $\phi_c = 1.0$ simulation with the linear Lagrange elements. This error is comparable to the lowest uncertainly in clinically measured activation times[GBGS$^+$11, VKS$^+$14]. Figure 3.5.D demonstrates that the high-order methods also have smaller RMS error than the linear elements on a degree of freedom basis.

3.4 Discussion

The above results are in agreement with previous studies demonstrating higher convergence rates with cubic Hermite and other high-order basis functions [RCM97, ABK12, CYK$^+$14] . The application of cubic Hermite-style serendipity basis functions and the cell Thiele modulus to the cardiac electrophysiology problem are, to our knowledge, novel contributions.

The solutions to the cardiac electrophysiology benchmark problem converged to the consensus total activation time and compare favorably to the other solvers reported by Niederer et al. [NKB$^+$11]. The behavior of the linear Lagrange solution suggests the convergence of hexahedral element meshes is not limited by their element choice. The slow conduction velocities exhibited at larger spatial scales by all of the solvers using hexahedral element meshes in the Niederer et al. paper were likely due to their choice of mass lumping as suggested by Pathmanathan et al. [PBN$^+$12] , and not the type of element. Solutions obtained using cubic Hermite and serendipity Hermite basis functions had substantially less error in total activation time at the same spatial discretization compared with our linear Lagrange solution and with solutions from the

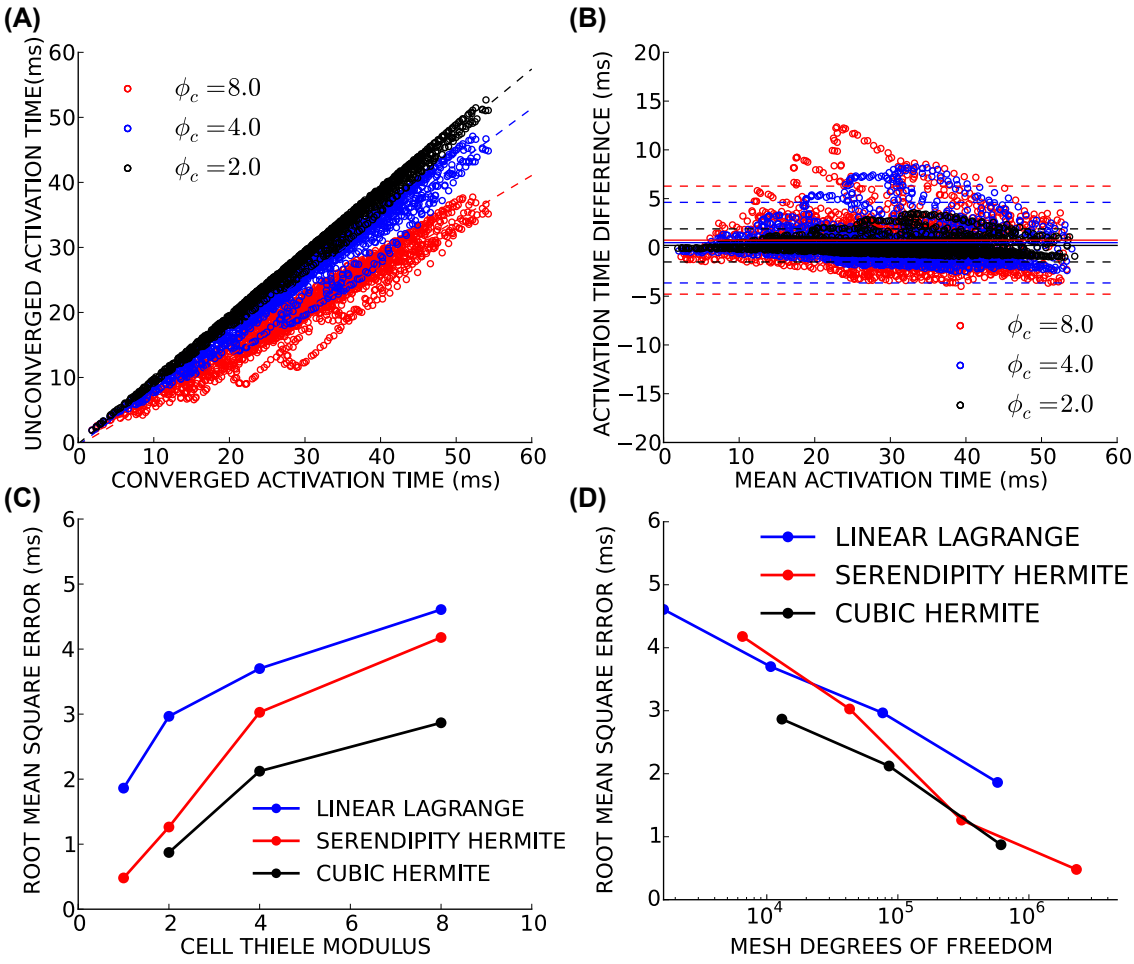

Figure 3.5: **Convergence results on a physiological mesh.** (A) Activation times from three unconverged electrophysiology simulations using cubic Hermite elements (black, $\phi_c = 2.0$; blue, $\phi_c = 4.0$; and red, $\phi_c = 8.0$) are plotted against activation times at the same location on the mesh of a converged ($\phi_c = 1.0$) reference solution. Regression lines are shown for each unconverged solution as a broken line. The activation times in the unconverged location were scaled so that regression line had a slope of 1.0. (B) These scaled activation times are compared with the converged activation times using a Bland-Altman plot where solid lines represent the mean difference between the two solutions and the broken lines are two standard deviations in the residuals from the regression line. (C) The root mean squared (RMS) error between the unconverged and fully converged activation patterns decreases with the cell Thiele modulus of the simulation. (D) The high-order methods have a smaller RMS error compared to the linear method on a degree of freedom basis particularly as the size of the problem increases.

solvers tested by Niederer et al. [NKB+11]. At 0.5 mm element size, Hermite solutions were as close to the consensus solution as most of the other solvers achieved at 0.1 mm discretization. This is unsurprising due to their additional degrees of freedom, but it also suggests that the 0.1 mm element edge length recommended by the benchmark exercise may be an overly stringent criterion. Results from Krishnamoorthi et al. [KSK13] suggest that our choice to integrate the cell ionic model at the Gauss-Legendre points (as opposed to at the nodes) was responsible for fast conduction in unconverged solutions in contrast to most of the solvers used in the benchmarking exercise.

A direct comparison of the three element types demonstrated that solutions using serendipity Hermite basis function have a convergence advantage per degree of freedom compared with linear Lagrange and cubic Hermite elements. These new cubic Hermite-style serendipity methods, applied to the cardiac electrophysiology problem for the first time here, balance the convergence benefits of high-order interpolation with lower computational demands.

Discussions of convergence criteria in cardiac electrophysiology simulations have focused on the element edge lengths [RM94a, CP08, NKB+11] despite a well-known dependence of the solutions on the conductivity[PBS93] [CHR+13] (Pollard et al., 1993; Rogers et al., 1997; Costa et al., 2013) and the stiffness of the cellular ODE model [BVP02] . We have introduced a new dimensionless parameter analogous to the Thiele modulus from mass transport theory that can be used to specify convergence criteria. The cell Thiele modulus compares the discretization length to the characteristic length of the monodomain equation. The characteristic length of the monodomain equation is the square root of reaction rate over the diffusivity (see Supplementary Material). For simplified ionic currents where the reaction rate is clearly defined (i.e., the bistable

equation where the ionic model is a cubic function), the characteristic length is the width of the propagating wavefront. Rescaling the non-linear ionic current component monodomain equation is more complex with a realistic cellular model, and we have defined the rate of reaction as the normalized $\mathrm{dV/dt}_{max}$ of the ionic model with units of ms^{-1}. Alternatively, the reaction rate could be selected as the maximum time-varying conductance of the fast sodium channel ($g_{na}(u)$; units of pS/nF or equivalently ms^{-1}). This would shift the cell Thiele modulus results but not change the relationship as $\mathrm{dV/dt}_{max}$ and $g_{na}(u)_{max}$ are closely related. The components of this metric are often reported in papers, but in isolation they provide an incomplete description of the convergence. The cell Thiele modulus is more complete measure of the numerical convergence and stability.

We demonstrated that the cell Thiele modulus is proportional to the wave speed error and can be used to determine the presence of non-physiological oscillations in poorly converged solutions. The sharp decrease in oscillation amplitude with decreasing cell Thiele modulus and the corresponding low wave speed errors suggest that a lack of oscillations is a good criterion for convergence. The oscillations are a manifestation of the Gibbs phenomenon [GS97]. Methods to eliminate these oscillations include mass lumping and modified ODE integration schemes [TZMSS14] . It has been suggested that these methods may not improve the underlying numerical stability of the solutions [GL81]. The cell Thiele modulus threshold where oscillations disappear is dependent on the order of the solution scheme. Our results suggest that a cell Thiele modulus of 3.0 is a reliable convergence and stability criterion when using the Hermite and serendipity Hermite elements and a cell Thiele modulus of 1.0 is sufficient for linear Lagrange elements. Additionally, by quantifying the discretization error and

solution stability (i.e., the presence or absence of oscillations), the cell Thiele modulus could provide reasonable bounds during parameterization or optimization and could help guide adaptive schemes especially in the presence or anisotropic conduction or heterogeneous conductivities.

The small spatial discretization often cited for fully converged solutions can become computationally limiting particularly for applications such as patient-specific modeling [VKS+14], that may necessitate parameter optimizations requiring hundreds or thousands of simulations. In these problems the total activation time is known whereas the conductivity is typically unknown and the available data may be too limited to allow highly detailed representations of the conducting system, ionic currents or tissue microstructure. We found that fully converged electrophysiology solutions were not required to obtain activation patterns to within clinically practical tolerances when the total activation time was known. For test simulations in a human biventricular model, activation patterns with RMS errors less than 2.5 ms were obtained using a cell Thiele modulus as high as 4.0 with cubic Hermite elements. The greatest errors were found on the basal right ventricular free wall where activation was mainly due to crossfiber conduction.

The simulations run at a high cell Thiele modulus can provide a reliable activation pattern but cannot guarantee biophysical fidelity due to the presence of oscillations. The utility of such simulations is therefore limited to applications such as the one described above where only the activation pattern is required. Other computational approaches to determine activation patterns, such as eikonal methods [PTH02], could be considered for this application. However, the monodomain solutions may be preferred especially if they are part of a coarse grain parameter optimization for

subsequent fine grain simulations. Finally, the specific solution scheme presented here may not be optimal for conduction velocity tuning schemes as increased discretization error speeds up propagation necessitating decreased conductivities, and decreasing the conductivity to account for fast conduction will further increase the cell Thiele modulus

Limitations

The above results compare the numerical convergence for an electrophysiology solver using different basis functions. However, the rate of numerical convergence is not the only consideration when comparing solution schemes. High-order Hermite methods are necessarily more complex to implement, and the optimal selection of a preconditioner for the linear system arising from the use of high-order methods is a long-standing issue in numerical analysis due to the poor condition number (relative to linear methods). The generation of high quality cubic Hermite hexahedral meshes for cardiac geometries from medical imaging data is a challenging problem and the resulting workflows may be more complex than automated methods for linear tetrahedral meshes [ZLM$^+$12, GSK$^+$13]. Simulation time is also an important consideration, particularly for clinical applications. However, solution times are dependent on hardware, code optimization and architecture. The accuracy and stability of a numerical scheme as presented here on a degree of freedom basis is independent of the performance of a specific solver. Finally, as discussed in Costa et al. [CHR$^+$13] , uncertainties introduced by numerical error may be minimal relative to the uncertainties in the parameterization of the models from physiological data. However, numerical error is problematic in biophysically detailed studies, as instabilities (i.e., the oscillations

observed in Figure 3.4) will alter the cellular dynamics.

3.5 Conclusions

The current analysis demonstrates that very small spatial discretizations (0.1 mm) are not necessarily required for well converged cardiac electrophysiology simulations under a variety of conditions. High-order cubic Hermite and cubic Hermite-style serendipity elements reached converged solutions with fewer degrees of freedom and longer element edge lengths than traditional linear elements. We suggest that since convergence also depends on membrane kinetics and conductivity parameters, the cell Thiele modulus is a more useful metric for determining solution convergence than element size alone. Finally, we found that clinically useful activation patterns can be obtained from cardiac electrophysiology solutions that are not close to being fully converged in situations such as patient-specific modeling where the total activation time is known a priori.

3.6 Acknowledgements

This work was supported by the National Institutes of Health (1R01 HL105242, 1R01 HL96544, 8 P41 GM103426, P50 GM094503, and 1R01 HL121754), NIH predoctoral training grants (T32 EB009380 and T32 HL105373), and the National Science Foundation (DMS Award 0715146, DMS Award 1318480, and Graduate Fellowship DGE-1144086). SP was supported by the ERC Advanced Grant Mathcard (227058).

The content of this chapter is, in full, a reprint of a previously published manuscript with minor edits to fit the format of this dissertation. The citation is

Vincent KP, Gonzales MJ, Gillette AK, Villongco CT, Pezzuto S, Omens JH, Holst MJ, McCulloch AD, "High-order finite element methods for cardiac monodomain simulations", *Front Physiol*, 6:217, 2015. This paper was published with a Creative Commons Attribution License. The dissertation author was the primary author of this paper.

The three-dimensional cubic Hermite-style serendipity basis functions are provided below for parametric coordinates ξ_1, ξ_2, and ξ_3 each on the interval [0,1]

3.7 Appendix I

Below is a derivation of the cell Thiele modulus by non-dimensionalization of the monodomain equation. We begin with the monodomain equation:

$$\chi\left(C_m\frac{\partial u}{\partial t}+I_{ionic}(u)\right)=\frac{\partial}{\partial x}\left(\boldsymbol{\sigma}\frac{\partial u}{\partial x}\right) \tag{3.3}$$

We then scale the monodomain equation by the characteristic time, τ_m, and characteristic length, λ_m:

$$t\rightarrow\frac{t}{\tau_m} \tag{3.4}$$

$$\frac{\partial u}{\partial t}\rightarrow\frac{1}{\tau_m}\frac{\partial u}{\partial t} \tag{3.5}$$

$$x\rightarrow\frac{x}{\lambda_m} \tag{3.6}$$

$$\frac{\partial^2 u}{\partial x^2}\rightarrow\frac{1}{\lambda_m}\frac{\partial^2 u}{\partial x^2} \tag{3.7}$$

Replacing the nonlinear ionic current term with a normalized current term,

$f(u)$, and the maximum rate of reaction, k.

$$I_{ionic}(u) = kf(u) \tag{3.8}$$

and substituting back into the monodomain equation we obtain:

$$\frac{1}{k\tau_m}\frac{\partial u}{\partial t} + f(u) = \frac{1}{kC_m\chi\lambda_m^2}\boldsymbol{\sigma}\frac{\partial^2 u}{\partial x^2} \tag{3.9}$$

The conductivity tensor can be replaced by the diffusivity in direction of wave propogation, D.

$$D = \frac{1}{C_m\chi}\boldsymbol{\sigma n}\cdot\boldsymbol{n} \tag{3.10}$$

The characteristic time constant and characteristic length constant can then be selected to nondimensionalize the monodomain equation.

$$\tau_m = \frac{1}{k} \tag{3.11}$$

$$\lambda_m = \sqrt{\frac{D}{k}} \tag{3.12}$$

$$\frac{\partial u}{\partial t} + f(u) = \frac{\partial^2 u}{\partial x^2} \tag{3.13}$$

Finally, we define the cell Thiele modulus as the ratio of the discretization length, h, to the characteristic length.

$$\phi_c \equiv \frac{h}{\lambda_m} = h\sqrt{\frac{k}{D}} \tag{3.14}$$

Chapter 4

Structural contributions to fibrillatory rotors in a patient-derived computational model of the atria

4.1 Introduction

The mechanisms by which atrial fibrillation (AF) initiates, sustains, and can be eliminated have been the subject of extensive investigation[SVKG11, Jal11, TDI09]. The local source hypothesis attributes persistent and permanent AF to a small number of sources including reentrant rotors or focal beats [Jal03, PJ13]. Recent computational mapping studies have revealed rotors or focal drivers in nearly all patients with wide presentations of AF [NKR12, NKS$^+$12], in multicentre studies of Focal Impulse and Rotor Mapping (FIRM)[SEH$^+$12, MKS$^+$14]. Although such AF rotors precess in

limited spatial areas for prolonged periods of time[NKER12, NSK$^+$13], the conditions that permit such precession (minimal meander) are unclear. Clinical observations suggest that rotors may preferentially locate to discontinuities in the fibre architecture, particularly in the right atrium [KOK$^+$98, SQAC$^+$02], and recent clinical studies show that human atria exhibit considerable fibrosis and scar outside the pulmonary veins that may contribute to the mechanisms for AF in many patients [MWH$^+$14].

Here we use a computational model to examine rotor behaviour in a realistic human atrial geometry. We demonstrate that meandering rotors can become transiently or permanently trapped by abrupt discontinuities in the fibre architecture. Furthermore, modelling of progressively larger regions of inexcitable tissue near the rotor core at the fibre discontinuity to simulate fibrosis or scar can anchor a meandering rotor, converting fibrillation to excitable gap reentry (macro-reentry). Macro-reentry may then terminate via established approaches including invasion of the excitable gap by external waves.

4.2 Methods

A male patient with a history of persistent AF was referred to the VA San Diego Healthcare System. He gave informed consent to participate in an Institutional Review Board-approved research study. He underwent a computed tomography (CT) study to evaluate atrial structure. At electrophysiology study, he underwent FIRM mapping, which uses phase-based algorithms to identify sources during AF (Topera, Inc.) [NKR12]. Focal Impulse and Rotor Mapping maps indicated a rotor in the lateral right atrial wall and a concurrent left atrial focal source (Figure 4.1), as previously reported [NKC$^+$13].

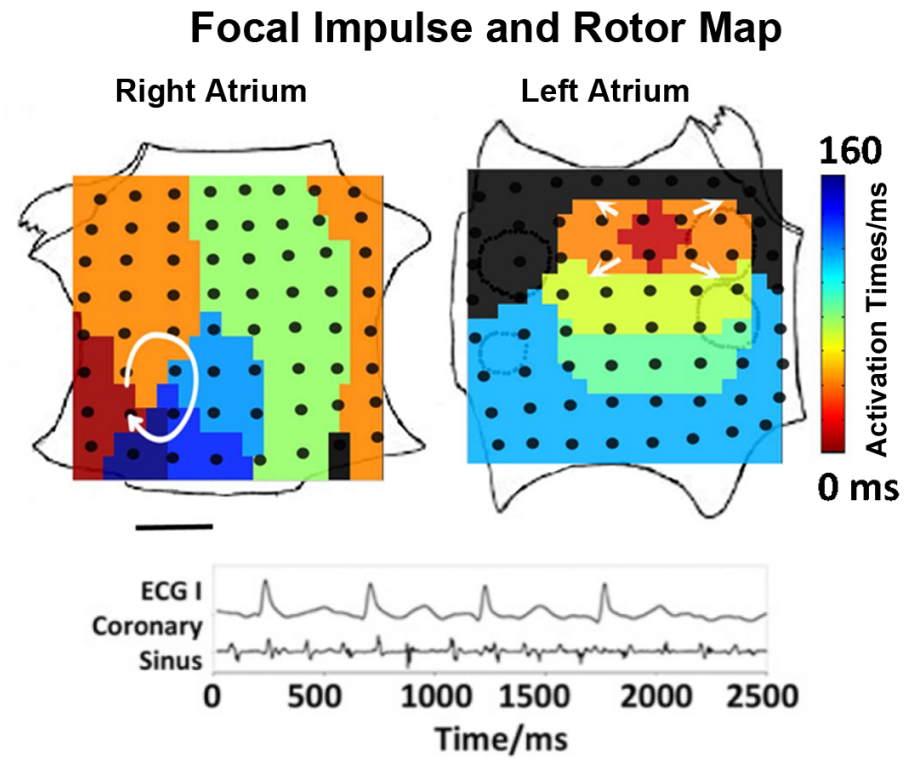

Figure 4.1: **Example of focal impulse and rotor mapping (FIRM)** reveals two independent sources: an AF rotor in an unconventional lateral RA location and a concurrent left atrial focal source. Orientation right atrium: Top, superior vena cava; Left, lateral tricuspid. Left atrium: Top, superior mitral annulus. AF rotor in lateral RA on patient-specific electroanatomic shell. The right atrial AF rotor was the basis for subsequent modeling. Modified from Narayan et al. [NKS+12]

The CT images, combined with consensus literature fibre orientations and regional wall thicknesses, were used to construct a one element thick tricubic Hermite finite element model as described previously [GSK+13]. This three-dimensional biatrial model was used for Galerkin finite element simulations of the monodomain equation using high-order cubic Hermite basis functions for the geometric and dependent variables. The electrophysiology model had 19 359 nodes, 154 872 degrees of freedom, and a mean element edge length of 1.9 mm. Operator splitting was used to simplify calculations, and a time step of 0.1 ms was used to solve the partial differential equation while the ordinary differential equations corresponding to the cellular ionic model were solved with a time step of 0.01 ms. Conductivities spanning two orders of magnitudes have been used to simulate electrical propagation in the atria; in the present work, the specific conductivity tensor was transversely isotropic with components: $D_{fibre} = 0.9$ mm^2/ms, and $D_{cross-fibre} = 0.1$ mm^2/ms for normal atrial propagation and $D_{fibre} = 0.4$ mm^2/ms, and $D_{cross-fibre} = 0.1$ mm^2/ms to account for decreased anisotropy of conduction seen with pathological remodelling during AF [KKS+02]. Point stimulus in the region of the sinoatrial node with these diffusivities gave rise to a total biatrial activation time of ∼130 ms with the Fenton–Karma ionic model (typical p-wave durations are 80 ms, and customarily are longer in patients with atrial enlargement, as is the case here). The total activation time differed by $< 5\%$ from the total activation time computed using a more refined model (114 670 nodes, 919 760 degrees of freedom). In a simple cuboid mesh with the same ionic model and conductivity parameters as the atrial electrophysiology simulations, the conduction velocity measured when the mesh was discretized to the same mean element edge length as the atrial model were within 0.5% of the

converged conduction velocity measured using a 0.1-mm element edge length. The base parameter set used for the Fenton–Karma model was parameter set 1 in Fenton et al [FK98]. The excitability value of the model could be adjusted by the parameter $\overline{g_{fi}}$—increasing (decreasing) excitability also caused the action potential duration to increase (decrease) by increasing (decreasing) magnitude of the fast inward current. The value used for $\overline{g_{fi}}$ was 2.95, except as noted because this gave rise to reentrant rotors with frequency approximately equal to that observed of the reentrant rotors in the patient (5 Hz). Action potential morphology (Figure 4.5.C) was dependent both on the ionic model parameters (e.g. $\overline{g_{fi}}$) and the source-sink relationship along the rotor. In the simulations below, rotors were initialized with broken waves by depolarizing a line of tissue and altering the initial conditions on one side of the stimulus to make that region refractory [RM94b]. Structural remodelling (fibrosis and scarring) was simulated by decreasing the excitability in the scar region to zero and setting the diffusivities to one-tenth of their original value. Finally, it should also be noted that the atrial model is static–i.e. its mechanics are not being considered.

4.3 Results

The computational model of action potential propagation on a realistic human atrial geometry was first used to investigate how normal physiology in the atria (vs. pathologic remodelling) might prevent a broken wave from stabilizing as a rotor. With normal cellular excitability, action potential duration (APD), conduction velocity and conduction anisotropy, a broken wave on the lateral wall of the right atrium was unable to sustain a rotor. Images from a representative simulation are presented in Figure 4.2.A. Owing to the extended wave tail of the physiological action potential, the

wavefront collided with the refractory wavetail causing it to extinguish. Even with an inexcitable region about which to rotate (data not shown), normal myocyte properties prevented a localized source from forming. An anisotropy ratio of nine still prevented the broken wave from sustaining a rotor (Figure 4.2.B) despite shortening the APD and effective refractory period (ERP) to broadly simulate the cellular remodelling seen in AF. Subsequent simulations all used an anisotropy ratio of four and reduced $\overline{g_{fi}}$ to emulate AF remodelling as these parameters consistently maintained rotors (Figure 4.2.C). Importantly, the conduction velocity in the primary fibre direction was reduced by 47% with these modified parameters.

In Figure 4.2.C, a rotor initiated with a broken wave drifted towards the tricuspid valve orifice. The circumferential fibres about the orifice did not allow the spiral to continue rightward and annihilate at the valve orifice but instead pulled the spiral away from the boundary and allowed it to pivot back towards the fibre discontinuity and become transiently attached at the interface between the adjacent fibre regions (continued in Figure 4.3.A). The rotor continued to meander in the superior–inferior direction for the remainder of the 5 s simulation (Figure 4.3.B), similar to the behaviour observed clinically in this patient (Figure 4.1). In simulations lacking this fibre discontinuity (not shown), the rotor did not become transiently fixed to this region, and instead meandered to the posterior right atrium.

Rotors that meandered to the posterior right atrium were often trapped near the crista terminalis. Figure 4.4 depicts two rotors that meandered across the posterior right atrium and became trapped by the abrupt change in the fibre architecture and wall thickness at the crista terminalis. The counter-clockwise rotor in Figure 4.4.A was confined to the discontinuity near the superior vena cava for 2000 ms before precessing

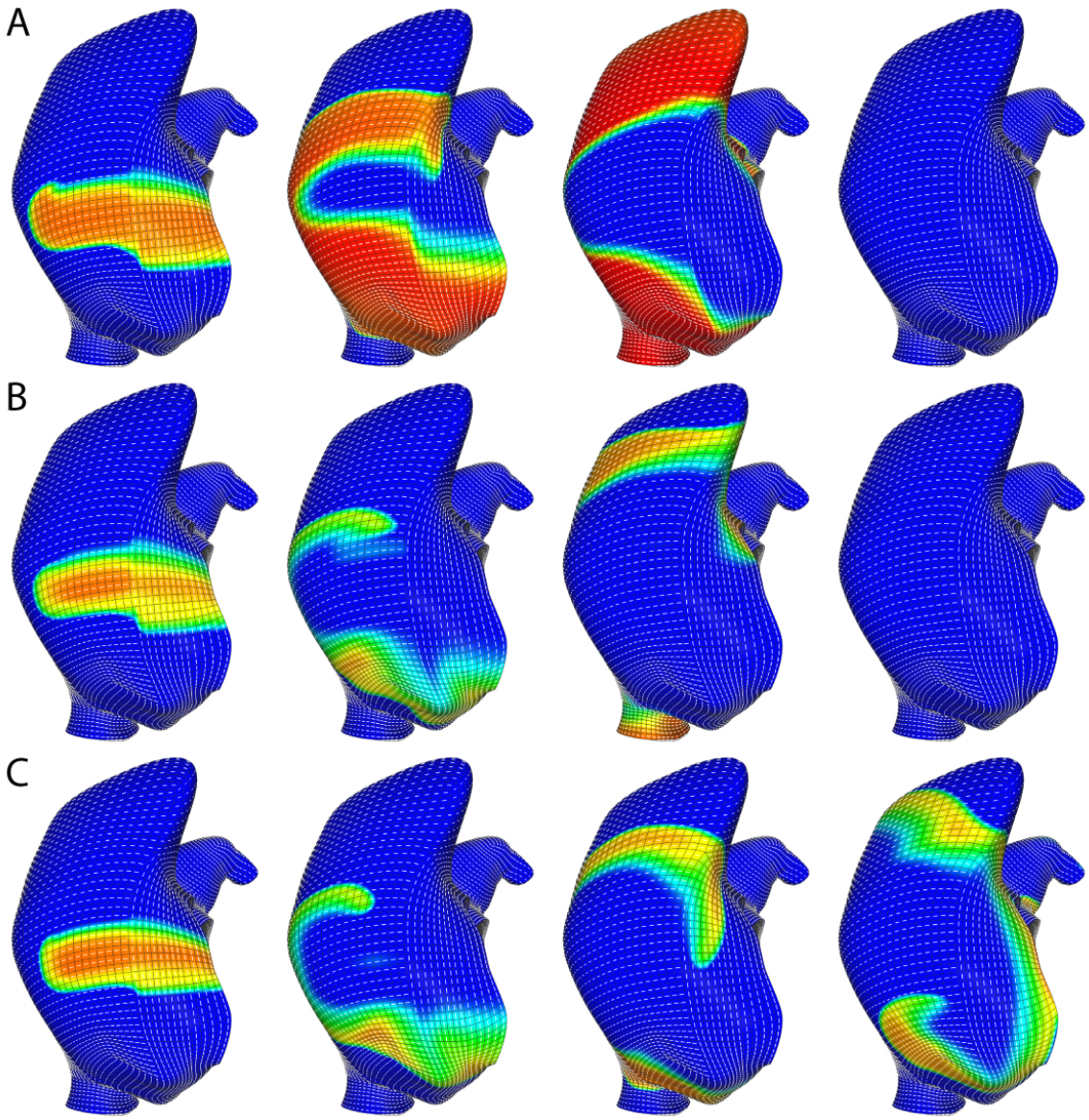

Figure 4.2: **Action potential duration, effective refractory period, and conduction anisotropy all protect normal atrial tissue from sustaining a rotor from a broken wave on the lateral wall of the right atrium.** (A) With healthy atrial parameters the broken wave runs into its wave tail. The normal atrial action potential has an extended repolarization phase (phase 3), which prohibits formation of reentry, especially at resting activation rates. (B) Despite decreased APD, an anisotropy ratio of nine still prevents the broken wave sustaining a rotor. (C) Decreasing cellular APD together with a decreased anisotropy ratio of four readily permits rotor maintenance. Red and yellow regions are depolarized cardiac tissue while blue regions are quiescent. Orientation: lateral right atrial view; Top, superior vena cava; Right, lateral tricuspid.

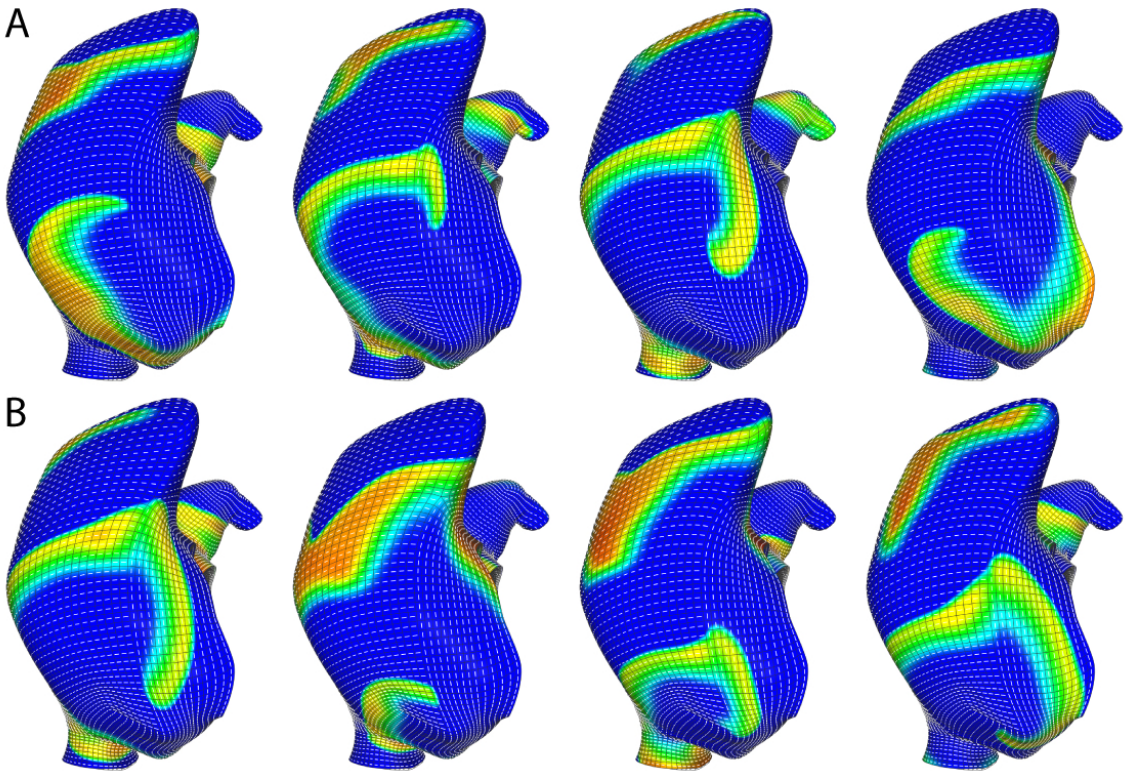

Figure 4.3: **Fiber discontinuities help to stabilize a meandering rotor.** (A) A broken wave on the lateral wall of the right atrium sustains a rotor. After briefly meandering towards the posterior RA, the rotor was pulled to the fiber discontinuity surrounding the tricuspid valve annulus. (B) The rotor precessed inferiorly along the fiber discontinuity and anchoring transiently to it repeatedly for the remainder of the five-second simulation. Orientation: lateral right atrial view; Top, superior vena cava; Right, lateral tricuspid.

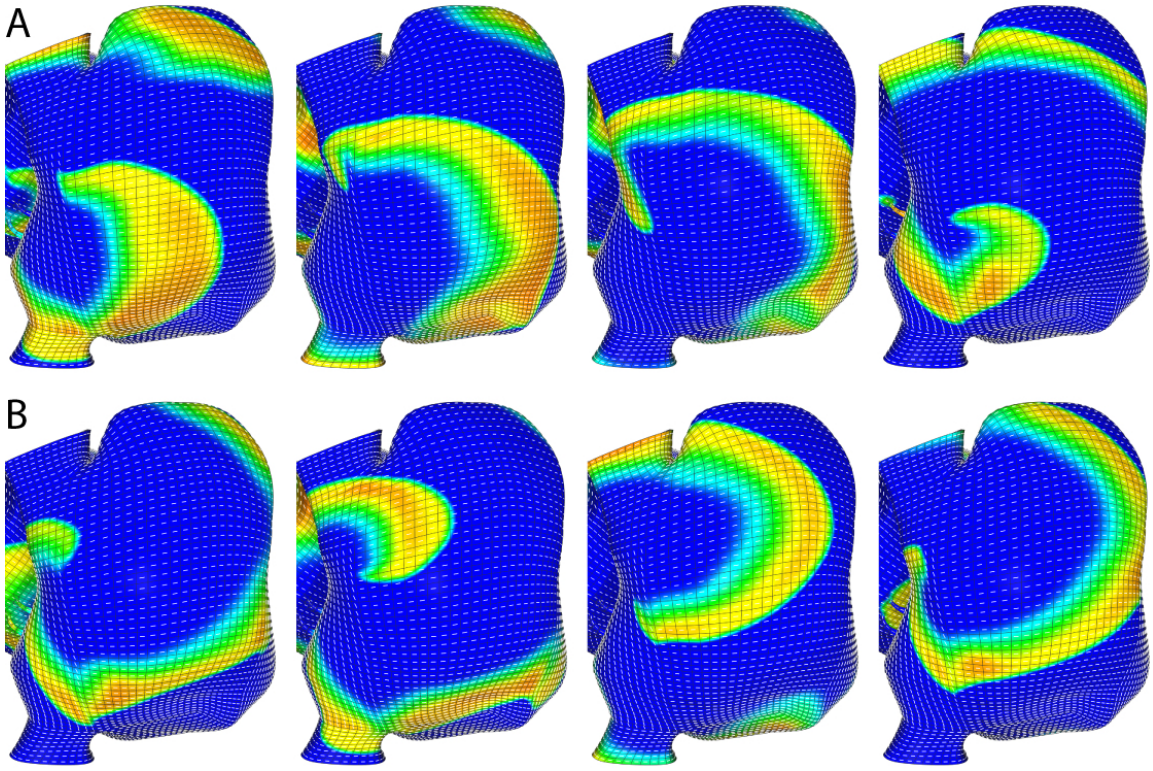

Figure 4.4: **Fiber discontinuities can trap a meandering rotor.** Rotors drifting across the posterior right atrium were pulled to the fiber discontinuity at the crista terminalis. (A) A couter-clockwise rotor became trapped by the fiber discontinuity for ∼2000 ms before precessing inferiorly along the crista terminalis. (B) A clockwise rotor became trapped by the fiber discontinuity and remained there for the remainder of the five-second simulation. Orientation: posterior right atrial view; Top, superior vena cava; Right, lateral right atrium

inferiorly along the crista terminalis (Figure 4.4.C). A rotor with the opposite chirality (Figure 4.4.B) became permanently affixed to this region. Interestingly, the counter-clockwise rotor had a smaller precession area than the trapped clockwise rotor.

The impact of structural remodelling was now simulated by placing inexcitable scar near the rotor core at the fibre discontinuity. After adding a scar near the tricuspid valve annulus, the rotor meandered about the scar initially before converting to stable macro-reentry about the inexcitable region (Figure 4.5). Broadly, the AF remodelling parameters allowed a fibrillatory rotor to readily attach to inexcitable

regions, causing conversion to stable excitable gap reentry or macro-reentry. Increasing the size of the scar increased the path length for reentry and decreased its rotational frequency (Figure 4.5.B). Similarly, the AF rotor near the crista terminalis became fixed to simulated dense scar (Figure 4.6), again converting it to excitable gap reentry. Again, increasing the size of the scar decreased the rotational frequency of the rotor. Decreasing the frequency of the rotor increased its spatially excitable gap. In Figure 4.6, an external wave invaded the excitable gap and displaced reentry away from its fixed location.

4.4 Discussion

This study provides insights into the relatively stable, precessing rotors recently described during human AF in multicentre clinical studies. Our observations emphasize the potential importance of structural features of the myocardium in rotor dynamics, by showing that discontinuities in the fibre architecture and inexcitable regions can constrain rotors transiently or persistently. Moreover, structural remodelling in the form of scar or fibrosis near the centre of the rotor core can convert fibrillation to excitable-gap reentry, which can be terminated.

The normal atria may be protected from AF by all of the following: the absence of triggers, although recently challenged by data suggesting that triggers may exist for decades in patients without clinical AF [DVM$^+$13], the unlikelihood of wavebreak due to protective conduction or repolarization dynamics [NKKR08, NFC$^+$11, LSG$^+$12], and the absence of substrates for rotor maintenance or attachment. Our modelling results support two protective mechanisms in the normal atria. First, the prolonged spatial wavetail of an action potential in a normal atrial myocyte may prevent reentrant

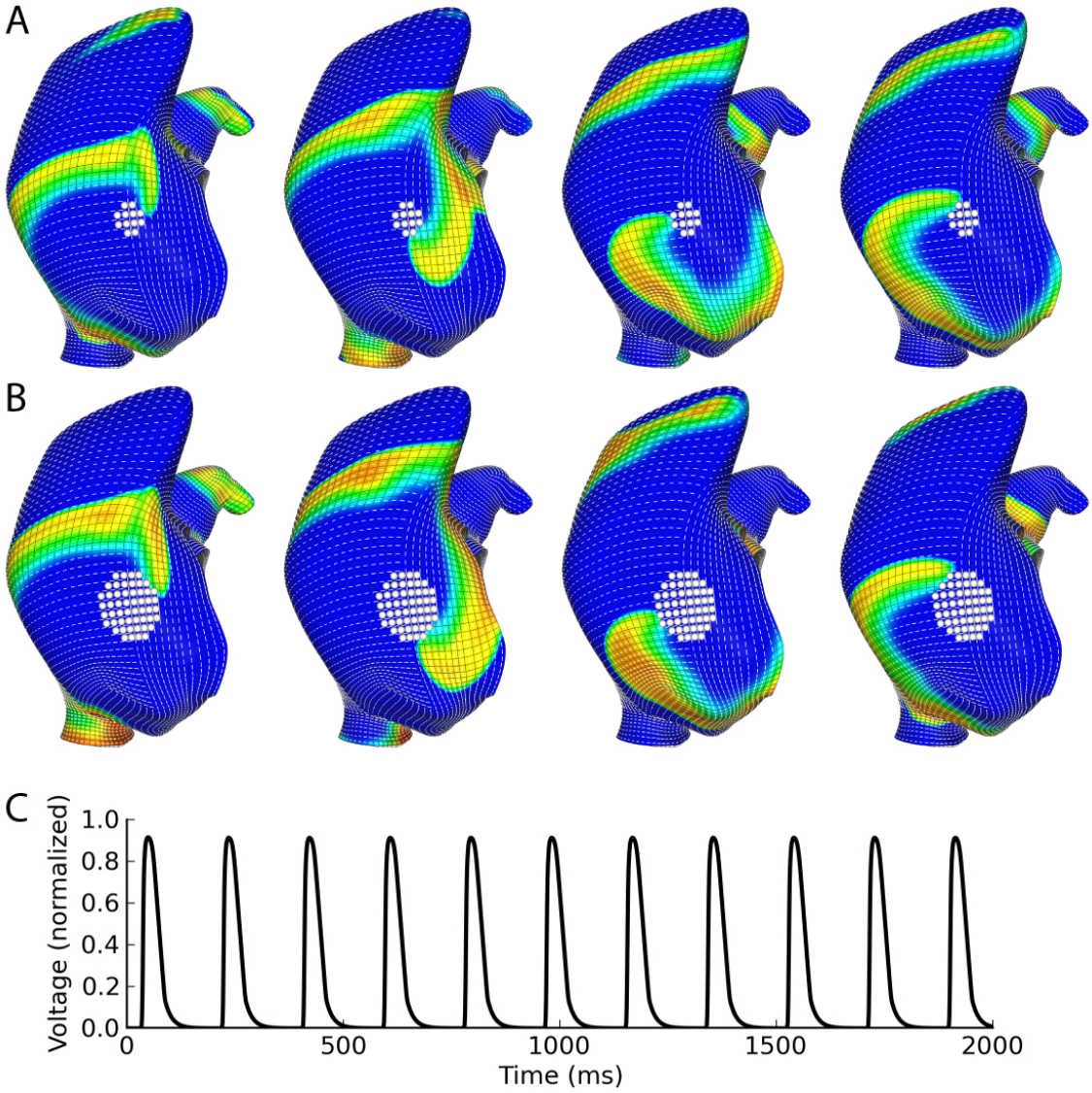

Figure 4.5: **Structural remodeling (fibrosis, scar) simulated by placing an inexcitable region near the rotor core trapped the meandering rotor from Figure 4.3 and converted it to stable macro-reentry.** In (A) the rotor initially meanders around the inexcitable region and eventually becomes trapped indefinitely. This small scar area increased the rotational frequency of the rotor to 8.5 Hz. Increasing scar area (B) decreased its rotational frequency to 5.5 Hz. Decreasing the frequency also increased the spatially excitable gap. Panel (C) demonstrates the action potential morphology for a location between the inexcitable region and the tricuspid valve annulus in (B). Orientation: lateral right atrial view; Top, superior vena cava; Right, lateral tricuspid.

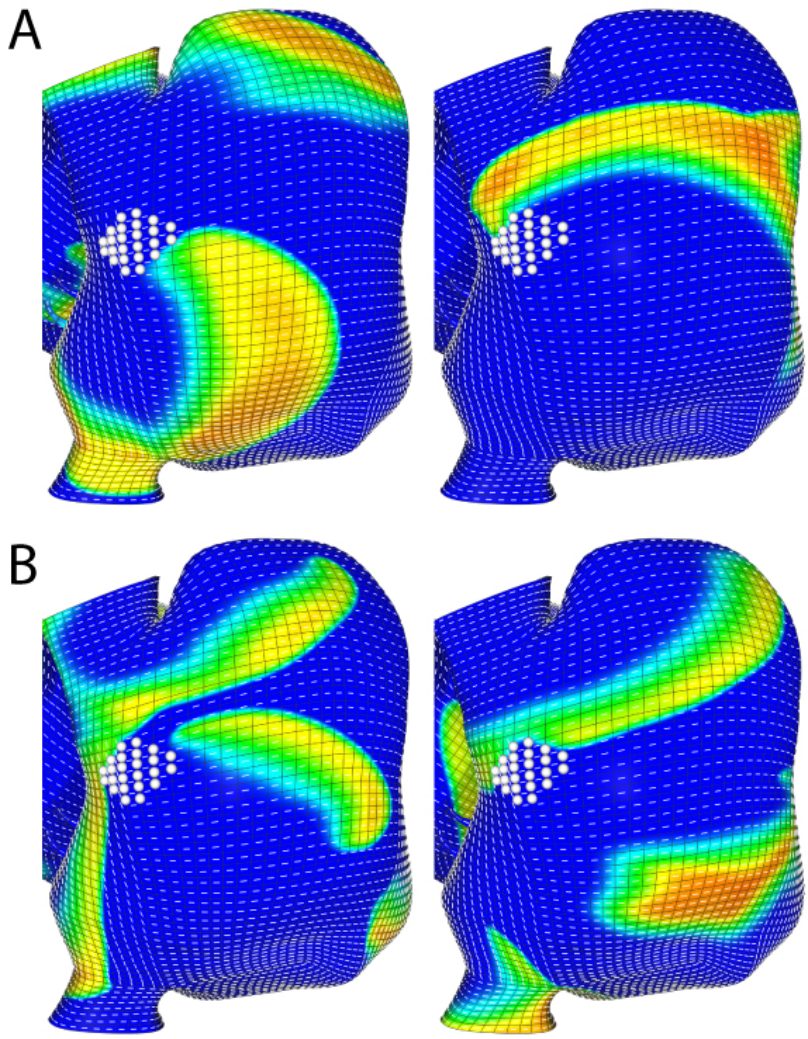

Figure 4.6: **Structural remodeling (fibrosis) near the crista terminalis altered reentry dynamics and resulted in the rotor being displaced.** (A) The rotor displaced from the fiber discontinuity and attached to the scar, with decreasing rotational frequency as in Figure 4.5. (B) The increased spatially excitable gap permits a wave (driven by more rapid activity originating in the left atrium) to impinge on the rotor core. Eventually the rotor is displaced by the invading wavefront suggesting that regions of fibrosis may enable the localized source to convert to macro-reentry with an excitable gap. Orientation: posterior right atrial view; Top, superior vena cava; Right, lateral right atrium

rotor formation by causing conduction block and propagation failure when a broken wave is pivoting (Figure 4.2.A) or in the process of anchoring about an inexcitable region.

It is well known that ionic current remodelling promotes AF. Ionic currents such as I_{K1} [ZGZH05] and I_{CaL} [CBW$^+$04] change in magnitude in AF, shortening the ERP and APD. Specific ionic effects were not considered in the present study, but others have demonstrated the importance of these changes in atrial myoyte ionic current magnitudes on rotor dynamics in AF. Atienza et al. [AAM$^+$06] demonstrated that upregulated I_{K1} promotes AF stability by increasing rotor frequency in human studies and simulations. Sarmast et al. [SKZ$^+$03] showed that rotor frequencies increase and AF stabilizes by increased $I_{K,Ach}$ in a cholinergic model of AF owing to the shorter ERP and APD. It is well known that short ERP and APD, dynamic oscillations in APD [NFC$^+$11, NBKF02] and potentially steep rate response in APD [NKKR08] can facilitate AF. It remains unclear under what conditions such AF can terminate in healthy control subjects.

The above results also support a protective role for normal conduction anisotropy and conduction velocity in preventing sustained rotor activity. The idea that normal uniform anisotropy of conductivity could be anti-arrhythmic was first proposed by Spach and Starmer [SS95]. In Figure 4.2.B, an anisotropy ratio of nine again causes the wavefront to extinguish at the tricuspid valve orifice after running into its tail. The large electrotonic loads near the rotor core present with increased anisotropy may also prevent sustained rotors and the attachment of scroll waves to inexcitable regions. Whether anisotropy ratio increases or decreases in AF is somewhat controversial, but here we modelled the anisotropy ratio as decreased in AF. The rationale

for this is the report of lateralization of connexin 43 in AF and a concomitant decrease in the anisotropy of apparent conduction velocity in intact tissue preparations in AF [PHE$^+$01]. Others have argued that anisotropy might increase, since it is known that there is increased fibrotic septation between juxtaposed sheets of cells [YHP$^+$03]. These findings could be reconciled by the dependence of conduction anisotropy not only on gap junction connections but also on the magnitude of the fast inward sodium current, which may be depressed in AF [GBBAN97], disproportionately decreasing the conduction velocity along the fibre axis. Recent clinical studies demonstrate conduction slowing (restitution) with markedly anisotropic dynamics (i.e. an abrupt shift in the vector of conduction slowing) immediately prior to AF onset [LSG$^+$12, SJW$^+$09, MSH$^+$03]. Further studies are required to elucidate the tissue properties that underlie these mechanisms.

Clinical studies of FIRM demonstrate that rotors typically precess in areas of 2 to 3 cm2 [NSK$^+$13]. The numerical simulations presented in Figures 4.3 and 4.4 suggest that discontinuities in the fibre architecture could play a role in such precession. Indeed, ongoing studies are exploring the relationship between rotor precession mapped by FIRM and areas of well-known fibre discontinuities. The ease with which rotors became trapped and converted into macro-reentry at sites of abrupt discontinuity in fibre orientation, particularly at the crista terminalis, is also consistent with previous clinical data. In 23 patients with suspected right atrial tachycardia, Kalman et al. [KOK$^+$98] identified 18 focal arrhythmias originating from the crista terminalis with eight of these located in the high lateral region as in Figure 4.4. Interestingly, three focal right atrial tachycardias were localized to the lateral side of the triscuspid valve annulus as in this patient and Figure 4.3. Computationally,

a recently published model of arrhythmias in a three-dimensional geometric model of normal human atria incorporating fibre orientations and wall thicknesses derived from the literature developed atrial flutter and a reentrant rotor in the high lateral crista terminalis region after nearby burst pacing [TRVH$^+$13]. Locally increased wall thickness at the crista terminalis was visible in the CT imaging data of our patient, and included in the geometric model [GSK$^+$13]. Electrotonic effects due to this thickening may theoretically aid in the permanent attachment of the rotor to this region. Both the fibre discontinuity and wall thickening in the crista terminalis region are supported by anatomical and histological measurements in cadaver hearts [SQAC$^+$02].

Of note, while the patient in Figure 4.1 had an AF rotor in lateral right atrium, several other right (and left) atrial locations have been noted for human AF rotors [NKC$^+$13]. Moreover, AF rotor locations often do not demonstrate signal characteristics consistent with dense scar or borderzone, in that voltages may be preserved and signals may lack fractionation [NSK$^+$13]. Detailed studies are thus required to define a structure–function relationship for AF rotor and focal impulse locations.

The importance of abrupt changes in the fibre architecture on rotor dynamics demonstrated here builds on previous experimental, computational, and analytical analyses. Indeed, much of our understanding of rotor behavior comes from simple two-dimensional computational models or chemical systems [PJ13]. Early experimental findings in excitable chemical media showed that spatial inhomogeneities are not required to sustain a rotor and that stable meander could result from the interaction between a spiral wave and its refractory tail [SS91]. Early numerical studies demonstrated that smooth gradients in fibre orientation [RM94b], refractory period [ZLK93] or ex-

citability [PE88] can lead to spiral wave drift. More recently, Kuklik et al. identified inhomogeneity of conduction anisotropy as one functional mechanism that can permanently trap rotors but stable meandering was not observed [KSSZ13]. A limitation for these investigations was the use of a simple two-dimensional geometry as surface curvature is an important determinant of rotor behaviour [ZLK93, DZ91, DBVP13]. The complex three-dimensional atrial geometry may require additional stabilizing influences to trap or confine rotors. A more recent simulation study using an atrial myocyte ionic model showed that functional heterogeneities alone are capable of constraining rotors to small regions of space, at least for the time course of seconds [CN11]; whether or not functional heterogeneities or fibre discontinuities are able to spatially constrain rotors for longer periods of time (hours to days) is unclear.

These data also demonstrate how structural remodelling can convert a fibrillatory rotor to excitable gap reentry. In Figure 4.5 the precessing AF rotor anchored to inexcitable scar, with development of an excitable gap. Similarly, the rotor in Figure 4.6 released from the fibre discontinuity at the crista terminalis and anchored to the scar. Increasing the size of this scar altered the dynamics of re-entry as anticipated, decreasing the rotational frequency and widening the spatially excitable gap. A depolarization wave was then able to invade the rotor core and displace reentry away from its original location (Figure 4.6.B). These data support a mechanism, previously suggested by Kawase et al. [KIN$^+$03], by which increasing the excitable gap of a rotor can result in its termination.

4.5 Limitations

One limitation of the present study is that the model uses a phenomenological ionic model (Fenton–Karma) rather than a biophysical ionic model such as Courtemanche–Ramirez–Nattel [CRN98] or Maleckar–Giles–Trayanova [MGGT09]. This limitation means that the present work can only suggest phenomenological mechanisms, not more meaningful biophysical mechanisms. For example, the Fenton–Karma model can be used to examine the effect of depressed excitability and of spatial variations in excitability, but cannot distinguish between changes in the biophysical constituents of excitability such as sodium channel remodelling, increased cardiomyocyte-fibroblast coupling, or resting membrane potential elevation. Moreover, the parameter governing excitability in the Fenton–Karma model ($\overline{g_{fi}}$) is not based on an actual biophysical measurement; in contrast, excitability in biophysical models is based on measurements of the fast inward sodium current. Additionally, inhibiting the fast inward current by modifying $\overline{g_{fi}}$ decreases both excitability and APD in the Fenton–Karma model, whereas in biophysical models of the action potential, decreasing the conductance of the fast sodium channel may increase APD (e.g. class 1a antiarrhythmic drugs). The extent to which these differences lead to different conditions for wavebreak and wave fractionation is unknown.

On the other hand, several insights gained into rotor dynamics and specifically into AF by computational models are completely attributable to the shape of the action potential waveform and its effect on spiral tip meander, dominant frequency, and fractionation [AAM$^+$06, KKZ$^+$05]. Consequently, results depending principally on the wave shape, such as the number of wavelets that can be supported in a normal vs. an enlarged atrium, should be unchanged if the Fenton–Karma model

can recapitulate the action potential shape of a more detailed model. A principal reason that we used the Fenton–Karma model in the present study is that in a recent computational study [WHM+12] both normal and AF parameter values in five recent human atrial myocyte models failed to capture clinically measured APD and CV restitution behaviours observed by groups including our own [NKKR08]. Specifically, the restitution curves for normal and AF parameters were far more flat than has been observed experimentally, and the disagreement was worst at the fast rates (> 4 Hz) of sources typical for rotors mapped by FIRM. In the future, the current study should be completed with more biophysically detailed models if parameter values can be found that agree with experimental APD and CV restitution curves.

Our model incorporated patient-specific CT anatomy, electrophysiological mapping of rotors and ablation results, although a limitation is that patient-specific APD and CV restitution curves were not incorporated. Unfortunately, with current technology such data cannot be obtained at high resolution in vivo. In explanted hearts, however, APD and CV restitution curves could be used to modify the parameters of the ionic model (whether phenomenological or biophysical) to make it subject specific although at the expense of an altered metabolic, haemodynamic, and autonomic milieu. Accordingly, while no model based on human measurements is currently available, Cherry et al. have published a similar model based on canine measurements [CENF07]. Like many of the biophysically detailed models, the restitution behavior of this model at fast rates is not as steep as clinical measurements.

Finally, this study is limited because it considers only the geometry of one patient. Future studies should test if these results can provide patient-specific information on rotor stability; these simulations might differ from the results presented

here due to differences in the distance of a focal source from a boundary, the location of sources relative to high-curvature regions (e.g. the pulmonary vein ostia), or the location of sources relative to well-known locations of fibre discontinuity.

4.6 Conclusion

Results from the computational model suggested mechanisms for the maintenance of rotors for human AF. Our data are consistent with the concept that discontinuities in the fibre architecture and inexcitable regions are important structural features that can trap rotors transiently or permanently. The addition of structural remodelling (inexcitable scars) can convert precessing AF rotors to macro-reentry, whose spatially excitable gap can be a target for extermination by external stimuli.

4.7 Acknowledgements

This work was supported by the National Institutes of Health [1R01HL105242, 1R01HL96544, 8P41 GM103226, P50 GM0945503, A.D.M.]; [HL083359, S.M.N. and W.J.R.]; [HL103800, S.M.N.]; and an NIH pre-doctoral training grant [T32 EB009380, M.J.G. and K.P.V.].

The content of this chapter is, in full, a reprint of a previously published manuscript with minor edits to fit the format of this dissertation. The citation is Gonzales MJ, Vincent KP, Rappel W-J, Narayan SM, McCulloch AD , Euclid, "Structural contributions to fibrillatory rotors in a patient-derived computational model of the atria", *Europace*, 16:iv3-iv10, 2014. This work is republished with permission of Oxford University Press.

Chapter 5

Toward a hierarchy of mechanisms in CaMKII-mediated arrhythmia

5.1 Introduction

Calcium/calmodulin-dependent protein kinase II (CaMKII) is a key regulator of excitation-contraction coupling in cardiac myocytes. As described in detail elsewhere in this special issue, CaMKII modulates the function and expression of numerous myocyte ion channels and calcium handling proteins (Figure 5.1). These include $Na_V1.5$, the L-type Ca^{2+} channel (LCC), several potassium channel subunits, the cardiac isoform of the ryanodine receptor (RyR2), and phospholamban (PLN; [BG09a]). Many of the effects at these targets are proarrhythmic [SPS+11, FNM13], although some are antiarrhythmic by conventional paradigms [TKK+99, EHBN+09, CXL+12], and therefore need to be considered in combination. Integrating these pleiotropic effects is further complicated by the temporal, spatial, and biochemical complexities of CaMKII activation (see articles herein from Erickson [Eri14] and Gray and Heller

Brown [GHB14]) in the intact myocyte. Thus, deciphering how CaMKII activity contributes to arrhythmia in any disease context is complex and non-intuitive.

These complexities notwithstanding, the potential for CaMKII inhibition to reduce arrhythmogenic outcomes has been demonstrated in animal models of a remarkably broad range of human diseases: from genetic channelopathies, such as catecholaminergic polymorphic tachycardia (CPVT), to etiologically complex pathologies such as heart failure, atrial fibrillation (AF), and ischemia/reperfusion injury (I/R). For this reason, and in addition to its potential as a target for anti-hypertrophic therapy, CaMKII has become a leading candidate for anti-arrhythmic targeting in the heart. Here we use this diverse range of disease models to develop a conceptual hierarchy of mechanisms in CaMKII-mediated arrhythmia. Specifically, we interrogate whether current evidence suggests that CaMKII promotes arrhythmia via multiple mechanisms, each of which can be recruited by particular disease etiologies, or alternatively, that CaMKII drives the same terminal mechanism irrespective of the specific underlying pathology. We contend that, while CaMKII disrupts ionic homeostasis and impairs repolarization through its actions at many different targets, the available evidence suggests that these mechanisms eventually converge to result in spontaneous Ca^{2+} release (SCR) from the sarcoplasmic reticulum (SR) and delayed afterdepolarizations (DADs). Thus we suggest that this is a dominant terminal mechanism of CaMKII-mediated arrhythmia, and may explain why experimental manipulation of CaMKII phosphorylation at RyR2 has proven effective in many models of arrhythmogenic disease.

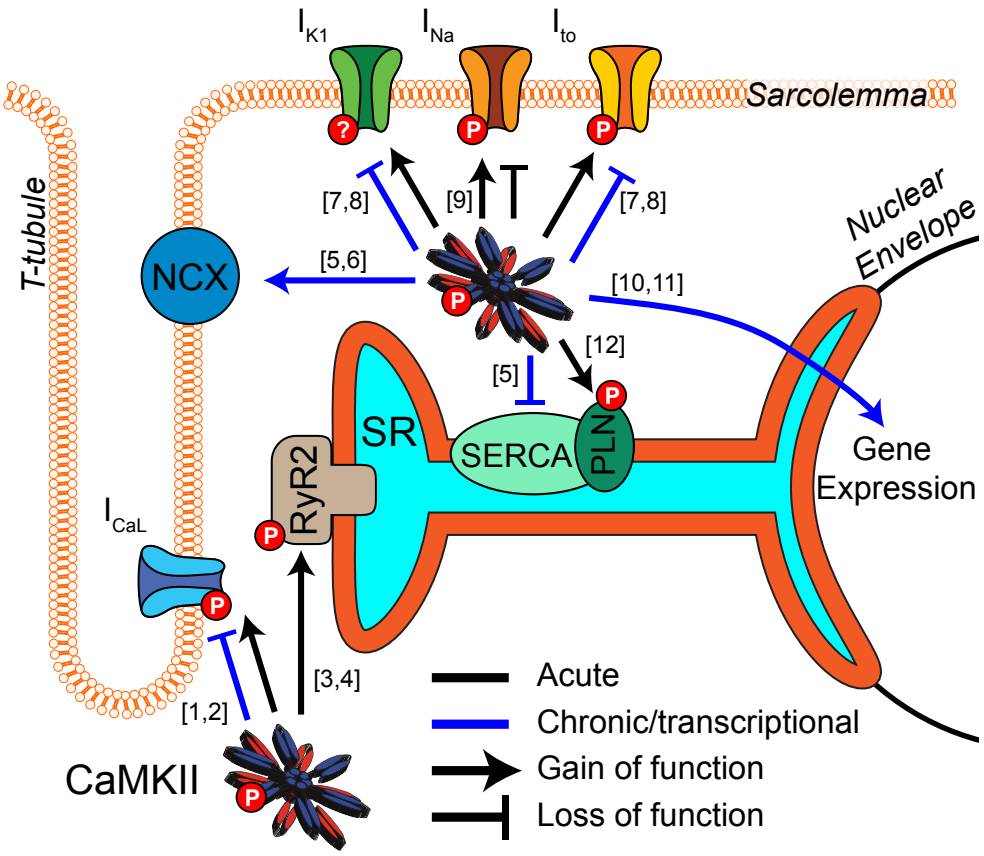

Figure 5.1: **CaMKII regulation of cardiomyocyte electrophysiology and Ca^{2+} handling.** CaMKII exerts acute (black) and transcriptional (blue) regulation ([10]- Wu et al., [WZB+06]; [11]-Backs et al., [BSB+06]) of many key proteins in cardiac electrophysiology and calcium handling. Acute phosphorylation of LCCs by CaMKII potentiates I_{CaL} and slows inactivation ([1]-Yuan and Bers,[YB94]). Transcriptional effects are less established but likely downregulate channel expression ([2]-Ronkainen et al., [RHK+11]). Phosphorylation of RyR2 by CaMKII promotes Ca^{2+} release from the SR and is implicated in many proarrhythmic contexts ([3]-Witcher et al., [WKS+91]; [4]-Wehrens et al., [WLRM04]). Available data suggest CaMKII transcriptional regulation promotes Ca^{2+} extrusion from the cell by increasing NCX expression and decreasing SERCA ([6]-Mani et al., [MEA+10]; [5]-Lu et al.,[LRD+11]). I_{to} and I_{K1} are enhanced by acute CaMKII phosphorylation ([7]-Li et al., [LMZ+06]), and transcriptional downregulation of these currents is a well-established effect of long term CaMKII activity. This reduces repolarization reserve and may destabilize resting membrane potential ([8]-Wagner et al., [WHG+09]). Acute regulatory effects of CaMKII on $Na_V1.5$ enhance inactivation, decrease availability and potentiate I_{NaL}, but again any transcriptional regulation is unclear ([9]-Wagner et al., [WDR+06]). Acute phosphorylation of PLN disinhibits SERCA and enhances SR Ca^{2+} reuptake ([12]-Karczewski et al., [KKB+97]).

5.2 Cellular Mechanisms of CaMKII-Mediated Arrhythmia

A key feature of CaMKII signaling in arrhythmia is the presence of several positive feedback mechanisms, whereby CaMKII target phosphorylation results in changes to Ca^{2+} homeostasis (or metabolism) that further activate the kinase. These mechanisms are likely to contribute both during acute homeostatic challenge, such as β-adrenergic stimulation, and to the chronic disruption of ionic homeostasis in acquired disease. Figure 5.2 shows two major forms of this feedback. Hyper-phosphorylation of LCCs, PLN, (Figure 5.3.A, mechanism 1) and $Na_V1.5$ (Figure 5.3.A, mechanism 2) increase whole-cell Ca^{2+} load either directly (LCC and PLN) or by impairing forward mode Na^+/Ca^{2+} exchange ($Na_V1.5$). This both promotes SCR in and of itself, and also further activates CaMKII, which independently drives SCR through phosphorylation of RyR2 (Figure 5.3.A, mechanism 3; [WLRM04]). While it is not shown in Figure 5.2, the increased cytosolic Ca^{2+} also causes mitochondrial Ca^{2+} loading and probably invokes a third positive feedback loop involving ROS-dependent CaMKII activation (see Joiner and Koval in this issue [JK14]). Of course, the actions of CaMKII at LCCs, I_{Na}, and certain potassium currents also directly result in proarrhythmic changes to the action potential (AP), including prolonged repolarization and early afterdepolarizations (EADs, Figure 5.3.B; [GZMB06]). Thus, even at the level of integrated physiological outcomes, there are a number of CaMKII-dependent mechanisms capable of disrupting cardiac ionic homeostasis and electrophysiology. Our focus here is to understand which of these predominates in experimental models of human disease.

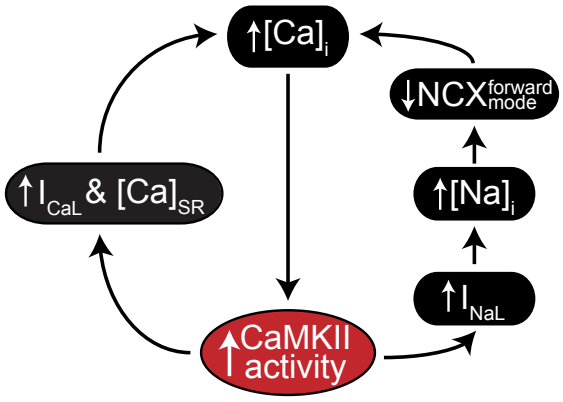

Figure 5.2: **CaMKII positive feedback mechanisms involved in cardiac disease.** As a Ca^{2+} regulated kinase, CaMKII is sensitive to any physiological mechanism that alters intracellular Ca^{2+} cycling. Many of its own catalytic actions result in such alterations, and two gain-of-function effects that create positive feedback by enhancing Ca^{2+} cycling occur at I_{CaL} (left) and I_{Na} (right). CaMKII regulation of I_{Na} is thought to increase intracellular Na^{+} via enhanced late I_{Na}, which in turn reduces the thermodynamic potential for Ca^{2+} extrusion via NCX. CaMKII regulation of I_{CaL} more directly enhances Ca^{2+} cycling by increasing Ca^{2+} influx through slightly elevated peak current and slowed inactivation.

5.3 Arrhythmogenic Influence of CaMKII in Congenital Heart Disease

The last 20 years have witnessed rapid progress in understanding the molecular and genetic basis of congenital arrhythmogenic diseases [CST+95, CNP12, NBMP12]. Somewhat surprisingly, CaMKII activity and hyperactivity have been shown to contribute in many experimental models of these diseases, even those with minimal or undetectable remodeling of myocardial structure. As such, these models offer a unique perspective of how CaMKII promotes arrhythmia in the absence of sequelae associated with structural disease. In this section, we review examples of CaMKII involvement in congenital arrhythmogenic disease, and identify key questions that remain for defining the roles, limits, and potential for therapeutic targeting of CaMKII

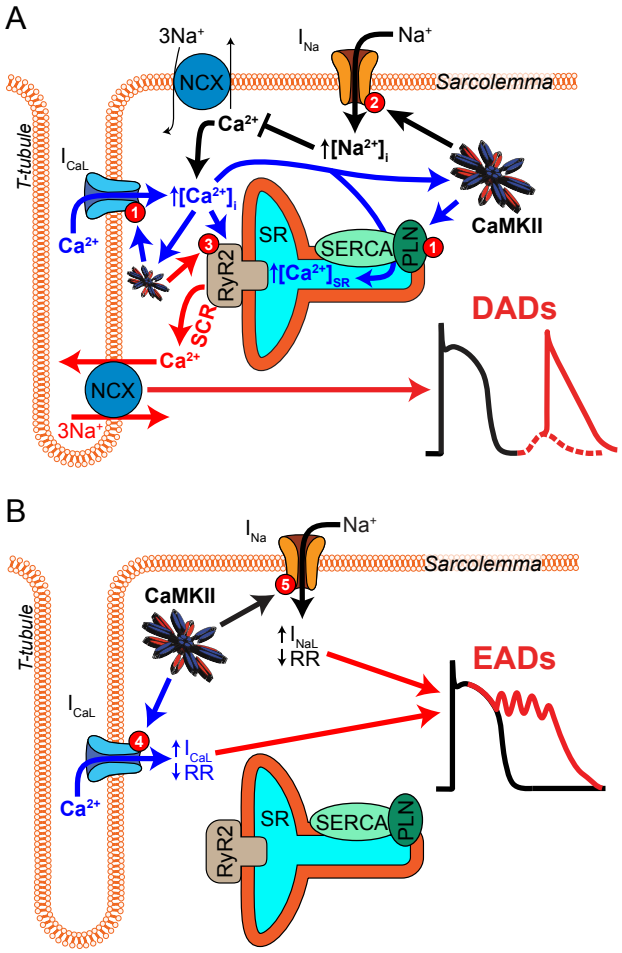

Figure 5.3: **Mechanisms of CaMKII-mediated afterdepolarizations.** **(A)** Pathological CaMKII regulation can trigger diastolic SR Ca^{2+} release resulting in electrogenic Ca^{2+} extrusion by NCX and DADs (red arrows). This results from pro-arrhythmic CaMKII regulation at multiple target proteins, which together drive 3 mechanisms through which CaMKII promotes SCR. First, CaMKII elicits gain-of-function effects at I_{CaL} and SERCA (via PLN-mediated disinhibition), thereby increasing Ca^{2+} influx and resulting in Ca^{2+} overload (mechanism 1, blue arrows). Second, CaMKII hyper-phosphorylation of $Na_V1.5$ can elevate intracellular Na^+ resulting in Na^+-induced Ca^{2+}-overload by decreasing Ca^{2+} efflux through NCX (mechanism 2, black arrows). Third, CaMKII directly phosphorylates RyR2, which has been shown to promote SCR and has been strongly implicated in a number of different models of arrhythmogenic disease (mechanism 3, red arrow). **(B)** CaMKII phosphorylation of depolarizing currents reduces repolarization reserve and promotes EADs (red arrows) in certain disease contexts. Altered LCC gating due to CaMKII hyper-activity can elicit EADs by increasing and prolonging I_{CaL} (mechanism 4, blue arrows). $Na_V1.5$ phosphorylation increases I_{NaL} and may lead to non-equilibrium reactivation of I_{Na} (mechanism 5, black arrows), both of which can trigger EADs.

in these contexts. Impressively, the available data suggest that CaMKII-dependent regulation of RyR2 is an important contributor to arrhythmogenesis in the majority of these congenital disease models. Here we focus specifically on how this regulation contributes to electrophysiologic instability, and suggest the review contributed by Camors and Valdivia [CV14] for those interested in a more mechanistic description of CaMKII-dependent regulation of RyR2.

Catecholaminergic Polymorphic Ventricular Tachycardia

The autosomal dominant form of CPVT has become the prototypical disease of RyR2-mediated arrhythmia, and accounts for at least half of all positive CPVT diagnoses [PNM$^+$02]. This channelopathy results from a family of RyR2 mutations that cause channel hyperactivity due to increased receptor Ca^{2+} sensitivity. The outstanding physiological ramification of these mutations is increased myocyte susceptibility to SCR and DADs during catecholamine-induced Ca^{2+} overload. As such, β-blocker therapy is a front-line treatment for CPVT patients. However, in $\sim$50% of cases, episodes of VT still present during β-blockade, and more aggressive treatment (including ICD implantation) is often required [PNM$^+$02, WK11]. Thus, efforts to define additional effective pharmacotherapeutic approaches for this disease remain a high priority.

Conceptually, CaMKII presents an attractive target in CPVT because its established actions at various Ca^{2+} handling proteins would all be expected to exacerbate arrhythmia resulting from RyR2 hyperactivity. Indeed, transgenic overexpression of CaMKIIC in the R4496C (+/-) mouse model of CPVT worsened the arrhythmia phenotype and increased mortality [DSN$^+$11]. However, few studies have assessed whether, and how, CaMKII activity contributes to arrhythmia in CPVT. Liu et al.

[LRD+11] showed that both chronic and acute administration of KN-93 dramatically reduced the incidence of arrhythmia in the R4496C (+/-) mouse. More specific CaMKII blockade by autocamtide-2 related inhibitory peptide (AIP) also markedly decreased the incidence of SCR, DADs, and triggered activity in isolated R4496C (+/-) ventricular myocytes (VMs). Interestingly, while AIP did remove signature effects of CaMKII on Ca^{2+} handling (e.g., frequency dependent acceleration of relaxation, FDAR), it did not achieve those effects by reducing SR Ca^{2+} load at any baseline pacing frequency or during isoproterenol (Iso) challenge. Thus, the antiarrhythmic actions of CaMKII blockade were unlikely to result from reduced SR or whole cell Ca^{2+} overload. Instead, they appeared to rely on reduction of CaMKII-induced RyR hyperactivity (Figure 5.3.A, mechanism 3), as measured by triggered fractional release, and spark frequency. AIP reduced both of these measures in R4496C (+/-) myocytes, particularly during Iso challenge, and KN-93 reduced RyR2 phosphorylation at the established CaMKII site, Ser-2814. Thus, this study suggests that, even in myocytes already expressing hyperactive mutant RyR2, CaMKII phosphoregulation of this critical SR Ca^{2+} release channel may further contribute to in vivo arrhythmogenesis.

Congenital Long QT Syndrome

Recent work has suggested that CaMKII is involved in several rare forms of congenital long QT (LQT) syndrome. Importantly, CaMKII mutations have not been established as the source of genetic susceptibility in these, or to date, any congenital arrhythmogenic disease. Rather, in all existing studies, CaMKII exerts its proarrhythmic influence by exacerbating the effects of disease-associated mutations occurring in other electrophysiologic or calcium handling proteins, many of which are

CaMKII targets.

Ankyrin-B syndrome/LQT4

After remaining elusive for over 10 years, the molecular basis for type 4 LQT syndrome was identified in 2003 as a family of loss-of-function mutations in Ankyrin-B [MSG$^+$03]. The electrophysiologic dysfunction associated with these mutations is broad, and often also involves sinus bradycardia and catecholamine-induced arrhythmia, but is not associated with gross structural defects. LQT is relatively mild in most cases, and absent for some mutations even though individuals harboring these mutations remain arrhythmia susceptible [MSN$^+$04]. Owing to this spectrum phenotype and clear molecular source, LQT4 is now often referred to as Ankyrin B syndrome [YTW03]. Heterozygous deletion of AnkB in the mouse recapitulates many signatures of human LQT4 [MSG$^+$03], including inducible polymorphic VT, and this model has now been used extensively to study mechanisms of the disease.

In neonatal AnkB(+/-) myocytes, LQT4 mutations consistently reduce expression and disrupt localization of the myocardial Na^+/Ca^{2+} exchanger (NCX1), Na^+/K^+ ATPase (NKA), and inositol triphosphate (IP3) receptor [MSG$^+$03, MSN$^+$04]. In adult myocytes, these changes promote signature arrhythmogenic changes including AP prolongation [DNK$^+$12], a prominent increase in Ca^{2+} waves [CMBD12] and afterdepolarizations [DNK$^+$12]. The mechanistic link between altered AnkB molecular anchoring and these arrhythmogenic outcomes is not fully established, but recent studies summarized below have suggested an important role for altered Ca^{2+} homeostasis, and particularly for CaMKII-dependent regulation of RyR2.

Given the observed changes to expression and distribution of major Na^+

transporters, Camors et al. [CMBD12] investigated whether altered Na^+ handling could explain arrhythmogenicity in AnkB(+/-) myocytes. They found that, while maximal NKA function was depressed, this had little impact on measures of basal or challenged Na^+ homeostasis, and did not increase diastolic $[Ca^{2+}]_i$. However, AnkB(+/-) myocytes did exhibit slightly increased SR Ca^{2+} load, enhanced Ca^{2+} transient amplitude and fractional release, and a marked increase in spark frequency and Ca^{2+} waves. Soon after, the same group was able to show that these effects are associated with RyR2 hyperactivity and increased phosphorylation of RyR2 at the primary CaMKII site, S2814 [DNK$^+$12]. These effects could be normalized by crossing the AnkB(+/-) mouse with one expressing the CaMKII inhibitory peptide, AC3-I. These mice were also resistant to both cellular afterdepolarizations and organ level arrhythmia present in the AnkB(+/-) mice during adrenergic challenge [DNK$^+$12].

While the authors acknowledged that these RyR2 effects are one component of what are probably many alterations associated with AnkB loss-of function, the observed changes in Ca^{2+} handling are consistent with a mechanism involving RyR2 hyperactivity [CMBD12]. Because AnkB is not known to anchor CaMKII itself, the authors instead suggested that loss of AnkB may have disrupted local phosphatase activity because protein phosphatase 2A is a known binding partner of AnkB and regulator of RyR2 phosphorylation.

Timothy syndrome/LQT8

The extremely rare LQT8, more frequently referred to as Timothy syndrome (TS), results from substitution mutations in the alpha subunit ($Ca_V1.2$) of the cardiac L-type calcium current (I_{CaL}). Only two mutations have been described to date, and both

replace glycine residues with either arginine (pos. 406) or serine (pos. 402; [STS$^+$04, STD$^+$05]. These mutations profoundly impair voltage-dependent inactivation of I_{CaL} (VDI), and this is generally accepted to be the proximal molecular dysfunction associated with the disease [BT08]. The cardiac signatures of TS include a range of cardiac structural defects and markedly prolonged ventricular repolarization [STS$^+$04, STD$^+$05]. Supraventricular arrhythmia has also been noted, particularly AV block [MWCK95], but ventricular arrhythmogenesis is the most serious presentation of the disease, and most TS patients experience life-threatening events in the first years of life [STS$^+$04]. The existence and severity of the TS phenotype has forced clinicians and scientists to broadly reconsider the importance of VDI in normal and pathologic cardiac electrophysiology.

Since the original mechanistic descriptions from Splawski et al. [STS$^+$04, STD$^+$05], a number of experimental models have been developed to investigate how these point mutations destabilize cardiac electrophysiology. In general, those models have provided compelling (albeit not entirely consistent) evidence for the involvement of CaMKII. Erxleben et al. [ELG$^+$06] were the first to suggest a role for CaMKII, and observed that heterologous expression of TS-mutated (G406R) rabbit $Ca_V1.2$ yielded LCCs exhibiting more frequent prolonged openings (mode-2 gating). In noticing that this substitution also created a consensus site for CaMKII at nearby rabbit Ser-439 (homologous to human Ser-409), they hypothesized that CaMKII activity may be required for both mode-2 gating and slowed macroscopic inactivation of I_{CaL} in TS. CaMKII inhibition by KN-62, and genetic ablation of the putative CaMKII phosphoacceptor (S439A) indeed eliminated the increased intrinsic mode-2 openings of the mutant channels in that study. Thiel et al. [TCH$^+$08] extended this work

to adult VMs by double-mutating $Ca_V1.2$ to include both G406R and resistance to dihydropiridine inhibition via T1066Y. This permitted the authors to modulate the contribution of endogenous LCCs to macroscopic I_{CaL} via nifedipine, and thereby study the effects of the loss of I_{CaL} control, independent of differences in peak I_{CaL}. Unlike Erxleben et al. [ELG+06], they were unable to observe a requirement for CaMKII in the loss of VDI accompanying the G406R mutation. However, they did observe an interaction between VDI loss and CaMKII, whereby TS myocytes exhibited greater I_{Ca} facilitation than WT, and this could be removed through peptide blockade of CaMKII via AC3-I. To explain this they suggested that Ca^{2+} loading due to impaired VDI caused enhanced secondary activation of CaMKII, which in turn exaggerated I_{Ca} facilitation. They also observed a pronounced increase in SCR and DADs, both of which could be prevented by AC3-I. As a result they reasoned that DADs occurring secondary to Ca^{2+} overload may reflect the dominant arrhythmogenic role of CaMKII in TS, and mathematical modeling supported this contention. Thus, in VMs, CaMKII activation may compound the effects of TS mutations by enhancing I_{CaL} facilitation in response to impaired VDI and increased Ca^{2+} influx.

Further cardiac-specific models of TS have now been developed, most notably the G436R transgenic mouse developed by Cheng et al. [CYN+11]. This model exhibits increased $Ca_V1.2$ expression, and the entirety of this increase ($\sim$40%) is due to expression of the G436R transgene. Somewhat surprisingly this additional $Ca_V1.2$ does not increase peak I_{CaL} in these mice but does slow VDI in the expected manner, and intriguingly, this effect required the anchoring protein AKAP150. To explain this result, the authors suggest that AKAP150 provides a key structural link among LCCs within the dyadic ensemble, and they provide evidence that, in the presence of

G436R-mutated channels, AKAP150 promotes coupled gating of LCCs and increases mode-2 behavior. Similarly to Thiel et al. [TCH$^+$08] , Yarotskyy et al. [YGPE09], and Cheng et al. [CYN$^+$11] observed that slowed inactivation in this model is not impacted by CaMKII inhibition, and therefore suggest that the gating effects underlying TS are probably not reliant upon G436R-mediated creation of a CaMKII phosphorylation site at Ser-439/409. They did, however, observe markedly enhanced Ca^{2+} cycling, prolonged AP duration, and exaggerated susceptibility to cellular afterdepolarizations. These effects were confirmed in a recent and more detailed study of Ca^{2+} handling in these mice [DDY$^+$14], and again like Thiel et al. [TCH$^+$08] the authors conclude that Ca^{2+} overload and SCR are the likely terminal mechanisms of arrhythmogenesis in this model.

In summary, these investigations suggest that CaMKII plays an important role in TS arrhythmogenesis, but at least in VMs it seems probable that this accompanies Ca^{2+} overload secondary to the intrinsic effects of the TS mutations on LCC gating. An important qualifier here is that, to date, all experiments suggesting this role for CaMKII have been conducted in primary cardiomyocytes from rodents. The rapid repolarization of these cells probably biases arrhythmogenic mechanisms away from disrupted repolarization and toward SCR and arrhythmia arising during diastole. Thus, similarly detailed investigations in large mammalian myocytes remain desirable for clarifying if changes in I_{CaL} gating are capable of playing a more direct role in human TS arrhythmia, and if CaMKII still contributes in a similar manner and to a similar degree.

Phosphomimetic mutation of $Na_V1.5$

CaMKII is an established regulator of the myocardial Na^+ current (I_{Na}), and simultaneously potentiates late I_{Na} (I_{NaL}) while decreasing channel availability [HBG13]. While the specific phosphorylations required for these effects remain debated, available evidence suggests that either or both Ser-571 and Ser-516 may be key sites [HKL$^+$10, AHG$^+$12, KSW$^+$12, HBG13], and it is generally agreed that the I-II intracellular linker is the critical phosphoregulatory domain.

An interesting line of investigation has suggested that mutation of residues immediately adjacent to Ser-571 are associated with congenital disease, and may result in phosphomimetic effects at I_{Na}. Two mutations, A572D and Q573E, were originally uncovered by genetic screening of Romano-Ward syndrome probands, and therefore thought to be novel forms of LQT3 [PMG$^+$03, TWHA05]. The A572D mutation has since been dismissed as an independent source of LQT3 susceptibility, but may still be associated with arrhythmogenic cardiac diseases because it cosegregates with the established arrhythmogenic mutation H558R [TVHK$^+$10]s. Having previously identified Ser-571 as a potential site for CaMKII regulation, Koval et al. [KSW$^+$12] recently investigated whether the functional effects of these mutations exhibited any dependence on CaMKII activity. They showed that heterologous expression of either A572D or Q573E recapitulated CaMKII-dependent effects at I_{Na}. Neither constitutively active CaMKII nor blockade of endogenous CaMKII altered these effects, suggesting that they are autonomous to the mutant $Na_V1.5$ and independent of additional CaMKII phosphoregulation. Further, the mutant gating defects could be reconstituted in primary mouse VMs transfected with channels sensitive to low dose tetrodotoxin to allow silencing of the exogenous $Na_V1.5$. While conflicting results

from other groups [TVHK$^+$10, AHG$^+$12] suggest that these findings require further interrogation, they provide the first evidence that CaMKII regulation of I_{Na} may be sufficient to induce an arrhythmogenic phenotype in the absence of structural or ischemic disease.

5.4 Arrhythmogenic Influence of CaMKII in Acquired Heart Disease

An extensive literature describes the arrhythmogenic mechanisms attributable to CaMKII hyperactivity in acquired heart disease. A large portion of this is related to heart failure, but significant effort has also been invested in AF and ischemia/reperfusion challenge (I/R). The CaMKII-dependent mechanisms involved in AF and I/R are detailed separately in this issue by Heijman et al. [HVWD14] and Bell et al. [BVPD14] and we direct the interested reader to those comprehensive treatments. For the purposes of this review it suffices to note that recent studies of AF and I/R mechanisms in mice and humans have again implicated RyR2 dysregulation, and SR Ca^{2+} handling in general [SBP$^+$08, SBV$^+$11, VLW$^+$12, PRG$^+$13]. These aspects are consistent among the various acquired disease even though other important pathological conditions differ. For example, some signature electrophysiologic alterations apparent in AF [NBD08], such as shortened APD and more negative resting potential, are precisely the opposite of the alterations present in failing VMs [TM99].

As might be expected of the pathologic complexity in acquired disease, the range of CaMKII-dependent mechanisms thought to contribute to arrhythmia is also broader than for congenital disease. Specifically, CaMKII has been shown to

contribute to Na^+ overload in heart failure (Figure 5.3.A, mechanism 2), and several studies have suggested that CaMKII effects at I_{CaL} may be sufficient to directly destabilize electrophysiology in the failing ventricle (Figures 5.3.A,B). An additional feature of CaMKII-dependent arrhythmia in heart failure and AF, and probably in acquired disease in general, is the importance of CaMKII-oxidation as a source of kinase hyperactivity ([LA14]; see also the review by Erickson in this special issue [Eri14]). This mode of CaMKII activation appears to be particularly important in sinus node (SN) dysfunction accompanying heart failure [SPS+11], in AF [PRG+13], and diabetic cardiomyopathy [LGL+13]. Finally, one of the most important roles that CaMKII plays in acquired disease is as a controller of the expression of several key ion channels and transporters, and many disease-associated changes in expression of these proteins appear to require CaMKII. The best-described of these involve K^+ currents, namely the transient outward current (I_{to}) and inward rectifier current (I_{K1}; [WHG+09]; reviewed elsewhere in this issue by Mustroph et al., 2014), but this transcriptional regulation may also extend to I_{CaL} [RHK+11], NCX1 [MEA+10] , and SERCA2 [LHS+11].

Heart Failure

The role of CaMKII in heart failure pathophysiology has been the subject of intense investigation since elevated CaMKII levels were first found in the myocardial tissue of heart failure patients [HMH+99, KSSN99]. Increased CaMKII expression and activity have since been mechanistically linked to structural and electrophysiological dysfunction in numerous experimental models of severe cardiomyopathy and heart failure. However, deciphering precisely how CaMKII is driving electrophysiologic dys-

function is made all the more difficult by the extensive structural and electrophysiologic remodeling that accompanies CaMKII hyperactivity in the failing heart.

Target-specific roles of CaMKII in heart failure

Murine models of heart failure, CaMKII hyperactivity (overexpression), and CaMKII regulation of RyR2 have provided a wealth of information describing how CaMKII contributes to both arrhythmogenesis and disease progression in cardiomyopathy. Cardiac restricted overexpression of CaMKIIC in the mouse leads to heart failure, inducible arrhythmia, and premature death [ZMD$^+$03, WDR$^+$06] . In these mice, acute inhibition of CaMKII (via KN-93) prevents catecholaminergic arrhythmia in vivo, and RyR2 dysfunction was implicated in this arrhymogenic mechanism (Figure 5.3, mechanism 3) by a substantial and CaMKII-dependent increase in SR Ca^{2+} leak, elevated diastolic Ca^{2+}, and DADs during Iso challenge [SWK$^+$09]. SR-targeted inhibition of CaMKII with SR-AIP restored calcium handling but worsened the heart failure phenotype suggesting that other CaMKII mechanisms are integral to pathological remodeling [HDK$^+$11]. The phosphomimetic (S2814D) and non-phosphorylatable (S2814A) RyR2 mutants developed by Wehrens et al. [WLRM04], have provided a powerful model for investigating the role of CaMKII-dependent RyR2 regulation in a large number of acute and chronic diseases. Most recently, the knock-in mice expressing these engineered RyR2 variants have provided compelling evidence that CaMKII regulation of this protein contributes to arrhythmogenesis in several models of acquired disease. The S2814D mouse slowly develops a heart failure phenotype and is susceptible to sustained VT during epinephrine/caffeine challenge, and pressure-overload initiated prior to overt heart failure also increased mortality due to arrhythmias in these mice

[vMD$^+$10]. Genetic ablation of CaMKII-dependent RyR2 phosphorylation in the S2814A mouse provides protection from pacing-induced arrhythmias after pressure-overload, slows the development of contractile dysfunction, and reduces ventricular remodeling and cellular SCR [vMD$^+$10, RvL$^+$12].

CaMKII has also been shown to contribute to heart failure arrhythmias in large mammals. A series of studies in a rabbit model of non-ischemic heart failure provides further mechanistic evidence of the importance of CaMKII regulation of RyR2 in heart failure arrhythmogenesis. In this model, total CaMKII expression was elevated and the amount and activity of CaMKII localized to RyR2 was increased in failing ventricular tissue, thus leading to enhanced CaMKII-dependent phosphorylation of RyR2 [ACS$^+$05]. Elevated SR Ca^{2+} leak was significantly reduced with inhibition of CaMKII but not PKA [ACS$^+$05], and Iso-induced SCR events (Ca^{2+} waves) were CaMKII-dependent [CBS$^+$10]. Belevych et al. [BTT$^+$11] also described progressive pathological RyR2 dysfunction in a tachycardia-induced canine model of heart failure. Mirroring changes in SR Ca^{2+} leak observed in the rabbit, phosphorylation of RyR2 by CaMKII but not PKA was increased after 1- and 16-months of tachycardic pacing. CaMKII inhibition with KN-93 abolished proarrhythmic diastolic calcium waves after 1 month but not 16-months. Instead, the increased wave frequency at 16 months was attributed to increased ROS production, which highlights the progressive nature of arrhythmia mechanisms in heart failure, and suggests that CaMKII hyperactivity may contribute more greatly to arrhythmogenesis early in heart failure progression. Significantly, the clinical importance of CaMKII modulation of RyR2 was reinforced recently when Fischer et al. [FHT$^+$13] demonstrated that CaMKII inhibition with KN-93 or AIP reduced SR Ca^{2+} leak in myocytes isolated from failing human hearts.

CaMKII regulation of cardiac Na^+ currents is another potential source of arrhythmogenic regulation during heart failure. The mechanisms of this regulation are presented briefly in Figures 5.2 and 5.3 and in detail elsewhere in this issue (see [GH14]), thus we only briefly mention them in the context of their importance in heart failure. I_{NaL} is increased in human heart failure [VCP+05], and evidence from numerous animal models suggests CaMKII inhibition normalizes I_{NaL}. In a murine TAC-induced heart failure model, CaMKII inhibition by AIP reversed increases in I_{NaL}, APD90, Iso-induced DAD frequency, and SR Ca^{2+} leak [THW+13]. In that study, CaMKII phosphorylation of $Na_V1.5$ was increased during decompensated heart failure and application of ranolazine had a similar result to CaMKII inhibition suggesting an important role for CaMKII regulation of Na^+ handling. Interestingly, myocytes from pressure-overloaded hearts did not exhibit EADs in that study, suggesting that Na^+ does not carry the arrhythmogenic current. Instead, the authors suggested that I_{NaL} was indirectly responsible for DADs by causing Na^+-induced Ca^{2+}-overload (Figure 5.2). This idea is consistent with reports from several other studies. Most recently Morotti et al. [MEM+14] have suggested that Na^+-induced Ca^{2+}-overload is a component of a positive feedback loop that is quantitatively capable of eliciting CaMKII hyperactivity, which in turn promotes arrhythmogenic outcomes and, probably, further Na^+ loading (Figure 5.2). Indeed, experiments involving Na^+ overload induced by anemone toxin (ATX-II, a potent agonist of I_{NaL}) and an LQT3 mutation (N1325S), have shown these maneuvers to be capable of inducing CaMKII activation and arrhythmia [YFJ+11]. Similar effects have been observed during glycoside-induced Na^+ overload [GSR+11, HLS+13], and arrhythmias resulting from glycoside treatment were susceptible to both SR-targeted peptide inhibition of CaMKII [GSR+11] and

ablation of CaMKII phosphorylation at RyR2 via S2814A mutagenesis [HLS$^+$13]. Thus, it may again be that these Na^+-dependent forms of arrhythmogenesis converge at CaMKII-dependent regulation of RyR2. It should be noted that some evidence in large mammals also supports a more direct arrhythmogenic role for CaMKII-dependent regulation of Na^+ currents (Figure 5.3.B). In a canine model of dyssynchronous heart failure with extensive electrophysiological remodeling [AHB$^+$09], CaMKII expression, activity and autophosphorylation were all increased, particularly in the late-activated lateral LV wall [CDT$^+$08]. Myocytes isolated from these dogs exhibited shifted voltage-dependent availability, enhanced intermediate inactivation, increased I_{NaL} and ranolazine sensitive EADs [ABH$^+$13]. Although inhibition studies were not performed in these dogs, Maltsev et al. [MRU$^+$08] had previously identified CaMKII as an important regulator of I_{NaL} in the failing canine heart.

Regulation of LCCs by CaMKII presents a third potential mechanism for proarrhythmic function during heart failure. However, as for I_{Na} the sites of CaMKII phosphorylation of LCCs remain somewhat controversial, and this has caused mutagenic approaches to investigating LCC-dependent mechanisms to be more challenging. Similarly to TS, CaMKII regulation of I_{CaL} in heart failure is thought to elicit arrhythmia either by disrupting repolarization and driving EADs (Figure 5.3.B), or by promoting cellular Ca^{2+} overload (Figures 5.2 and 3A). Again, a complete treatment of CaMKII effects at I_{Ca} is provided elsewhere in this issue (see the review from Bers), but briefly, heart failure-associated changes to LCC gating are quite similar to those accompanying CaMKII regulation [SHB$^+$98, DWC$^+$00]. Specifically, CaMKII elicits mode-2 gating in single channels, and slows inactivation while hastening recovery from inactivation of the macroscopic current [GZMB06]. All of these effects would

be expected to promote EADs by reducing repolarization reserve, independently promoting I_{CaL} reactivation, or both [ABSP94, HGW10, KGW$^+$10]. The most direct evidence for the ability of CaMKII to elicit EADs via I_{CaL} (in large mammal VMs), was presented by Koval et al. [KGW$^+$10]. In that study, the $Ca_V1.2$ β2a regulatory subunit was expressed in rabbit VMs, which increased I_{Ca} facilitation and promoted EADs. Those effects were reversed by peptide (CaMKIIN) or shRNA inhibition of CaMKII, and ablation of the proposed CaMKII phosphorylation or binding sites [KGW$^+$10]. Two caveats when extending these findings to CaMKII hyperactivity in normal or failing myocytes are: (1) the β2a subunit is probably a lesser component of LCCs in non-diseased hearts, although its expression may be increased in heart failure [HMv$^+$07], and (2) the slowed inactivation in this study also increased total Ca^{2+} influx without destabilizing the AP. In vivo, the effect of this on whole-cell and SR Ca^{2+} overload could easily be as or more important than effects upon repolarization.

Together these studies suggest that CaMKII-mediated ventricular DADs and EADs exert a proarrhythmic influence in the failing heart, and that the specific mode of arrhythmia initiation and maintenance is likely dictated by the underlying etiology and stage of disease development. The genetic tools available for studying the role of CaMKII regulation of RyR2 in mice have provided compelling evidence that this target is central to the acute arrhythmogenic outcomes of CaMKII in the failing ventricle, and this contention is largely supported by studies in large mammals. Given the extensive structural and electrophysiological remodeling accompanying heart failure, and relatively poor specificity of small molecule inhibitors available for in vivo CaMKII blockade, it is still not entirely clear how effective acute CaMKII inhibition may be as an anti-arrhythmic strategy in heart failure. However, evidence published to date

support an optimistic outlook for potential therapeutic applications in this and other acquired cardiac diseases.

Sinus node dysfunction in heart failure

Another series of recent studies, reviewed in this issue by Wu and Anderson [WA14], has suggested that oxidized-CaMKII (ox-CaMKII) plays a critical role in SN dysfunction accompanying heart failure, and that this involves pronounced structural remodeling of the SN. Swaminathan et al. [SPS+11] first observed that, relative to non-diseased controls and heart failure patients without SN dysfunction, heart failure patients with SN dysfunction exhibit increased ox-CaMKII in right atrial tissue. This comprehensive study observed an analogous effect in a canine model of pacing-induced heart failure, and utilized their previously developed model of Ang II-dependent oxidation/activation of CaMKII to elicit and study the mechanisms of SN dysfunction in mice. With this model ∼70% of mice develop sinus pause or exit block after 3 weeks of Ang II infusion, and heart rate at rest and during activity is blunted compared to untreated controls. SN dysfunction was absent in AC3-I (cardiac specific) mice treated with Ang II even though the pressor response to Ang II was similar to WT. The observed dysfunction was associated with increased apoptosis and fibrosis within the SN, and structurally based computational analysis suggests that the cell loss observed experimentally may be sufficient to explain both reduced SN firing frequency, and episodes of exit block. One particularly elegant component of this study showed that local adenoviral gene transfer of the CaMKIIN inhibitory peptide (via painting of the SN) was capable of preventing Ang II-driven SN dysfunction in WT mice. Thus providing proof-of-principle that gene transfer of CaMKII-inhibitors may be a viable

therapeutic avenue for this specific heart failure phenotype. A follow-up study from Luo et al. [LGL$^+$13] investigating SN dysfunction in a mouse model of combined insulin deficiency and myocardial infarction, suggests that the mechanistic cascade described by Swaminathan et al. [SPS$^+$11], may extend to other cardiac conditions exhibiting pronounced oxidative stress.

The role of oxidized CaMKII in driving structural remodeling and dysfunction of the SN in response to oxidative stress highlights the ability of CaMKII to impact arrhythmogenic outcomes via structural as well as functional changes. To date, the impact of these tissue-level effects in CaMKII-mediated arrhythmia has not been studied to the same extent as the effects on cellular electrophysiology and Ca^{2+} handling. This aspect of CaMKII-driven arrhythmia warrants further work, as some evidence suggests that effects at this level may be important. For example, CaMKII activity may exhibit regional heterogeneity in the heart [CDT$^+$08] . Even without considering this heterogeneity of kinase action, transmural dispersion of repolarization is a predicted result of CaMKII hyperactivity [BG09b] due exclusively to its effects at I_{to}. Thus, putative roles for CaMKII in reentrant or alternans-driven arrhythmias remain largely untested.

5.5 Summary and Conclusion

The ability of CaMKII to contribute to arrhythmia in models of cardiac disease that result from widely varying etiologies is testament to the importance of this kinase in the control of cardiac electrophysiology and calcium handling. It also suggests that CaMKII exerts its proarrhythmic influence either by regulating some convergent mechanism that is active in all of these diseases, or by regulating a divergent range of

proarrhythmic mechanisms, which contribute to differing degrees in each disease. To date, the available mechanistic evidence suggests that CaMKII-dependent regulation of diastolic SR Ca^{2+} release is the dominant cellular mechanism by which the kinase promotes arrhythmia (Figure 5.3.A). Of the various CaMKII targets capable of driving this mechanism, RyR2 is the most clearly implicated. This may in part be due to the quality of the tools available for genetically manipulating CaMKII phosphorylation and regulation of RyR2, but it also suggests that developing exogenous compounds capable of impairing the ability of CaMKII to phosphorylate RyR2 could constitute a broadly applicable therapeutic strategy. Additional effects of CaMKII upon I_{Na} and I_{CaL} may also directly contribute to arrhythmia in some contexts (Figure 5.3.B), but in several of the examples described above it appears likely that these effects again converge to elicit arrhythmia via SCR and DADs (Figure 5.3.A).

Both SCR and DADs are generally induced by some form of acute Ca^{2+} overload, and it is probable that this partially explains why CaMKII-dependent arrhythmia most often requires conditions of tachycardia and, notably, β-adrenergic challenge. The involvement of this additional signaling cascade brings in further complexity that is almost certainly important in defining the transition from stable to unstable electrophysiology. As suggested by studies involving the Ankyrin B (+/-) mouse [DNK+12], this may depend on less well-understood aspects of the signaling network, such as local phosphatase balance. As such, strong conclusions regarding any one CaMKII target as being crucial for broad arrhythmia phenotypes should remain contentious until these finer details have been described with some clarity.

Tissue-level effects of CaMKII are also undeniably important, as highlighted by SN dysfunction in heart failure, but beyond these investigations, little direct

evidence is available to describe how CaMKII disrupts normal propagation of the cardiac AP. By incorporating regional heterogeneities in cellular electrophysiology, computational modeling may aide in understanding these tissue level effects provided sufficient experimental data for parameterization and validation are available. The reviews by Onal et al. (2014), Greenstein et al. (2014), and Yaniv and Maltsev (2014) offer a comprehensive survey of previous work modeling CaMKII on the cellular and tissue levels.

5.6 Caveats and Important Future Directions

Even with the wealth of information that has amassed to describe the role of CaMKII in cardiac arrhythmia over the last 20 years, several key aspects either remain challenging or are otherwise conspicuously absent from the existing literature. First, no study has been capable of identifying a gain-of-function mutation in CaMKII that is an independent risk for arrhythmogenic cardiac disease, or indeed, any form of cardiac disease. This is surprising given the data available from studies involving the various CaMKII inhibitors. Second, a key unrealized objective of the CaMKII field is to have more specific CaMKII inhibitors that can be applied acutely and in vivo (see the review from Pellicena and Schulman in this special issue [PS14]). This is particularly true for studies of arrhythmia, where such inhibitors would allow more straightforward translation between cell-based experiments and arrhythmia outcomes in intact animals, and perhaps eventually humans. Indeed, as mentioned above, the tissue-level effects of CaMKII activity and hyperactivity are poorly understood compared to the cellular effects, and one reason for this is the lack of suitably specific small molecule inhibitors. Third, as mentioned with respect to TS, the use of murine

myocytes for cell-based arrhythmia assays probably biases the active mechanisms away from those occurring during repolarization (EADs), and toward those that are active during diastole (DADs). This is because the rapidly repolarizing murine myocyte has markedly increased repolarization reserve, and current dynamics during repolarization that are at least very different to those in large mammals and humans [Ner04]. As techniques for differentiating and reprogramming h-IPSCs improve, models based on this approach may offer a useful new tool for studying the role of CaMKII in congenital arrhythmogenic diseases at least. Examples of early studies in this direction have recently appeared for CPVT [DPLM$^+$13] and TS [YHJ$^+$11]. However, concerns surrounding how well these cells recapitulate adult cardiomyocyte Ca^{2+} handling are particularly poignant in these and other Ca^{2+}-related arrhythmogenic diseases. As such, the evidence supporting myocyte-specific differentiation should be considered carefully and specifically for any such future model.

5.7 Acknowledgments

This work was supported by the National Institutes of Health (1R01HL105242, 1R01HL96544, 8 P41 GM103426, P50 GM094503, Andrew D. McCulloch), postdoctoral fellowships from the American Heart Association and Heart Rhythm Society (Andrew G. Edwards) and an NIH pre-doctoral training grant (T32 EB009380, Kevin P. Vincent).

The content of this chapter is, in full, a reprint of a previously published manuscript with minor edits to fit the format of this dissertation. The citation is Vincent KP, Gonzales MJ, Gillette AK, Villongco CT, Pezzuto S, Omens JH, Holst MJ, McCulloch AD, "High-order finite element methods for cardiac monodomain

simulations", *Front Physiol*, 6:217, 2015. This paper was published with a Creative Commons Attribution License and the authors retain copyright.

Chapter 6

Experimental Techniques and Analytical Methods for Cardiac Optical Mapping

The ability to optically record transmembrane electrical potential in *ex-vivo* hearts with high temporal and spatial resolution has greatly aided the understanding of healthy and pathological cardiac electrophysiology. This experimental technique combines one of the oldest and most impactful cardiac experimental preparations (Langendorff perfusion) with emerging technologies (high speed CMOS cameras and voltage sensitive dyes). In this chapter I will review the basics and some practical considerations for cardiac optical mapping beginning with the isolated heart preparation.

6.1 The Langendorff Perfused Isolated Heart

Building on the isolated frog heart experiments of Carl Ludwig and Elias Cyon at the University of Leipzig, Oscar Langendorff pioneered the first retrograde mammalian heart preparation in 1895 while working at the University of Rostock, Germany [Lan95, Zim98]. Langendorff's eponymous experimental preparation has proven to be a foundational achievement in cardiac physiology, and it continues to enable discovery over a century after his death.

In brief, the heart is excised via thoracotomy and a cannula is inserted into the severed aorta and secured with a suture. A solution (defibrinated cat blood in Langendorff's original experiments) is perfused retrograde into the aorta forcing the aortic valve closed. Pressure develops between the aortic valve and the suture diverting the solution into the coronary ostia at the base of the aorta. The perfusate then flows through the coronary vessels providing oxygen, nutrients and electrolytes to the myocytes before emptying into the right atrium via the coronary sinus. When performed carefully, this technique can keep an *ex-vivo* heart viable for experiments for an hour or longer depending on species. However, the relative ease, modest price and near ubiquity of Langendorff perfusion conceal many potential pitfalls.

Perfusate Solutions

The careful selection and preparation of an asanguineous electrolyte solution is necessary for relevant and reproducible experimental results. As demonstrated recently by Poelzing and colleagues, even small differences in the perfusate cation composition can modulate macroscopic electrophysiological changes in genetically modified mice [GSL$^+$15, GP16, GBZ$^+$16]. The most commonly used contemporary perfusates are

Krebs-Henseleit buffer and Tyrode's solution. Solutions recipes are frequently modified based on animal specifies or experimenter preference, but each is composed of essential electrolytes (e.g., Na^+, K^+, Ca^{2+}, Cl^-, and Mg^{2+}), metabolic substrate (typically D-glucose), and a buffering agent (e.g., bicarbonate or HEPES). Solutions should be prepared with ultra-pure water to prevent impurities and filtered at 0.2 μm to remove bacteria. Although it presents a practical challenge, solutions should be warmed and aerated with the proper gas before the pH is tested and adjusted.

Proper electrolyte balance is necessary to provide accurate extracellular ionic concentrations for cardiomyocytes. Typical extracellular potassium values are between 5-6 mM, but the concentration concentration can increase substantially during ischemia [Klé83]. High extracellular potassium can be useful in cardioplegic solutions to inhibit depolarization or perfusion solutions to suppress spontaneous arrhythmias. However, hyperkalemic solutions alter conduction velocity in a biphasic manner with a small increase in $[K^+]_o$ (up to 8mM) increasing conduction velocity but further increases to $[K^+]_o$ decreasing conduction velocity [NG00]. Typical extracellular sodium values are between 140-150 mM. Decreasing extracellular sodium is known to decrease excitability and reduce conduction velocity [BDE75, YMA$^+$01]. CaAlthough it presents a practical challenge, solutions should be warmed and aerated with the proper gas before the pH is tested and adjusted. concentration is particularly important for studies where calcium dysregulation is expected to be arrhythmogenic. Krebs-Henseleit solution was originally composed with 2.4 mM Ca^{2+} as this is the concentration in whole blood. However, Krebs & Henseleit did not consider that much of the Ca^{2+} is bound to proteins, and free Ca^{2+} levels are lower. A calcium concentration of 1.2-1.8 mM is more typical of contemporary perfusate recipes. Physiological extracellular calcium

concentration for a mouse is on the lower end of that range (1.35 mM) [SSBH03]. EDTA is occasionally added to chelate heavy metals. This will buffer free calcium and must be compensated for when determining the free Ca^{2+} concentration.

D-Glucose (Dextrose) is the most common metabolic substrate in perfusate solutions. However, as Bell et al. point out, glucose is not the preferred metabolic substrate for normoxic myocardium [BMY11]. Fatty acid oxidation is responsible for over 60% of ATP production in human and mouse myocardium [LUF$^+$10]. Belke et al. demonstrated that *ex-vivo* mouse hearts prefer free fatty acids and will derive over 90% of ATP from them if modestly supraphysiological concentrations are included in the perfusate (1.2mM palmitate in perfusate vs. 0.7 mM in mouse plasma)[BLLS99]. However, free fatty acids are poorly suited for aerated solutions due to the tendency to froth. Therefore, glucose is commonly the only metabolic substate as ex-vivo hearts can readily metabolize glucose through glucose oxidation and glycolysis [LUF$^+$10]. Most perfusate recipes include glucose at very high concentrations (11.1 mM compared to 5-6 mM in healthy mouse plasma) which are close to the concentration in mouse models of type II diabetes [BMY11]. The use of glucose as the primary metabolic substrate may not be prudent in models of diabetes, mice with genetically altered metabolic proteins or when metabolism is of particular interest.

Well regulated perfusate pH is essential to maintaining viable and properly functioning myocardium. Perfusion solutions achieve a balanced, physiological pH (7.4) using either bicarbonate, which mimics the innate pH homeostasis mechanism, or organic buffers (i.e., HEPES). Classically, Krebs solutions are bicarbonate buffered and Tyrode's solutions are HEPES buffered. HEPES buffered solutions maintain superior buffering capacity and efficiency at low temperatures (5°C) compared to bicarbonate

buffered solutions and may be better suited for cold cardioplegic solutions [BT02]. Although rarely considered, the choice of buffering agent may impact electrophysiology. Fülöp et al. demonstrated increased action potential duration and decreased calcium transient amplitude with HEPES buffered compared to bicarbonate buffered solution in isolated guinea-pig hearts and canine Purkinje fibers [FSM+03].

Asanguineous solutions have low oxygen carrying capacity due to their lack of hemoglobin. Bicarbonate buffered perfusates must be aerated with carbogen (95% oxygen/5% carbon dioxide) whereas HEPES buffered solutions are aerated with 100% oxygen. Aerating with 95% oxygen results in P_{O2} of >500mmHg, and compensates for the low oxygen carrying capacity of the electrolyte solutions [LPL12].

The use of a crystalloid perfusion solutions rather than whole blood has important physiological effects that should be considered when planning and interpreting experiments. First, asanguineous solutions result in supra-physiological coronary flow rates. Qiu et al. [QH92] demonstrated coronary flow rates over five times greater in crystalloid-perfused compared to blood-perfused isolated rabbit hearts. Thus, the hearts should be considered maximally vasodilated. Second, The lack of serum albumin results in low colloid osmotic pressure. This causes progressive tissue edema that may degrade experiment quality over time.

Temperature

Maintaining a constant physiological temperature of 37°C is essential for a viable experimental preparation. The importance of temperature on heart rate and cardiac function is so fundamental that it was the topic of Langendorff's original paper (this is apparent even without translating it from his native German) [Lan95]. The high

surface area per volume in the mouse heart makes it particularly sensitive to ambient temperature. Sutherland et al. demonstrated that heart rate and developed LV pressure drop precipitously above and below 37°C in the mouse heart [SSBH03]. This is avoided by warming the perfusion solution in jacketed glassware and by submerging the heart in warmed perfusate. Difficulties arise when the perfusate reservoir and the hear perfusion chamber are far apart as is common in passive constant pressure set-ups). The warmed perfusate must travel through almost a meter of tubing before perfusing the heart. If the tubing isn't jacketed or insulated, the perfusate will cool by the time it reaches the heart. Compensating for this by increasing the reservoir temperature will likely over heat the heart perfusion chamber. Additionally, changes in perfusion flow rate will alter the temperature. To avoid this, the tubing should be as short as possible and insulated when possible. The most most reliable experimental set-up will have a temperature control system to actively regulate the temperature throughout an experiment.

Electrical Stimulation

Langendorff perfused hearts spontaneously beat, but many experiments require electrical stimulation of the heart. This includes arrhythmia protocols (e.g., S1-S2 or rapid pacing), anterior LV pacing for conduction velocity measurements, effective refractory period protocols, or pacing at a physiological rate for a more controlled experiment (necessary for APD measurements). Noble metals (e.g., platinum or stainless steel) are preferred over more common AgCl electrodes due to the minimal chemical reactions at their electrode-electrolyte interface [Web09]. Although unipolar stimulation pulses are common, bipolar pulses should be considered when extensive

stimulation is required to minimize electrode erosion. As a practical consideration, it is important that the stimulating and ground electrode be of the same metal and that no solder or joint are exposed to the perfusion bath.

Other Considerations

Rapid excision and cannulation of the heart is essential to obtaining a viable Langendorff preparation. After excision the heart is commonly submerged in a cold cardioplegic solution (low Ca^{2+} and high K^{+}) to suppress spontaneous beating. Sutherland et al. [SSBH03] demonstrated that the cold transfer solutions has little or no effect on heart rate or developed pressure, but they still advocated for regular use of a cold transfer solution.

Finally, Langendorff heart preparations are subject to error and as such, exclusion criteria should be defined prior to experiments. Surgical time, flow rate, and heart rate should all be within normal parameters for reliable and reproducible experiments. The time from heart excision to clearing of the coronaries should be under 5 minutes and ideally closer to 2 minutes. Acceptable coronary flow rates are typically considered >1 mL/min and <5 mL/min. Due to adrenergic stimulus and anesthesia effects during the excision, the heart rate should be allowed to equilibrate for 10-15 minutes. Acceptable heart rates are generally above 300 bpm.

6.2 Optical Mapping of Cardiac Action Potentials

The first successful optical mapping of transmembrane potential was published in 1973 using a merocyanine dye to image the action potential in a giant squid axon [DSCW73], and within three years Salaman and Morad used Merocyanine 540 to

optically map action potentials in bullfrog hearts [SM76]. Since those initial studies, technological advances have propelled optical mapping to become one of the most useful experimental techniques in cardiac research for understanding the coupling between excitation and [ENS04, HLJ12]. Cardiac optical mapping enables the measurement of tissue properties such as total activation time, conduction velocity, and tissue space constant. It also allows the visualization and localization of abnormal electrical activity to better understand arrhythmia initiation, maintenance, and termination. The use of optical mapping in mice has been particularly important due to the malleability of the murine genome.

Potentiometric dyes

Potentiometric dyes are the foundation of optical mapping. These fluorescent molecules embed themselves in the myocyte membrane and their spectral properties are altered by the transmembrane potential. Contemporary dyes exhibit a left shift in their emission spectra that is linearly proportional to the change in membrane potential. The most commonly used dyes are the styrl dyes developed by Leslie Loew and colleagues including di-4-ANEPPS and di-8-ANEPPS [FBL85, LCD$^+$92, GBL94]. The di-4-ANEPPS dye is common for whole heart preparations, but di-8-ANEPPS is more common in cells and monolayers due to reduced phytotoxicity [RS94]. Another common dye is RH237 which was developed by Grinvald and Hildesheim [GHFA82]. RH237 is frequently used in multiparametric experiments as its shares an excitation peak of 540 nm with the intracellular Ca^{2+} dye Rhod-2, but the two dyes have distinct emission peaks[CS00]. RH237 may also be preferable in isolated atrial preparations as di-4-ANEPPS has been shown to alter SA nodal cycle length [GFA$^+$10]

Illumination source and light path

Light emitting diodes (LEDs) have emerged as the preferred light source for most tissue scale optical mapping applications. Their low cost and ease of use allowed them to quickly overtake xenon and halogen lamps. The specificity of LED emission wavelength can eliminate the need for an excitation filter in some configurations, and the ability of micro-controllers to rapidly switch between different wavelengths makes ratiometric and multiparametric experiments much easier[BGS$^+$11].

Light from the LED passes typically passes through an excitation filter and is reflected off a dichroic mirror. Dichroic mirrors have unique optical properties that allow them to reflect light with a wavelength below a given threshold while longer wavelength light passes through. A dichroic mirror is not needed with certain experimental configurations if the heart is directly illuminated. After the light illuminates the heart, the potentiometric dye emits photons at a longer wavelength. This emitted light passes back through the dichroic mirror to the emission filter. A high quality emission filter that closely matches the emission spectra peak for a chosen dye is essential to obtaining high quality data with a low signal-to-noise ratio.

Uncouplers

Motion artifact is an inherent complication during optical mapping due to the contractile nature of the heart. However, if the total activation time is less that the electro-mechanical delay, the motion can generally be ignored and reliable activation maps can be obtained. Any measurements involving repolarization (e.g., APD or dispersion of repolarization) are require an excitation-contraction uncoupler. Early inhibitors of muscle contraction for optical mapping had pronounced side effects.

Cytochalasin-D, which inhibits actin filament polymerization, reduced conduction velocity, prolonged APD, and altered Ca^{2+} handling [BWC+04]. 2,3 butanedione monoxime, which is a noncompetitive inhibitor of myosin II, also altered action potential duration and conduciton delay [KWC+04].

Blebbistatin has emerged as the preferred excitation-contraction uncoupler thanks to its reduced electrophysiological side effects. Blebbistatin functions by inhibiting myosin-II ATPase [FTM+08], and only the levo-rotary (−) form of blebbistatin is active [EMM+07]. A typical concentration for blebbistatin for optical mapping applications is 10 μM. To avoid the development of crystalline precipitate in the coronary vasculature, the perfusate solution should be warmed above physiological temperature ($\sim$45°C) before adding the blebbistatin. Some investigators still caution that blebbistatin causes important changes to the native electrophysiology [BNWN13]

References

[AA11] Douglas N. Arnold and Gerard Awanou. The Serendipity Family of Finite Elements. *Found Comput Math*, 11(3):337–344, March 2011.

[AA14] Douglas Arnold and Gerard Awanou. Finite element differential forms on cubical meshes. *Math. Comp.*, 83(288):1551–1570, 2014.

[AAM+06] Felipe Atienza, Jesús Almendral, Javier Moreno, Ravi Vaidyanathan, Arkazdi Talkachou, Jérôme Kalifa, Angel Arenal, Julian P Villacastín, Esteban G Torrecilla, and Ana Sánchez. Activation of Inward Rectifier Potassium Channels Accelerates Atrial Fibrillation in Humans Evidence for a Reentrant Mechanism. *Circulation*, 114(23):2434–2442, 2006.

[ABH+13] Takeshi Aiba, Andreas S. Barth, Geoffrey G. Hesketh, Yasmin L. Hashambhoy, Khalid Chakir, Richard S. Tunin, Joseph L. Greenstein, Raimond L. Winslow, David A. Kass, and Gordon F. Tomaselli. Cardiac resynchronization therapy improves altered Na channel gating in canine model of dyssynchronous heart failure. *Circ Arrhythm Electrophysiol*, 6(3):546–54, June 2013.

[ABK12] Christopher J. Arthurs, Martin J. Bishop, and David Kay. Efficient simulation of cardiac electrical propagation using high order finite elements. *J. Comput. Phys.*, 231(10):3946–3962, May 2012.

[ABK13] Christopher J. Arthurs, Martin J. Bishop, and David Kay. Efficient simulation of cardiac electrical propagation using high-order finite elements II: Adaptive p-version. *Journal of Computational Physics*, 253:443–470, November 2013.

[ABSP94] M. E. Anderson, A. P. Braun, H. Schulman, and B. A. Premack. Multifunctional Ca2+/calmodulin-dependent protein kinase mediates Ca(2+)-induced enhancement of the L-type Ca2+ current in rabbit ventricular myocytes. *Circ Res*, 75(5):854–61, November 1994.

[ACS+05] Xun Ai, Jerry W. Curran, Thomas R. Shannon, Donald M. Bers, and Steven M. Pogwizd. Ca2+/calmodulin-dependent protein kinase mod-

ulates cardiac ryanodine receptor phosphorylation and sarcoplasmic reticulum Ca2+ leak in heart failure. *Circ Res*, 97(12):1314–22, December 2005.

[AHB+09] Takeshi Aiba, Geoffrey G. Hesketh, Andreas S. Barth, Ting Liu, Samantapudi Daya, Khalid Chakir, Veronica Lea Dimaano, Theodore P. Abraham, Brian O'Rourke, Fadi G. Akar, David A. Kass, and Gordon F. Tomaselli. Electrophysiological consequences of dyssynchronous heart failure and its restoration by resynchronization therapy. *Circulation*, 119(9):1220–30, March 2009.

[AHG+12] Nicole M. Ashpole, Anthony W. Herren, Kenneth S. Ginsburg, Joseph D. Brogan, Derrick E. Johnson, Theodore R. Cummins, Donald M. Bers, and Andy Hudmon. Ca2+/calmodulin-dependent protein kinase II (CaMKII) regulates cardiac sodium channel NaV1.5 gating by multiple phosphorylation sites. *J Biol Chem*, 287(24):19856–69, June 2012.

[ANC09] Rebecca C. Ahrens-Nicklas and David J. Christini. Anthropomorphizing the mouse cardiac action potential via a novel dynamic clamp method. *Biophys. J.*, 97(10):2684–2692, November 2009.

[Ant06] Charles Antzelevitch. Brugada Syndrome. *Pacing Clin. Electrophysiol.*, 29(10):1130–1159, October 2006.

[APC+07] Charles Antzelevitch, Guido D. Pollevick, Jonathan M. Cordeiro, Oscar Casis, Michael C. Sanguinetti, Yoshiyasu Aizawa, Alejandra Guerchicoff, Ryan Pfeiffer, Antonio Oliva, Bernd Wollnik, Philip Gelber, Elias P. Bonaros, Elena Burashnikov, Yuesheng Wu, John D. Sargent, Stefan Schickel, Ralf Oberheiden, Atul Bhatia, Li-Fern Hsu, Michel Haïssaguerre, Rainer Schimpf, Martin Borggrefe, and Christian Wolpert. Loss-of-Function Mutations in the Cardiac Calcium Channel Underlie a New Clinical Entity Characterized by ST-Segment Elevation, Short QT Intervals, and Sudden Cardiac Death. *Circulation*, 115(4):442–449, January 2007.

[ARR01] F. G. Akar, B. J. Roth, and D. S. Rosenbaum. Optical measurement of cell-to-cell coupling in intact heart using subthreshold electrical stimulation. *Am J Physiol Heart Circ Physiol*, 281(2):H533–42, August 2001.

[ASKV+11] Jazmin Aguado-Sierra, Adarsh Krishnamurthy, Christopher Villongco, Joyce Chuang, Elliot Howard, Matthew J. Gonzales, Jeff Omens, David E. Krummen, Sanjiv Narayan, Roy C. P. Kerckhoffs, and Andrew D. McCulloch. Patient-specific modeling of dyssynchronous heart failure: A case study. *Prog Biophys Mol Biol*, 107(1):147–55, October 2011.

[AUGC10] Aintzane Alday, Janire Urrutia, Monica Gallego, and Oscar Casis. α1-Adrenoreceptors regulate only the caveolae-located subpopulation of cardiac KV4 channels. *Channels*, 4(3):168–178, May 2010.

[BDB+07] Ravi Balijepalli, Brian Delisle, Sadguna Y. Balijepalli, Jason D. Foell, Jessica K. Slind, Timothy J. Kamp, and Craig T. January. Kv11.1 (ERG1) K+ Channels Localize in Cholesterol and Sphingolipid Enriched Membranes and Are Modulated by Membrane Cholesterol. *Channels*, 1(4):263–272, July 2007.

[BDE75] F. Ballantyne, L. D. Davis, and Reynolds Ew. Cellular basis for reversal of hyperkalemic electrocardiographic changes by sodium. *Am. J. Physiol. – Leg. Content*, 229(4):935–940, October 1975.

[Ber01] Donald M. Bers. *Excitation-Contraction Coupling and Cardiac Contractile Force*. Springer Science & Business Media, August 2001. Google-Books-ID: 00PLwEsg1ccC.

[BF11] Anna Biernacka and Nikolaos G Frangogiannis. Aging and Cardiac Fibrosis. *Aging Dis*, 2(2):158–173, March 2011.

[BFB+11] Jabe M. Best, Jason D. Foell, Courtney R. Buss, Brian P. Delisle, Ravi C. Balijepalli, Craig T. January, and Timothy J. Kamp. Small GTPase Rab11b regulates degradation of surface membrane L-type Cav1.2 channels. *Am. J. Physiol. - Cell Physiol.*, 300(5):C1023–C1033, May 2011.

[BFH+06a] Ravi C. Balijepalli, Jason D. Foell, Duane D. Hall, Johannes W. Hell, and Timothy J. Kamp. Localization of cardiac L-type Ca(2+) channels to a caveolar macromolecular signaling complex is required for beta(2)-adrenergic regulation. *Proc. Natl. Acad. Sci. U.S.A.*, 103(19):7500–7505, May 2006.

[BFH+06b] Ravi C. Balijepalli, Jason D. Foell, Duane D. Hall, Johannes W. Hell, and Timothy J. Kamp. Localization of cardiac L-type Ca2+ channels to a caveolar macromolecular signaling complex is required for β2-adrenergic regulation. *PNAS*, 103(19):7500–7505, September 2006.

[BFW+08] Ravi C. Balijepalli, Jason D. Foell, Jing Wang, Jabe M. Best, and Timothy J. Kamp. Targeting of CaV1.2 Channels to Caveolae Requires CaVβ Subunit Association with Caveolin-3 in the Cardiomyocytes. *Circulation*, 118(Suppl 18):S_339–S_339, October 2008.

[BG09a] Donald M. Bers and Eleonora Grandi. Calcium/calmodulin-dependent kinase II regulation of cardiac ion channels. *J Cardiovasc Pharmacol*, 54(3):180–7, September 2009.

[BG09b] Donald M. Bers and Eleonora Grandi. CaMKII regulation of cardiac ion channels. *J. Cardiovasc. Pharmacol.*, 54(3):180, 2009.

[BGR+04] Andrea Barbuti, Biagio Gravante, Monica Riolfo, Raffaella Milanesi, Benedetta Terragni, and Dario DiFrancesco. Localization of pacemaker channels in lipid rafts regulates channel kinetics. *Circ. Res.*, 94(10):1325–1331, May 2004.

[BGS+11] A. D. Bachtel, R. A. Gray, J. M. Stohlman, E. B. Bourgeois, A. E. Pollard, and J. M. Rogers. A Novel Approach to Dual Excitation Ratiometric Optical Mapping of Cardiac Action Potentials With Di-4-ANEPPS Using Pulsed LED Excitation. *IEEE Trans. Biomed. Eng.*, 58(7):2120–2126, July 2011.

[BH82] Alexander N. Brooks and Thomas J. R. Hughes. Streamline upwind/Petrov-Galerkin formulations for convection dominated flows with particular emphasis on the incompressible Navier-Stokes equations. *Computer Methods in Applied Mechanics and Engineering*, 32(1):199–259, September 1982.

[BJ98] Omer Berenfeld and José Jalife. Purkinje-Muscle Reentry as a Mechanism of Polymorphic Ventricular Arrhythmias in a 3-Dimensional Model of the Ventricles. *Circ. Res.*, 82(10):1063–1077, June 1998.

[BKov] Ravi C. Balijepalli and Timothy J. Kamp. Caveolae, ion channels and cardiac arrhythmias. *Prog. Biophys. Mol. Biol.*, 98(2-3):149–160, 2008 Oct-Nov.

[BLLS99] Darrell D. Belke, Terje S. Larsen, Gary D. Lopaschuk, and David L. Severson. Glucose and fatty acid metabolism in the isolated working mouse heart. *Am. J. Physiol. - Regul. Integr. Comp. Physiol.*, 277(4):R1210–R1217, October 1999.

[BM70] J. Thomas Bigger and William J. Mandel. Effect of lidocaine on the electrophysiological properties of ventricular muscle and Purkinje fibers. *J Clin Invest*, 49(1):63–77, January 1970.

[BMY11] Robert M. Bell, Mihaela M. Mocanu, and Derek M. Yellon. Retrograde heart perfusion: The Langendorff technique of isolated heart perfusion. *J. Mol. Cell. Cardiol.*, 50(6):940–950, June 2011.

[BNE93] D. J. Beuckelmann, M. Näbauer, and E. Erdmann. Alterations of K+ currents in isolated human ventricular myocytes from patients with terminal heart failure. *Circ. Res.*, 73(2):379–385, August 1993.

[BNWN13] Kieran E. Brack, Ravi Narang, James Winter, and G. André Ng. The mechanical uncoupler blebbistatin is associated with significant electrophysiological effects in the isolated rabbit heart. *Exp Physiol*, 98(5):1009–27, May 2013.

[BOCF08] Alfonso Bueno-Orovio, Elizabeth M. Cherry, and Flavio H. Fenton. Minimal model for human ventricular action potentials in tissue. *J Theor Biol*, 253(3):544–60, August 2008.

[BPR+17] M. S. Bohnen, G. Peng, S. H. Robey, C. Terrenoire, V. Iyer, K. J. Sampson, and R. S. Kass. Molecular Pathophysiology of Congenital Long QT Syndrome. *Physiol. Rev.*, 97(1):89–134, January 2017.

[BPW14] Doug Bruce, Pras Pathmanathan, and Jonathan P. Whiteley. Modelling the Effect of Gap Junctions on Tissue-Level Cardiac Electrophysiology. *Bull Math Biol*, 76(2):431–454, February 2014.

[BR77] G. W. Beeler and H. Reuter. Reconstruction of the action potential of ventricular myocardial fibres. *J. Physiol. (Lond.)*, 268(1):177–210, June 1977.

[BSB+06] Johannes Backs, Kunhua Song, Svetlana Bezprozvannaya, Shurong Chang, and Eric N. Olson. CaM kinase II selectively signals to histone deacetylase 4 during cardiomyocyte hypertrophy. *J Clin Invest*, 116(7):1853–64, July 2006.

[BSD+11] David Benoist, Rachel Stones, Mark Drinkhill, Olivier Bernus, and Ed White. Arrhythmogenic substrate in hearts of rats with monocrotaline-induced pulmonary hypertension and right ventricular hypertrophy. *Am. J. Physiol. Heart Circ. Physiol.*, 300(6):H2230–2237, June 2011.

[BT02] Simona C Baicu and Michael J Taylor. Acid–base buffering in organ preservation solutions as a function of temperature: New parameters for comparing buffer capacity and efficiency. *Cryobiology*, 45(1):33–48, August 2002.

[BT08] Curtis F. Barrett and Richard W. Tsien. The Timothy syndrome mutation differentially affects voltage- and calcium-dependent inactivation of CaV1.2 L-type calcium channels. *Proc Natl Acad Sci U A*, 105(6):2157–62, February 2008.

[BTJKH02a] Julie Bossuyt, Bonnie E. Taylor, Marilyn James-Kracke, and Calvin C. Hale. The cardiac sodium-calcium exchanger associates with caveolin-3. *Ann. N. Y. Acad. Sci.*, 976:197–204, November 2002.

[BTJKH02b] Julie Bossuyt, Bonnie E. Taylor, Marilyn James-Kracke, and Calvin C. Hale. Evidence for cardiac sodium-calcium exchanger association with caveolin-3. *FEBS Lett.*, 511(1-3):113–117, January 2002.

[BTT+11] Andriy E. Belevych, Dmitry Terentyev, Radmila Terentyeva, Yoshinori Nishijima, Arun Sridhar, Robert L. Hamlin, Cynthia A. Carnes, and Sandor Györke. The relationship between arrhythmogenesis and impaired contractility in heart failure: Role of altered ryanodine receptor function. *Cardiovasc Res*, 90(3):493–502, June 2011.

[BVP02] Olivier Bernus, Henri Verschelde, and Alexander V. Panfilov. Modified ionic models of cardiac tissue for efficient large scale computations. *Phys Med Biol*, 47(11):1947–1959, June 2002.

[BVPD14] James R. Bell, Martin Vila-Petroff, and Lea M. D. Delbridge. CaMKII-dependent responses to ischemia and reperfusion challenges in the heart. *Front Pharmacol*, 5, May 2014.

[BWC+04] Linda C. Baker, Robert Wolk, Bum-Rak Choi, Simon Watkins, Patricia Plan, Anisha Shah, and Guy Salama. Effects of mechanical uncouplers, diacetyl monoxime, and cytochalasin-D on the electrophysiology of perfused mouse hearts. *Am. J. Physiol. - Heart Circ. Physiol.*, 287(4):H1771–H1779, October 2004.

[CBS+10] Jerry Curran, Kathy Hayes Brown, Demetrio J. Santiago, Steve Pogwizd, Donald M. Bers, and Thomas R. Shannon. Spontaneous Ca waves in ventricular myocytes from failing hearts depend on Ca(2+)-calmodulin-dependent protein kinase II. *J Mol Cell Cardiol*, 49(1):25–32, July 2010.

[CBW+04] T Christ, P Boknik, S Wöhrl, E Wettwer, EM Graf, RF Bosch, M Knaut, W Schmitz, U Ravens, and D Dobrev. L-type Ca2+ current downregulation in chronic human atrial fibrillation is associated with increased activity of protein phosphatases. *Circulation*, 110(17):2651–2657, 2004.

[CDT+08] Khalid Chakir, Samantapudi K. Daya, Richard S. Tunin, Robert H. Helm, Melissa J. Byrne, Veronica L. Dimaano, Albert C. Lardo, Theodore P. Abraham, Gordon F. Tomaselli, and David A. Kass. Reversal of global apoptosis and regional stress kinase activation by cardiac resynchronization. *Circulation*, 117(11):1369–77, March 2008.

[CENF07] E. M. Cherry, J. R. Ehrlich, S. Nattel, and F. H. Fenton. Pulmonary vein reentry–properties and size matter: Insights from a computational analysis. *Heart rhythm : the official journal of the Heart Rhythm Society*, 4(12):1553–62, December 2007.

[CF04] Elizabeth M. Cherry and Flavio H. Fenton. Suppression of alternans and conduction blocks despite steep APD restitution: Electrotonic, memory, and conduction velocity restitution effects. *Am. J. Physiol. Heart Circ. Physiol.*, 286(6):H2332–2341, June 2004.

[CGS87] S. E. Campbell, A. M. Gerdes, and T. D. Smith. Comparison of regional differences in cardiac myocyte dimensions in rats, hamsters, and guinea pigs. *Anat. Rec.*, 219(1):53–59, September 1987.

[CGT+09] Natalie J. Chandler, Ian D. Greener, James O. Tellez, Shin Inada, Hanny Musa, Peter Molenaar, Dario Difrancesco, Mirko Baruscotti, Renato Longhi, Robert H. Anderson, Rudolf Billeter, Vinod Sharma, Daniel C. Sigg, Mark R. Boyett, and Halina Dobrzynski. Molecular architecture of the human sinus node: Insights into the function of the cardiac pacemaker. *Circulation*, 119(12):1562–75, March 2009.

[CHAS+09] Stuart G. Campbell, Elliot Howard, Jazmin Aguado-Sierra, Benjamin A. Coppola, Jeffrey H. Omens, Lawrence J. Mulligan, Andrew D. McCulloch, and Roy C. P. Kerckhoffs. Effect of transmurally heterogeneous myocyte excitation-contraction coupling on canine left ventricular electromechanics. *Exp. Physiol.*, 94(5):541–552, May 2009.

[CHR+13] Caroline Mendonca Costa, Elena Hoetzl, Bernardo Martins Rocha, Anton J. Prassl, and Gernot Plank. Automatic Parameterization Strategy for Cardiac Electrophysiology Simulations. *Comput Cardiol (2010)*, 40:373–376, October 2013.

[CHSL04] Alex W. Cohen, Robert Hnasko, William Schubert, and Michael P. Lisanti. Role of caveolae and caveolins in health and disease. *Physiol. Rev.*, 84(4):1341–1379, October 2004.

[CHW+96] K. D. Costa, P. J. Hunter, J. S. Wayne, L. K. Waldman, J. M. Guccione, and A. D. McCulloch. A three-dimensional finite element method for large elastic deformations of ventricular myocardium: II–Prolate spheroidal coordinates. *J Biomech Eng*, 118(4):464–472, November 1996.

[CK08] Elizabeth D. Copene and James P. Keener. Ephaptic coupling of cardiac cells through the junctional electric potential. *J. Math. Biol.*, 57(2):265–284, August 2008.

[Cle76] L. Clerc. Directional differences of impulse spread in trabecular muscle from mammalian heart. *J. Physiol. (Lond.)*, 255(2):335–346, February 1976.

[CMBD12] Emmanuel Camors, Peter J. Mohler, Donald M. Bers, and Sanda Despa. Ankyrin-B reduction enhances Ca spark-mediated SR Ca release promot-

ing cardiac myocyte arrhythmic activity. *J Mol Cell Cardiol*, 52(6):1240–8, June 2012.

[CN11] P. Comtois and S. Nattel. Impact of tissue geometry on simulated cholinergic atrial fibrillation: A modeling study. *Chaos Interdiscip. J. Nonlinear Sci.*, 21(1):013108–013108–13, 2011.

[CNP12] Marina Cerrone, Carlo Napolitano, and Silvia G. Priori. Genetics of ion-channel disorders. *Curr Opin Cardiol*, 27(3):242–52, May 2012.

[CO06] Chantal E. Conrath and Tobias Opthof. Ventricular repolarization: An overview of (patho)physiology, sympathetic effects and genetic aspects. *Prog. Biophys. Mol. Biol.*, 92(3):269–307, November 2006.

[CP08] R. H. Clayton and A. V. Panfilov. A guide to modelling cardiac electrical activity in anatomically detailed ventricles. *Prog. Biophys. Mol. Biol.*, 96(1-3):19–43, Jan-Apr 2008.

[CRN98] Marc Courtemanche, Rafael J Ramirez, and Stanley Nattel. Ionic mechanisms underlying human atrial action potential properties: Insights from a mathematical model. *Am. J. Physiol.-Heart Circ. Physiol.*, 275(1):H301–H321, 1998.

[CS00] Bum-Rak Choi and Guy Salama. Simultaneous maps of optical action potentials and calcium transients in guinea-pig hearts: Mechanisms underlying concordant alternans. *J Physiol*, 529(Pt 1):171–188, November 2000.

[CSP+15] Fernando O. Campos, Yohannes Shiferaw, Anton J. Prassl, Patrick M. Boyle, Edward J. Vigmond, and Gernot Plank. Stochastic spontaneous calcium release events trigger premature ventricular complexes by overcoming electrotonic load. *Cardiovasc. Res.*, 107(1):175–183, July 2015.

[CST+95] Mark E. Curran, Igor Splawski, Katherine W. Timothy, G. Michael Vincen, Eric D. Green, and Mark T. Keating. A molecular basis for cardiac arrhythmia: HERG mutations cause long QT syndrome. *Cell*, 80(5):795 – 803, 1995.

[CV14] Emmanuel Camors and Héctor H. Valdivia. CaMKII regulation of cardiac ryanodine receptors and inositol triphosphate receptors. *Front. Pharmacol.*, 5:101, 2014.

[CVV+13] Jianding Cheng, Carmen R. Valdivia, Ravi Vaidyanathan, Ravi C. Balijepalli, Michael J. Ackerman, and Jonathan C. Makielski. Caveolin-3 suppresses late sodium current by inhibiting nNOS-dependent S-nitrosylation of SCN5A. *J. Mol. Cell. Cardiol.*, 61:102–110, August 2013.

[CXL+12] Jun Cheng, Lin Xu, Dongwu Lai, Arnaud Guilbert, Hyun Joung Lim, Thitima Keskanokwong, and Yanggan Wang. CaMKII inhibition in heart failure, beneficial, harmful, or both. *Am J Physiol Heart Circ Physiol*, 302(7):H1454–65, April 2012.

[CYK+07] Lisa B. Cronk, Bin Ye, Toshihiko Kaku, David J. Tester, Matteo Vatta, Jonathan C. Makielski, and Michael J. Ackerman. Novel mechanism for sudden infant death syndrome: Persistent late sodium current secondary to mutations in caveolin-3. *Heart Rhythm*, 4(2):161–166, February 2007.

[CYK+14] Chris D. Cantwell, Sergey Yakovlev, Robert M. Kirby, Nicholas S. Peters, and Spencer J. Sherwin. High-order spectral/hp element discretisation for reaction-diffusion problems on surfaces: Application to cardiac electrophysiology. *J Comput Phys*, 257(PA):813–829, January 2014.

[CYN+11] Edward P. Cheng, Can Yuan, Manuel F. Navedo, Rose E. Dixon, Madeline Nieves-Cintrón, John D. Scott, and Luis F. Santana. Restoration of normal L-type Ca2+ channel function during Timothy syndrome by ablation of an anchoring protein. *Circ Res*, 109(3):255–61, July 2011.

[DBVP13] H. Dierckx, E. Brisard, H. Verschelde, and A. V. Panfilov. Drift laws for spiral waves on curved anisotropic surfaces. *Physical review. E, Statistical, nonlinear, and soft matter physics*, 88(1):012908, July 2013.

[DDY+14] Benjamin M. L. Drum, Rose E. Dixon, Can Yuan, Edward P. Cheng, and Luis F. Santana. Cellular mechanisms of ventricular arrhythmias in a mouse model of Timothy syndrome (long QT syndrome 8). *J Mol Cell Cardiol*, 66:63–71, January 2014.

[DeS97] Regis A. DeSilva. George Ralph Mines, Ventricular Fibrillation and the Discovery of the Vulnerable Period1. *Journal of the American College of Cardiology*, 29(6):1397–1402, May 1997.

[DNK+12] Sean DeGrande, Derek Nixon, Olha Koval, Jerald W. Curran, Patrick Wright, Qiongling Wang, Farshid Kashef, David Chiang, Na Li, Xander H. T. Wehrens, Mark E. Anderson, Thomas J. Hund, and Peter J. Mohler. CaMKII inhibition rescues proarrhythmic phenotypes in the model of human ankyrin-B syndrome. *Heart Rhythm*, 9(12):2034–41, December 2012.

[DPLM+13] E. Di Pasquale, F. Lodola, M. Miragoli, M. Denegri, J. E. Avelino-Cruz, M. Buonocore, H. Nakahama, P. Portararo, R. Bloise, C. Napolitano, G. Condorelli, and S. G. Priori. CaMKII inhibition rectifies arrhythmic phenotype in a patient-specific model of catecholaminergic polymorphic ventricular tachycardia. *Cell Death Dis*, 4:e843, 2013.

[DRL+08] Stephan B. Danik, Gregg Rosner, Joshua Lader, David E. Gutstein, Glenn I. Fishman, and Gregory E. Morley. Electrical remodeling contributes to complex tachyarrhythmias in connexin43-deficient mouse hearts. *FASEB J*, 22(4):1204–1212, April 2008.

[DSCW73] H. V. Davila, B. M. Salzberg, L. B. Cohen, and A. S. Waggoner. A Large Change in Axon Fluorescence that Provides a Promising Method for Measuring Membrane Potential. *Nature*, 241(109):159–160, January 1973.

[DSN+11] Nataliya Dybkova, Simon Sedej, Carlo Napolitano, Stefan Neef, Adam G. Rokita, Mark Hünlich, Joan Heller Brown, Jens Kockskämper, Silvia G. Priori, Burkert Pieske, and Lars S. Maier. Overexpression of CaMKIIδc in RyR2R4496C+/- Knock-In Mice Leads to Altered Intracellular Ca2+ Handling and Increased Mortality. *Journal of the American College of Cardiology*, 57(4):469–479, January 2011.

[DSS+14] Stefan Dhein, Thomas Seidel, Aida Salameh, Joanna Jozwiak, Anja Hagen, Martin Kostelka, Gerd Hindricks, and Friedrich-Wilhelm Mohr. Remodeling of cardiac passive electrical properties and susceptibility to ventricular and atrial arrhythmias. *Front Physiol*, 5:424, 2014.

[DSW+96] Jane E. Dixon, Wenmei Shi, Hong-Sheng Wang, Christine McDonald, Hangang Yu, Randy S. Wymore, Ira S. Cohen, and David McKinnon. Role of the Kv4.3 K+ Channel in Ventricular Muscle. *Circ. Res.*, 79(4):659–668, October 1996.

[DVM+13] T. A. Dewland, E. Vittinghoff, M. C. Mandyam, S. R. Heckbert, D. S. Siscovick, P. K. Stein, B. M. Psaty, N. Sotoodehnia, J. S. Gottdiener, and G. M. Marcus. Atrial ectopy as a predictor of incident atrial fibrillation: A cohort study. *Annals of internal medicine*, 159(11):721–8, December 2013.

[DWC+00] I. Dzhura, Y. Wu, R. J. Colbran, J. R. Balser, and M. E. Anderson. Calmodulin kinase determines calcium-dependent facilitation of L-type calcium channels. *Nat Cell Biol*, 2(3):173–7, March 2000.

[dXQ12] Enno de Lange, Yuanfang Xie, and Zhilin Qu. Synchronization of early afterdepolarizations and arrhythmogenesis in heterogeneous cardiac tissue models. *Biophys J*, 103(2):365–73, July 2012.

[DZ91] V. A. Davydov and V. S. Zykov. Kinematics of Spiral Waves on Nonuniformly Curved Surfaces. *Physica D*, 49(1-2):71–74, April 1991.

[EGH+14] Andrew G. Edwards, Eleonora Grandi, Johan E. Hake, Sonia Patel, Pan Li, Shigeki Miyamoto, Jeffrey H. Omens, Joan Heller Brown, Donald M.

Bers, and Andrew D. McCulloch. Non-Equilibrium Reactivation of Na+ Current Drives Early Afterdepolarizations in Mouse Ventricle. *Circ. Arrhythm. Electrophysiol.*, page CIRCEP.113.001666, September 2014.

[EHBN+09] Saïd El-Haou, Elise Balse, Nathalie Neyroud, Gilles Dilanian, Bruno Gavillet, Hugues Abriel, Alain Coulombe, Andreas Jeromin, and Stéphane N. Hatem. Kv4 potassium channels form a tripartite complex with the anchoring protein SAP97 and CaMKII in cardiac myocytes. *Circ Res*, 104(6):758–69, March 2009.

[ELG+06] Christian Erxleben, Yanhong Liao, Saverio Gentile, David Chin, Claudio Gomez-Alegria, Yasuo Mori, Lutz Birnbaumer, and David L. Armstrong. Cyclosporin and Timothy syndrome increase mode 2 gating of CaV1.2 calcium channels through aberrant phosphorylation of S6 helices. *Proc Natl Acad Sci U A*, 103(10):3932–7, March 2006.

[ELM+91] D. S. Echt, P. R. Liebson, L. B. Mitchell, R. W. Peters, D. Obias-Manno, A. H. Barker, D. Arensberg, A. Baker, L. Friedman, and H. L. Greene. Mortality and morbidity in patients receiving encainide, flecainide, or placebo. The Cardiac Arrhythmia Suppression Trial. *N. Engl. J. Med.*, 324(12):781–788, March 1991.

[ELY+01] Benjamin C. Eloff, Deborah L. Lerner, Kathryn A. Yamada, Richard B. Schuessler, Jeffrey E. Saffitz, and David S. Rosenbaum. High resolution optical mapping reveals conduction slowing in connexin43 deficient mice. *Cardiovasc. Res.*, 51(4):681–690, September 2001.

[EMM+07] Thomas J. Eddinger, Daniel P. Meer, Amy S. Miner, Joel Meehl, Arthur S. Rovner, and Paul H. Ratz. Potent Inhibition of Arterial Smooth Muscle Tonic Contractions by the Selective Myosin II Inhibitor, Blebbistatin. *J Pharmacol Exp Ther*, 320(2):865–870, February 2007.

[ENS04] Igor R. Efimov, Vladimir P. Nikolski, and Guy Salama. Optical Imaging of the Heart. *Circ Res*, 95(1):21–33, September 2004.

[Eri14] Jeffrey R. Erickson. Mechanisms of CaMKII activation in the heart. *Front. Pharmacol.*, 5:59, 2014.

[FBD+04] Jason D. Foell, Ravi C. Balijepalli, Brian P. Delisle, Anne Marie R. Yunker, Seth L. Robia, Jeffrey W. Walker, Maureen W. McEnery, Craig T. January, and Timothy J. Kamp. Molecular heterogeneity of calcium channel β-subunits in canine and human heart: Evidence for differential subcellular localization. *Physiol. Genomics*, 17(2):183–200, April 2004.

[FBL85] Eric Fluhler, Valerie G. Burnham, and Leslie M. Loew. Spectra, membrane binding, and potentiometric responses of new charge shift probes. *Biochemistry*, 24(21):5749–5755, October 1985.

[FCHE02] Flavio H. Fenton, Elizabeth M. Cherry, Harold M. Hastings, and Steven J. Evans. Multiple mechanisms of spiral wave breakup in a model of cardiac electrical activity. *Chaos*, 12(3):852–892, September 2002.

[FHH+14] Péter Ferdinandy, Derek J. Hausenloy, Gerd Heusch, Gary F. Baxter, and Rainer Schulz. Interaction of risk factors, comorbidities, and comedications with ischemia/reperfusion injury and cardioprotection by preconditioning, postconditioning, and remote conditioning. *Pharmacol. Rev.*, 66(4):1142–1174, October 2014.

[FHT+13] Thomas H. Fischer, Jonas Herting, Theodor Tirilomis, André Renner, Stefan Neef, Karl Toischer, David Ellenberger, Anna Förster, Jan D. Schmitto, Jan Gummert, Friedrich A. Schöndube, Gerd Hasenfuss, Lars S. Maier, and Samuel Sossalla. Ca2+/calmodulin-dependent protein kinase II and protein kinase A differentially regulate sarcoplasmic reticulum Ca2+ leak in human cardiac pathology. *Circulation*, 128(9):970–981, August 2013.

[FK98] Flavio Fenton and Alain Karma. Vortex dynamics in three-dimensional continuous myocardium with fiber rotation: Filament instability and fibrillation. *Chaos*, 8(1):20–47, March 1998.

[FNM13] Thomas H. Fischer, Stefan Neef, and Lars S. Maier. The Ca-calmodulin dependent kinase II: A promising target for future antiarrhythmic therapies? *J Mol Cell Cardiol*, 58:182–7, May 2013.

[FRv+14] Magda S. C. Fontes, Antonia J. A. Raaijmakers, Tessa van Doorn, Bart Kok, Sylvia Nieuwenhuis, Roel van der Nagel, Marc A. Vos, Teun P. de Boer, Harold V. M. van Rijen, and Marti F. A. Bierhuizen. Changes in Cx43 and NaV1.5 expression precede the occurrence of substantial fibrosis in calcineurin-induced murine cardiac hypertrophy. *PLoS ONE*, 9(1):e87226, 2014.

[FSM+03] L. Fülöp, G. Szigeti, J. Magyar, N. Szentandrássy, T. Ivanics, Z. Miklós, L. Ligeti, A. Kovács, G. Szénási, L. Csernoch, P. P. Nánási, and T. Bányász. Differences in electrophysiological and contractile properties of mammalian cardiac tissues bathed in bicarbonate - and HEPES-buffered solutions. *Acta Physiol. Scand.*, 178(1):11–18, May 2003.

[FTM+08] Gerrie P. Farman, Kittipong Tachampa, Ryan Mateja, Olivier Cazorla, Alain Lacampagne, and Pieter P. de Tombe. Blebbistatin: Use as inhibitor of muscle contraction. *Pflugers Arch.*, 455(6):995–1005, March 2008.

[Fvdv12] Magda S. C. Fontes, Toon A. B. van Veen, Jacques M. T. de Bakker, and Harold V. M. van Rijen. Functional consequences of abnormal Cx43 expression in the heart. *Biochim. Biophys. Acta*, 1818(8):2020–2029, August 2012.

[Gab71] G. Gabella. Relationship between sarcoplasmic reticulum and caveolae intracellulares in the intestinal smooth muscle. *J. Physiol. (Lond.)*, 216(1):42P–44P, July 1971.

[Gar14] Walter E. Garrey. The nature of fibrillary contraction of the heart.—Its relation to tissue mass and form. *Am. J. Physiol.*, 33:397–414, March 1914.

[GBBAN97] Rania Gaspo, Ralph F Bosch, Elias Bou-Abboud, and Stanley Nattel. Tachycardia-induced changes in Na+ current in a chronic dog model of atrial fibrillation. *Circ. Res.*, 81(6):1045–1052, 1997.

[GBGS+11] Michael R. Gold, Ulrika Birgersdotter-Green, Jagmeet P. Singh, Kenneth A. Ellenbogen, Yinghong Yu, Timothy E. Meyer, Milan Seth, and Patrick J. Tchou. The relationship between ventricular electrical delay and left ventricular remodelling with cardiac resynchronization therapy. *Eur. Heart J.*, 32(20):2516–2524, October 2011.

[GBL94] E. Gross, R. S. Bedlack, and L. M. Loew. Dual-wavelength ratiometric fluorescence measurement of the membrane dipole potential. *Biophys J*, 67(1):208–216, July 1994.

[GBZ+16] Sharon A. George, Mohammad Bonakdar, Michael Zeitz, Rafael V. Davalos, James W. Smyth, and Steven Poelzing. Extracellular sodium dependence of the conduction velocity-calcium relationship: Evidence of ephaptic self-attenuation. *Am. J. Physiol. - Heart Circ. Physiol.*, 310(9):H1129–H1139, May 2016.

[GCJ+10] Zhan Gao, Biyi Chen, Mei-ling A. Joiner, Yuejin Wu, Xiaoqun Guan, Olha M. Koval, Ashok K. Chaudhary, Shane R. Cunha, Peter J. Mohler, James B. Martins, Long-Sheng Song, and Mark E. Anderson. If and SR Ca2+ release both contribute to pacemaker activity in canine sinoatrial node cells. *Journal of Molecular and Cellular Cardiology*, 49(1):33–40, July 2010.

[GCKN00] Ihor Gussak, Bernard R. Chaitman, Stephen L. Kopecky, and Jeanne M. Nerbonne. Rapid Ventricular Repolarization in Rodents: Electrocardiographic Manifestations, Molecular Mechanisms, and Clinical Insights. *Journal of Electrocardiology*, 33(2):159–170, April 2000.

[GFA+10] Alexey V. Glukhov, Vadim V. Fedorov, Mark E. Anderson, Peter J. Mohler, and Igor R. Efimov. Functional anatomy of the murine sinus

node: High-resolution optical mapping of ankyrin-B heterozygous mice. *Am. J. Physiol. - Heart Circ. Physiol.*, 299(2):H482–H491, August 2010.

[GH14] Eleonora Grandi and Anthony W. Herren. CaMKII-dependent regulation of cardiac Na(+) homeostasis. *Front Pharmacol*, 5:41, 2014.

[GHB14] Charles Burdis Burns Gray and Joan Heller Brown. CaMKIIdelta subtypes: Localization and function. *Front. Pharmacol.*, 5:15, 2014.

[GHFA82] A Grinvald, R Hildesheim, I C Farber, and L Anglister. Improved fluorescent probes for the measurement of rapid changes in membrane potential. *Biophys J*, 39(3):301–308, September 1982.

[Gil14] Andrew Gillette. Hermite and Bernstein style basis functions for cubic serendipity spaces on squares and cubes. In Gregory E. Fasshauer and Larry L. Schumaker, editors, *Approximation Theory XIV: San Antonio 2013*, pages 103–121. Springer, New York, June 2014. Google-Books-ID: f6vIAwAAQBAJ.

[GKK+15] Tanush Gupta, Sahil Khera, Dhaval Kolte, Wilbert S. Aronow, and Sei Iwai. Antiarrhythmic properties of ranolazine: A review of the current evidence. *International Journal of Cardiology*, 187:66–74, May 2015.

[GKM+92] A. M. Gerdes, S. E. Kellerman, J. A. Moore, K. E. Muffly, L. C. Clark, P. Y. Reaves, K. B. Malec, P. P. McKeown, and D. D. Schocken. Structural remodeling of cardiac myocytes in patients with ischemic cardiomyopathy. *Circulation*, 86(2):426–430, August 1992.

[GL81] Philip M. Gresho and Robert L. Lee. Don't suppress the wiggles—They're telling you something! *Computers & Fluids*, 9(2):223–253, June 1981.

[GLBS+07] Nathalie Gaborit, Sabrina Le Bouter, Viktoria Szuts, Andras Varro, Denis Escande, Stanley Nattel, and Sophie Demolombe. Regional and tissue specific transcript signatures of ion channel genes in the non-diseased human heart. *J. Physiol. (Lond.)*, 582(Pt 2):675–693, July 2007.

[GMR+09] Betti Giusti, Marina Marini, Luciana Rossi, Ilaria Lapini, Alberto Magi, Andrea Capalbo, Rosa Lapalombella, Simona di Tullio, Michele Samaja, Fabio Esposito, Vittoria Margonato, Maria Boddi, Rosanna Abbate, and Arsenio Veicsteinas. Gene expression profile of rat left ventricles reveals persisting changes following chronic mild exercise protocol: Implications for cardioprotection. *BMC Genomics*, 10:342, July 2009.

[GMT+01] David E. Gutstein, Gregory E. Morley, Houman Tamaddon, Dhananjay Vaidya, Michael D. Schneider, Ju Chen, Kenneth R. Chien, Heidi

Stuhlmann, and Glenn I. Fishman. Conduction Slowing and Sudden Arrhythmic Death in Mice With Cardiac-Restricted Inactivation of Connexin43. *Circ. Res.*, 88(3):333–339, February 2001.

[GP16] Sharon A. George and Steven Poelzing. Cardiac conduction in isolated hearts of genetically modified mice – Connexin43 and salts. *Progress in Biophysics and Molecular Biology*, 120(1–3):189–198, January 2016.

[GS97] D. Gottlieb and C. Shu. On the Gibbs Phenomenon and Its Resolution. *SIAM Rev.*, 39(4):644–668, January 1997.

[GSK+13] Matthew J. Gonzales, Gregory Sturgeon, Adarsh Krishnamurthy, Johan Hake, René Jonas, Paul Stark, Wouter-Jan J. Rappel, Sanjiv M. Narayan, Yongjie Zhang, W. Paul Segars, and Andrew D. McCulloch. A three-dimensional finite element model of human atrial anatomy: New methods for cubic Hermite meshes with extraordinary vertices. *Med Image Anal*, 17(5):525–37, July 2013.

[GSL+15] Sharon A. George, Katherine J. Sciuto, Joyce Lin, Mohamed E. Salama, James P. Keener, Robert G. Gourdie, and Steven Poelzing. Extracellular sodium and potassium levels modulate cardiac conduction in mice heterozygous null for the Connexin43 gene. *Pflugers Arch*, March 2015.

[GSR+11] Luis A. Gonano, Marisa Sepúlveda, Yanina Rico, Marcia Kaetzel, Carlos A. Valverde, John Dedman, Alicia Mattiazzi, and Martin Vila Petroff. Calcium-calmodulin kinase II mediates digitalis-induced arrhythmias. *Circ Arrhythm Electrophysiol*, 4(6):947–57, December 2011.

[GXLN99] Weinong Guo, Haodong Xu, Barry London, and Jeanne M. Nerbonne. Molecular basis of transient outward K+ current diversity in mouse ventricular myocytes. *J. Physiol.*, 521(3):587–599, December 1999.

[GZMB06] Tao Guo, Tong Zhang, Ruben Mestril, and Donald M. Bers. Ca2+/Calmodulin-dependent protein kinase II phosphorylation of ryanodine receptor does affect calcium sparks in mouse ventricular myocytes. *Circ Res*, 99(4):398–406, August 2006.

[HBG13] Anthony W. Herren, Donald M. Bers, and Eleonora Grandi. Post-translational modifications of the cardiac Na channel: Contribution of CaMKII-dependent phosphorylation to acquired arrhythmias. *Am J Physiol Heart Circ Physiol*, 305(4):H431–45, August 2013.

[HCCS90] R. H. Hoyt, M. L. Cohen, P. B. Corr, and J. E. Saffitz. Alterations of intercellular junctions induced by hypoxia in canine myocardium. *Am. J. Physiol. - Heart Circ. Physiol.*, 258(5):H1439–H1448, May 1990.

[HDK+11] Sabine Huke, Jaime Desantiago, Marcia A. Kaetzel, Shikha Mishra, Joan H. Brown, John R. Dedman, and Donald M. Bers. SR-targeted CaMKII inhibition improves SR $Ca^{2\$}$+ handling, but accelerates cardiac remodeling in mice overexpressing CaMKIIδC. *J Mol Cell Cardiol*, 50(1):230–8, January 2011.

[Heu15] Gerd Heusch. Molecular basis of cardioprotection: Signal transduction in ischemic pre-, post-, and remote conditioning. *Circ. Res.*, 116(4):674–699, February 2015.

[HGW10] Yasmin L. Hashambhoy, Joseph L. Greenstein, and Raimond L. Winslow. Role of CaMKII in RyR leak, EC coupling and action potential duration: A computational model. *J Mol Cell Cardiol*, 49(4):617–24, October 2010.

[HH52] A. L. Hodgkin and A. F. Huxley. Propagation of Electrical Signals Along Giant Nerve Fibres. *Proceedings of the Royal Society of London. Series B, Biological Sciences*, 140(899):177–183, 1952.

[HKL+10] Thomas J. Hund, Olha M. Koval, Jingdong Li, Patrick J. Wright, Lan Qian, Jedidiah S. Snyder, Hjalti Gudmundsson, Crystal F. Kline, Nathan P. Davidson, Natalia Cardona, Matthew N. Rasband, Mark E. Anderson, and Peter J. Mohler. A β(IV)-spectrin/CaMKII signaling complex is essential for membrane excitability in mice. *J Clin Invest*, 120(10):3508–19, October 2010.

[HLJ12] Todd J. Herron, Peter Lee, and José Jalife. Optical imaging of voltage and calcium in cardiac cells & tissues. *Circ Res*, 110(4):609–23, February 2012.

[HLS+13] Hsiang-Ting T. Ho, Bin Liu, Jedidiah S. Snyder, Qing Lou, Elizabeth A. Brundage, Florencia Velez-Cortes, Honglan Wang, Mark T. Ziolo, Mark E. Anderson, Chandan K. Sen, Xander H. T. Wehrens, Vadim V. Fedorov, Brandon J. Biesiadecki, Thomas J. Hund, and Sándor Györke. Ryanodine receptor phosphorylation by oxidized CaMKII contributes to the cardiotoxic effects of cardiac glycosides. *Cardiovasc Res*, November 2013.

[HMH+99] B. Hoch, R. Meyer, R. Hetzer, E. G. Krause, and P. Karczewski. Identification and expression of delta-isoforms of the multifunctional Ca2+/calmodulin-dependent protein kinase in failing and nonfailing human myocardium. *Circ Res*, 84(6):713–21, April 1999.

[HMv+07] Roger Hullin, Jan Matthes, Sibylle von Vietinghoff, Ilona Bodi, Marta Rubio, Karen D'Souza, Ismail Friedrich Khan, Dennis Rottländer, Uta C. Hoppe, Paul Mohacsi, Eva Schmitteckert, Ralf Gilsbach, Moritz

Bünemann, Lutz Hein, Arnold Schwartz, and Stefan Herzig. Increased expression of the auxiliary beta(2)-subunit of ventricular L-type Ca(2)+ channels leads to single-channel activity characteristic of heart failure. *PLoS One*, 2(3):e292, 2007.

[Hod94] Alan Hodgkin. *Chance and Design: Reminiscences of Science in Peace and War*. Cambridge University Press, Cambridge England; New York, NY, USA, n edition edition edition, January 1994.

[HPK+11] Yousuke T. Horikawa, Mathivadhani Panneerselvam, Yoshitaka Kawaraguchi, Yasuo M. Tsutsumi, Sameh S. Ali, Ravi C. Balijepalli, Fiona Murray, Brian P. Head, Ingrid R. Niesman, Timo Rieg, Volker Vallon, Paul A. Insel, Hemal H. Patel, and David M. Roth. Cardiac-specific overexpression of caveolin-3 attenuates cardiac hypertrophy and increases natriuretic peptide expression and signaling. *J. Am. Coll. Cardiol.*, 57(22):2273–2283, May 2011.

[HPT+08] Yousuke T. Horikawa, Hemal H. Patel, Yasuo M. Tsutsumi, Michelle M. Jennings, Michael W. Kidd, Yasuko Hagiwara, Yoshihiro Ishikawa, Paul A. Insel, and David M. Roth. Caveolin-3 expression and caveolae are required for isoflurane-induced cardiac protection from hypoxia and ischemia/reperfusion injury. *J. Mol. Cell. Cardiol.*, 44(1):123–130, January 2008.

[HR14] Charles G. Hill and Thatcher W. Root. *Introduction to Chemical Engineering Kinetics and Reactor Design*. Wiley, 2nd edition, 2014.

[HTPR14] Yousuke T. Horikawa, Yasuo M. Tsutsumi, Hemal H. Patel, and David M. Roth. Signaling epicenters: The role of caveolae and caveolins in volatile anesthetic induced cardiac protection. *Curr. Pharm. Des.*, 20(36):5681–5689, 2014.

[HVWD14] Jordi Heijman, Niels Voigt, Xander H. T. Wehrens, and Dobromir Dobrev. Calcium dysregulation in atrial fibrillation: The role of CaMKII. *Front Pharmacol*, 5, March 2014.

[IMH+11] Ilanit Itzhaki, Leonid Maizels, Irit Huber, Limor Zwi-Dantsis, Oren Caspi, Aaron Winterstern, Oren Feldman, Amira Gepstein, Gil Arbel, Haim Hammerman, Monther Boulos, and Lior Gepstein. Modelling the long QT syndrome with induced pluripotent stem cells. *Nature*, 471(7337):225–229, March 2011.

[Jal03] José Jalife. Rotors and spiral waves in atrial fibrillation. *J Cardiovasc Electrophysiol*, 14(7):776–780, 2003.

[Jal11] J. Jalife. Deja vu in the theories of atrial fibrillation dynamics. *Cardiovascular research*, 89(4):766–75, March 2011.

[JK14] Mei-ling A. Joiner and Olha M. Koval. CaMKII and stress mix it up in mitochondria. *Front. Pharmacol*, 5:67, 2014.

[KCBS05] Peter Kohl, Patrizia Camelliti, Francis L. Burton, and Godfrey L. Smith. Electrical coupling of fibroblasts and myocytes: Relevance for cardiac propagation. *Journal of Electrocardiology*, 38(4, Supplement):45–50, October 2005.

[Kee90] J. P. Keener. The effects of gap junctions on propagation in myocardium: A modified cable theory. *Ann. N. Y. Acad. Sci.*, 591:257–277, 1990.

[KFP+11] Melissa H. Kong, Gregg C. Fonarow, Eric D. Peterson, Anne B. Curtis, Adrian F. Hernandez, Gillian D. Sanders, Kevin L. Thomas, David L. Hayes, and Sana M. Al-Khatib. Systematic Review of the Incidence of Sudden Cardiac Death in the United States. *J Am Coll Cardiol*, 57(7):794–801, February 2011.

[KGW+10] Olha M. Koval, Xiaoquan Guan, Yuejin Wu, Mei-Ling L. Joiner, Zhan Gao, Biyi Chen, Isabella M. Grumbach, Elizabeth D. Luczak, Roger J. Colbran, Long-Sheng S. Song, Thomas J. Hund, Peter J. Mohler, and Mark E. Anderson. CaV1.2 beta-subunit coordinates CaMKII-triggered cardiomyocyte death and afterdepolarizations. *Proc Natl Acad Sci U A*, 107(11):4996–5000, March 2010.

[KHG98] David A. Kass, Joshua M. Hare, and Dimitrios Georgakopoulos. Murine Cardiac Function. *Circ. Res.*, 82(4):519–522, March 1998.

[KHN+08] Prince J. Kannankeril, Paul A. Harris, Kris J. Norris, Irfan Warsy, Phillip D. Smith, and Dan M. Roden. Rate-independent QT shortening during exercise in healthy subjects: Terminal repolarization does not shorten with exercise. *J. Cardiovasc. Electrophysiol.*, 19(12):1284–1288, December 2008.

[KIN+03] A. Kawase, T. Ikeda, K. Nakazawa, T. Ashihara, T. Namba, T. Kubota, K. Sugi, and H. Hirai. Widening of the excitable gap and enlargement of the core of reentry during atrial fibrillation with a pure sodium channel blocker in canine atria. *Circulation*, 107(6):905–10, February 2003.

[KJC+11] Michael H. Kim, Stephen S. Johnston, Bong-Chul Chu, Mehul R. Dalal, and Kathy L. Schulman. Estimation of Total Incremental Health Care Costs in Patients With Atrial Fibrillation in the United States. *Circ. Cardiovasc. Qual. Outcomes*, 4(3):313–320, May 2011.

[KKB+97] P. Karczewski, M. Kuschel, L. G. Baltas, S. Bartel, and E. G. Krause. Site-specific phosphorylation of a phospholamban peptide by cyclic nucleotide- and Ca2+/calmodulin-dependent protein kinases of cardiac sarcoplasmic reticulum. *Basic Res Cardiol*, 92 Suppl 1:37–43, 1997.

[KKS+02] S. Kostin, G. Klein, Z. Szalay, S. Hein, E. P. Bauer, and J. Schaper. Structural correlate of atrial fibrillation in human patients. *Cardiovascular research*, 54(2):361–79, May 2002.

[KKY97] A. D. Krahn, G. J. Klein, and R. Yee. Hysteresis of the RT interval with exercise: A new marker for the long-QT syndrome? *Circulation*, 96(5):1551–1556, September 1997.

[KKZ+05] James Kneller, Jérôme Kalifa, Renqiang Zou, Alexey V Zaitsev, Mark Warren, Omer Berenfeld, Edward J Vigmond, L Joshua Leon, Stanley Nattel, and José Jalife. Mechanisms of atrial fibrillation termination by pure sodium channel blockade in an ionically-realistic mathematical model. *Circ. Res.*, 96(5):e35–e47, 2005.

[Klé83] A. G. Kléber. Resting membrane potential, extracellular potassium activity, and intracellular sodium activity during acute global ischemia in isolated perfused guinea pig hearts. *Circ Res*, 52(4):442–450, January 1983.

[KNC+96] Stefan Kääb, H. Bradley Nuss, Nipavan Chiamvimonvat, Brian O'Rourke, Peter H. Pak, David A. Kass, Eduardo Marban, and Gordon F. Tomaselli. Ionic Mechanism of Action Potential Prolongation in Ventricular Myocytes From Dogs With Pacing-Induced Heart Failure. *Circ. Res.*, 78(2):262–273, February 1996.

[KNLS15] Jong J. Kim, Jan Němec, Qiao Li, and Guy Salama. Synchronous Systolic Subcellular Ca2+-Elevations Underlie Ventricular Arrhythmia in Drug-Induced Long QT Type 2. *Circ. Arrhythm. Electrophysiol.*, 8(3):703–712, June 2015.

[KOK+98] J. M. Kalman, J. E. Olgin, M. R. Karch, M. Hamdan, R. J. Lee, and M. D. Lesh. "Cristal tachycardias": Origin of right atrial tachycardias from the crista terminalis identified by intracardiac echocardiography. *Journal of the American College of Cardiology*, 31(2):451–9, February 1998.

[KR04] André G. Kléber and Yoram Rudy. Basic Mechanisms of Cardiac Impulse Propagation and Associated Arrhythmias. *Physiol. Rev.*, 84(2):431–488, April 2004.

[KS98] James P. Keener and J Sneyd. *Mathematical Physiology*, volume 8 of *Interdisciplinary Applied Mathematics*. Springer-Verlag, New York, 1998.

[KSK13] Shankarjee Krishnamoorthi, Mainak Sarkar, and William S. Klug. Numerical quadrature and operator splitting in finite element methods for cardiac electrophysiology. *Int J Numer Method Biomed Eng*, July 2013.

[KSSN99] U. Kirchhefer, W. Schmitz, H. Scholz, and J. Neumann. Activity of cAMP-dependent protein kinase and Ca2+/calmodulin-dependent protein kinase in failing and nonfailing human hearts. *Cardiovasc Res*, 42(1):254–61, April 1999.

[KSSZ13] P. Kuklik, P. Sanders, L. Szumowski, and J. J. Zebrowski. Attraction and repulsion of spiral waves by inhomogeneity of conduction anisotropy–a model of spiral wave interaction with electrical remodeling of heart tissue. *Journal of biological physics*, 39(1):67–80, January 2013.

[KSW+12] Olha M. Koval, Jedidiah S. Snyder, Roseanne M. Wolf, Ryan E. Pavlovicz, Patric Glynn, Jerry Curran, Nicholas D. Leymaster, Wen Dun, Patrick J. Wright, Natalia Cardona, Lan Qian, Colleen C. Mitchell, Penelope A. Boyden, Philip F. Binkley, Chenglong Li, Mark E. Anderson, Peter J. Mohler, and Thomas J. Hund. Ca2+/calmodulin-dependent protein kinase II-based regulation of voltage-gated Na+ channel in cardiac disease. *Circulation*, 126(17):2084–94, October 2012.

[KV12] Sven Kaese and Sander Verheule. Cardiac electrophysiology in mice: A matter of size. *Front Physiol*, 3:345, 2012.

[KWC+04] S. Kettlewell, N. L. Walker, S. M. Cobbe, F. L. Burton, and G. L. Smith. The electrophysiological and mechanical effects of 2,3-butanedione monoxime and cytochalasin-D in the Langendorff perfused rabbit heart. *Exp. Physiol.*, 89(2):163–172, March 2004.

[KYC+02] Andrew D. Krahn, Raymond Yee, Vijay Chauhan, Allan C. Skanes, Jian Wang, Robert A. Hegele, and George J. Klein. Beta blockers normalize QT hysteresis in long QT syndrome. *Am. Heart J.*, 143(3):528–534, March 2002.

[LA14] Elizabeth D. Luczak and Mark E. Anderson. CaMKII oxidative activation and the pathogenesis of cardiac disease. *J Mol Cell Cardiol*, February 2014.

[Lam12] Rachel Lampert. Evaluation and management of arrhythmia in the athletic patient. *Prog Cardiovasc Dis*, 54(5):423–431, Mar-Apr 2012.

[Lan95] O. Langendorff. Untersuchungen am überlebenden Säugethierherzen. *Pflügers Arch.*, 61(6):291–332, August 1895.

[LCD+92] Leslie M. Loew, Lawrence B. Cohen, James Dix, Eric N. Fluhler, Valerie Montana, Guy Salama, and Wu Jian-young. A naphthyl analog of the aminostyryl pyridinium class of potentiometric membrane dyes shows consistent sensitivity in a variety of tissue, cell, and model membrane preparations. *J. Membarin Biol.*, 130(1):1–10, October 1992.

[LCWT01] Barry A. Love, Kathryn K. Collins, Edward P. Walsh, and John K. Triedman. Electroanatomic Characterization of Conduction Barriers in Sinus/Atrially Paced Rhythm and Association with Intra-Atrial Reentrant Tachycardia Circuits Following Congenital Heart Disease Surgery. *J. Cardiovasc. Electrophysiol.*, 12(1):17–25, January 2001.

[LD09] Edward G. Lakatta and Dario DiFrancesco. What keeps us ticking: A funny current, a calcium clock, or both? *Journal of Molecular and Cellular Cardiology*, 47(2):157–170, August 2009.

[LdG+15] Michael B. Liu, Enno de Lange, Alan Garfinkel, James N. Weiss, and Zhilin Qu. Delayed afterdepolarizations generate both triggers and a vulnerable substrate promoting reentry in cardiac tissue. *Heart Rhythm*, 12(10):2115–2124, October 2015.

[LFS+00] M. Löhn, M. Fürstenau, V. Sagach, M. Elger, W. Schulze, F. C. Luft, H. Haller, and M. Gollasch. Ignition of calcium sparks in arterial and cardiac muscle through caveolae. *Circ. Res.*, 87(11):1034–1039, November 2000.

[LGL+13] Min Luo, Xiaoqun Guan, Elizabeth D. Luczak, Di Lang, William Kutschke, Zhan Gao, Jinying Yang, Patric Glynn, Samuel Sossalla, Paari D. Swaminathan, Robert M. Weiss, Baoli Yang, Adam G. Rokita, Lars S. Maier, Igor R. Efimov, Thomas J. Hund, and Mark E. Anderson. Diabetes increases mortality after myocardial infarction by oxidizing CaMKII. *J Clin Invest*, 123(3):1262–74, March 2013.

[LHM+09] N. Lindegger, B. M. Hagen, A. R. Marks, W. J. Lederer, and R. S. Kass. Diastolic transient inward current in long QT syndrome type 3 is caused by Ca2+ overload and inhibited by ranolazine. *J. Mol. Cell. Cardiol.*, 47(2):326–334, August 2009.

[LHS+11] Ying-Mei M. Lu, Jiyun Huang, Norifumi Shioda, Kohji Fukunaga, Yasufumi Shirasaki, Xiao-Ming M. Li, and Feng Han. CaMKIIδB mediates aberrant NCX1 expression and the imbalance of NCX1/SERCA in transverse aortic constriction-induced failing heart. *PLoS One*, 6(9):e24724, 2011.

[Lio10] Fred Lionetti. *GPU Accelerated Cardiac Electrophysiology*. M.s. thesis, University of California San Diego, January 2010.

[LK14] Joyce Lin and James P. Keener. Microdomain Effects on Transverse Cardiac Propagation. *Biophys J*, 106(4):925–931, February 2014.

[LLS+00] Timothy P. Lockwich, Xibao Liu, Brij B. Singh, Julie Jadlowiec, Sharon Weiland, and Indu S. Ambudkar. Assembly of Trp1 in a Signaling

Complex Associated with Caveolin-Scaffolding Lipid Raft Domains. *J. Biol. Chem.*, 275(16):11934–11942, April 2000.

[LMZ+06] Jingdong Li, Céline Marionneau, Rong Zhang, Vaibhavi Shah, Johannes W. Hell, Jeanne M. Nerbonne, and Mark E. Anderson. Calmodulin kinase II inhibition shortens action potential duration by upregulation of K+ currents. *Circ Res*, 99(10):1092–9, November 2006.

[LPL12] Ronglih Liao, Bruno K. Podesser, and Chee Chew Lim. The continuing evolution of the Langendorff and ejecting murine heart: New advances in cardiac phenotyping. *Am. J. Physiol. - Heart Circ. Physiol.*, 303(2):H156–H167, July 2012.

[LPO+01] Hadas Lahat, Elon Pras, Tsviya Olender, Nili Avidan, Edna Ben-Asher, Orna Man, Etgar Levy-Nissenbaum, Asad Khoury, Avraham Lorber, Boleslaw Goldman, Doron Lancet, and Michael Eldar. A Missense Mutation in a Highly Conserved Region of CASQ2 Is Associated with Autosomal Recessive Catecholamine-Induced Polymorphic Ventricular Tachycardia in Bedouin Families from Israel. *The American Journal of Human Genetics*, 69(6):1378–1384, December 2001.

[LRD+11] Nian Liu, Yanfei Ruan, Marco Denegri, Tiziana Bachetti, Yang Li, Barbara Colombi, Carlo Napolitano, William A. Coetzee, and Silvia G. Priori. Calmodulin kinase II inhibition prevents arrhythmias in RyR2(R4496C+/-) mice with catecholaminergic polymorphic ventricular tachycardia. *J Mol Cell Cardiol*, 50(1):214–22, January 2011.

[LSG+12] G. G. Lalani, A. Schricker, M. Gibson, A. Rostamian, D. E. Krummen, and S. M. Narayan. Atrial conduction slows immediately before the onset of human atrial fibrillation: A bi-atrial contact mapping study of transitions to atrial fibrillation. *Journal of the American College of Cardiology*, 59(6):595–606, February 2012.

[LSW11] William E. Louch, Katherine A. Sheehan, and Beata M. Wolska. Methods in cardiomyocyte isolation, culture, and gene transfer. *Journal of Molecular and Cellular Cardiology*, 51(3):288–298, September 2011.

[LUF+10] Gary D. Lopaschuk, John R. Ussher, Clifford D. L. Folmes, Jagdip S. Jaswal, and William C. Stanley. Myocardial Fatty Acid Metabolism in Health and Disease. *Physiol. Rev.*, 90(1):207–258, January 2010.

[MBW+10] Alessandra Moretti, Milena Bellin, Andrea Welling, Christian Billy Jung, Jason T. Lam, Lorenz Bott-Flügel, Tatjana Dorn, Alexander Goedel, Christian Höhnke, Franz Hofmann, Melchior Seyfarth, Daniel Sinnecker, Albert Schömig, and Karl-Ludwig Laugwitz. Patient-Specific Induced Pluripotent Stem-Cell Models for Long-QT Syndrome. *N. Engl. J. Med.*, 363(15):1397–1409, October 2010.

[MEA+10] Santhosh K. Mani, Erin A. Egan, Benjamin K. Addy, Michael Grimm, Harinath Kasiganesan, Thirumagal Thiyagarajan, Ludivine Renaud, Joan Heller Brown, Christine B. Kern, and Donald R. Menick. Beta-Adrenergic receptor stimulated Ncx1 upregulation is mediated via a CaMKII/AP-1 signaling pathway in adult cardiomyocytes. *J Mol Cell Cardiol*, 48(2):342–51, February 2010.

[MEM+14] Stefano Morotti, Andrew G. Edwards, Andrew D. McCulloch, Donald M. Bers, and Eleonora Grandi. A novel computational model of mouse myocyte electrophysiology to assess the synergy between Na+ loading and CaMKII. *J Physiol*, January 2014.

[MFP+11] Yogananda S. Markandeya, Jonathan M. Fahey, Florentina Pluteanu, Leanne L. Cribbs, and Ravi C. Balijepalli. Caveolin-3 regulates protein kinase A modulation of the Ca(V)3.2 (alpha1H) T-type Ca2+ channels. *J. Biol. Chem.*, 286(4):2433–2444, January 2011.

[MGGT09] Mary M Maleckar, Joseph L Greenstein, Wayne R Giles, and Natalia A Trayanova. K+ current changes account for the rate dependence of the action potential in the human atrial myocyte. *Am. J. Physiol.-Heart Circ. Physiol.*, 297(4):H1398–H1410, 2009.

[MI89] A. J. Moss and CAST Investigators. Preliminary Report: Effect of Encainide and Flecainide on Mortality in a Randomized Trial of Arrhythmia Suppression after Myocardial Infarction. *N. Engl. J. Med.*, 321(6):406–412, August 1989.

[Min14] George Ralph Mines. On circulating excitations in heart muscles and their possible relation to tachycardia and fibrillation. *Trans R Soc Can*, 4:43–52, 1914.

[MJK98] G. F. Mitchell, A. Jeron, and G. Koren. Measurement of heart rate and Q-T interval in the conscious mouse. *Am. J. Physiol.*, 274(3 Pt 2):H747–751, March 1998.

[MKS+14] J. M. Miller, R. C. Kowal, V. Swarup, J. P. Daubert, E. G. Daoud, J. D. Day, K. A. Ellenbogen, J. D. Hummel, T. Baykaner, D. E. Krummen, S. M. Narayan, V. Y. Reddy, K. Shivkumar, J. S. Steinberg, and K. R. Wheelan. Initial Independent Outcomes from Focal Impulse and Rotor Modulation Ablation for Atrial Fibrillation: Multicenter FIRM Registry. *Journal of cardiovascular electrophysiology*, June 2014.

[MNA94] Zhen Ming, Charles Nordin, and Ronald S. Aronson. Role of L-Type Calcium Channel Window Current in Generating Current-Induced Early Afterdepolarizations. *J. Cardiovasc. Electrophysiol.*, 5(4):323–334, April 1994.

[MP06] Barry J. Maron and Antonio Pelliccia. The heart of trained athletes: Cardiac remodeling and the risks of sports, including sudden death. *Circulation*, 114(15):1633–1644, October 2006.

[MPW+15] Yogananda S. Markandeya, Laura J. Phelan, Marites T. Woon, Alexis M. Keefe, Courtney R. Reynolds, Benjamin K. August, Timothy A. Hacker, David M. Roth, Hemal H. Patel, and Ravi C. Balijepalli. Caveolin-3 Overexpression Attenuates Cardiac Hypertrophy via Inhibition of T-type Ca2+ Current Modulated by Protein Kinase Cα in Cardiomyocytes. *J. Biol. Chem.*, 290(36):22085–22100, September 2015.

[MRU+08] Victor A. Maltsev, Vitaliy Reznikov, Nidas A. Undrovinas, Hani N. Sabbah, and Albertas Undrovinas. Modulation of late sodium current by Ca2+, calmodulin, and CaMKII in normal and failing dog cardiomyocytes: Similarities and differences. *Am J Physiol Heart Circ Physiol*, 294(4):H1597–608, April 2008.

[MSG+03] Peter J. Mohler, Jean-Jacques . J. Schott, Anthony O. Gramolini, Keith W. Dilly, Silvia Guatimosim, William H. duBell, Long-Sheng . S. Song, Karine Haurogné, Florence Kyndt, Mervat E. Ali, Terry B. Rogers, W. J. . J. Lederer, Denis Escande, Herve Le Marec, and Vann Bennett. Ankyrin-B mutation causes type 4 long-QT cardiac arrhythmia and sudden cardiac death. *Nature*, 421(6923):634–639, February 2003.

[MSH+03] V. Markides, R. J. Schilling, S. Y. Ho, A. W. Chow, D. W. Davies, and N. S. Peters. Characterization of left atrial activation in the intact human heart. *Circulation*, 107(5):733–9, February 2003.

[MSN+04] Peter J. Mohler, Igor Splawski, Carlo Napolitano, Georgia Bottelli, Leah Sharpe, Katherine Timothy, Silvia G. Priori, Mark T. Keating, and Vann Bennett. A cardiac arrhythmia syndrome caused by loss of ankyrin-B function. *Proc. Natl. Acad. Sci. U. S. A.*, 101(24):9137–9142, June 2004.

[MSS+01] Jeffrey R. Martens, Naoya Sakamoto, Shelley A. Sullivan, Tammy D. Grobaski, and Michael M. Tamkun. Isoform-specific Localization of Voltage-gated K+Channels to Distinct Lipid Raft Populations TARGETING OF Kv1.5 TO CAVEOLAE. *J. Biol. Chem.*, 276(11):8409–8414, March 2001.

[MVS+99] G. E. Morley, D. Vaidya, F. H. Samie, C. Lo, M. Delmar, and J. Jalife. Characterization of conduction in the ventricles of normal and heterozygous Cx43 knockout mice using optical mapping. *J. Cardiovasc. Electrophysiol.*, 10(10):1361–1375, October 1999.

[MWCK95] M. L. Marks, S. L. Whisler, C. Clericuzio, and M. Keating. A new form of long QT syndrome associated with syndactyly. *J Am Coll Cardiol*, 25(1):59–64, January 1995.

[MWH+14] N. F. Marrouche, D. Wilber, G. Hindricks, P. Jais, N. Akoum, F. Marchlinski, E. Kholmovski, N. Burgon, N. Hu, L. Mont, T. Deneke, M. Duytschaever, T. Neumann, M. Mansour, C. Mahnkopf, B. Herweg, E. Daoud, E. Wissner, P. Bansmann, and J. Brachmann. Association of atrial tissue fibrosis identified by delayed enhancement MRI and atrial fibrillation catheter ablation: The DECAAF study. *JAMA : the journal of the American Medical Association*, 311(5):498–506, February 2014.

[MWK+12] Rachel C. Myles, Lianguo Wang, Chaoyi Kang, Donald M. Bers, and Crystal M. Ripplinger. Local β-adrenergic stimulation overcomes source-sink mismatch to generate focal arrhythmia. *Circ Res*, 110(11):1454–64, May 2012.

[MYB+13] Jonathan D. Moreno, Pei-Chi Yang, John R. Bankston, Eleonora Grandi, Donald M. Bers, Robert S. Kass, and Colleen E. Clancy. Ranolazine for Congenital and Acquired Late INa-Linked ArrhythmiasNovelty and Significance. *Circ. Res.*, 113(7):e50–e61, September 2013.

[MZH+00] A. J. Moss, W. Zareba, W. J. Hall, P. J. Schwartz, R. S. Crampton, J. Benhorin, G. M. Vincent, E. H. Locati, S. G. Priori, C. Napolitano, A. Medina, L. Zhang, J. L. Robinson, K. Timothy, J. A. Towbin, and M. L. Andrews. Effectiveness and limitations of beta-blocker therapy in congenital long-QT syndrome. *Circulation*, 101(6):616–623, February 2000.

[MZN+12] Christine L. Mummery, Jianhua Zhang, Elizabeth S. Ng, David A. Elliott, Andrew G. Elefanty, and Timothy J. Kamp. Differentiation of Human Embryonic Stem Cells and Induced Pluripotent Stem Cells to Cardiomyocytes. *Circ. Res.*, 111(3):344–358, July 2012.

[MZY+11] Jonathan D. Moreno, Z. Iris Zhu, Pei-Chi C. Yang, John R. Bankston, Mao-Tsuen T. Jeng, Chaoyi Kang, Lianguo Wang, Jason D. Bayer, David J. Christini, Natalia A. Trayanova, Crystal M. Ripplinger, Robert S. Kass, and Colleen E. Clancy. A computational model to predict the effects of class I anti-arrhythmic drugs on ventricular rhythms. *Sci Transl Med*, 3(98):98ra83, August 2011.

[NBD08] Stanley Nattel, Brett Burstein, and Dobromir Dobrev. Atrial remodeling and atrial fibrillation: Mechanisms and implications. *Circ Arrhythm Electrophysiol*, 1(1):62–73, April 2008.

[NBKF02] S. M. Narayan, F. Bode, P. L. Karasik, and M. R. Franz. Alternans of atrial action potentials during atrial flutter as a precursor to atrial fibrillation. *Circulation*, 106(15):1968–73, October 2002.

[NBMP12] Carlo Napolitano, Raffaella Bloise, Nicola Monteforte, and Silvia G. Priori. Sudden cardiac death and genetic ion channelopathies: Long QT, Brugada, short QT, catecholaminergic polymorphic ventricular tachycardia, and idiopathic ventricular fibrillation. *Circulation*, 125(16):2027–34, April 2012.

[Ner04] Jeanne M. Nerbonne. Studying cardiac arrhythmias in the mouse–a reasonable model for probing mechanisms? *Trends Cardiovasc Med*, 14(3):83–93, April 2004.

[NFC+11] S. M. Narayan, M. R. Franz, P. Clopton, E. J. Pruvot, and D. E. Krummen. Repolarization alternans reveals vulnerability to human atrial fibrillation. *Circulation*, 123(25):2922–30, June 2011.

[NG00] A. Nygren and W. R. Giles. Mathematical Simulation of Slowing of Cardiac Conduction Velocity by Elevated Extracellular [K+] in a Human Atrial Strand. *Annals of Biomedical Engineering*, 28(8):951–957, August 2000.

[NK05] Jeanne M. Nerbonne and Robert S. Kass. Molecular physiology of cardiac repolarization. *Physiol. Rev.*, 85(4):1205–1253, October 2005.

[NKB+11] Steven A. Niederer, Eric Kerfoot, Alan P. Benson, Miguel O. Bernabeu, Olivier Bernus, Chris Bradley, Elizabeth M. Cherry, Richard Clayton, Flavio H. Fenton, Alan Garny, Elvio Heidenreich, Sander Land, Mary Maleckar, Pras Pathmanathan, Gernot Plank, José F. Rodríguez, Ishani Roy, Frank B. Sachse, Gunnar Seemann, Ola Skavhaug, and Nic P. Smith. Verification of cardiac tissue electrophysiology simulators using an N-version benchmark. *Philos Trans Math Phys Eng Sci*, 369(1954):4331–51, November 2011.

[NKC+13] Sanjiv M Narayan, David E Krummen, Paul Clopton, Kalyanam Shivkumar, and John M Miller. Direct Or Coincidental Elimination of Stable Rotors or Focal Sources May Explain Successful Atrial Fibrillation Ablation: On-Treatment Analysis of the CONFIRM (CONventional ablation for AF with or without Focal Impulse and Rotor Modulation) Trial. *J Am Coll Cardiol*, http://dx.doi.org/10.1016/j.jacc.2013.03.021, 2013.

[NKER12] Sanjiv M. Narayan, David E. Krummen, Michael W. Enyeart, and Wouter-Jan J. Rappel. Computational mapping identifies localized mechanisms for ablation of atrial fibrillation. *PLoS One*, 7(9):e46034, 2012.

[NKKR08] Sanjiv M Narayan, Dhruv Kazi, David E Krummen, and Wouter-Jan Rappel. Repolarization and Activation Restitution Near Human Pulmonary Veins and Atrial Fibrillation InitiationA Mechanism for the Initiation of Atrial Fibrillation by Premature Beats. *J Am Coll Cardiol*, 52(15):1222–1230, 2008.

[NKR12] Sanjiv M Narayan, David E Krummen, and Wouter-Jan Rappel. Clinical mapping approach to diagnose electrical rotors and focal impulse sources for human atrial fibrillation. *J Cardiovasc Electrophysiol*, 23(5):447–454, 2012.

[NKS+12] Sanjiv M Narayan, David E Krummen, Kalyanam Shivkumar, Paul Clopton, Wouter-Jan Rappel, and John M Miller. Treatment of Atrial Fibrillation by the Ablation of Localized Sources: CONFIRM (Conventional Ablation for Atrial Fibrillation With or Without Focal Impulse and Rotor Modulation) Trial. *J Am Coll Cardiol*, 60(7):628–636, 2012.

[NLGSH91] P. M. Nielsen, I. J. Le Grice, B. H. Smaill, and P. J. Hunter. Mathematical model of geometry and fibrous structure of the heart. *Am. J. Physiol.*, 260(4 Pt 2):H1365–1378, April 1991.

[NN10] Noriko Niwa and Jeanne M. Nerbonne. Molecular determinants of cardiac transient outward potassium current (I(to)) expression and regulation. *J. Mol. Cell. Cardiol.*, 48(1):12–25, January 2010.

[Nob62] D. Noble. A modification of the Hodgkin—Huxley equations applicable to Purkinje fibre action and pacemaker potentials. *J Physiol*, 160(2):317–352, February 1962.

[Nob02] Denis Noble. Modeling the Heart–from Genes to Cells to the Whole Organ. *Science*, 295(5560):1678–1682, March 2002.

[NPC+11] Steven A. Niederer, Gernot Plank, Phani Chinchapatnam, Matthew Ginks, Pablo Lamata, Kawal S. Rhode, Christopher A. Rinaldi, Reza Razavi, and Nicolas P. Smith. Length-dependent tension in the failing heart and the efficacy of cardiac resynchronization therapy. *Cardiovasc Res*, 89(2):336–43, February 2011.

[NSK+13] S. M. Narayan, K. Shivkumar, D. E. Krummen, J. M. Miller, and W. J. Rappel. Panoramic electrophysiological mapping but not electrogram morphology identifies stable sources for human atrial fibrillation: Stable atrial fibrillation rotors and focal sources relate poorly to fractionated electrograms. *Circulation. Arrhythmia and electrophysiology*, 6(1):58–67, February 2013.

[NWH+13] John Noel, Hui Wang, Nankang Hong, Jian-Qin Tao, Kevin Yu, Elena M. Sorokina, Kristine DeBolt, Michelle Heayn, Victor Rizzo, Horace

Delisser, Aron B. Fisher, and Shampa Chatterjee. PECAM-1 and caveolae form the mechanosensing complex necessary for NOX2 activation and angiogenic signaling with stopped flow in pulmonary endothelium. *Am. J. Physiol. - Lung Cell. Mol. Physiol.*, 305(11):L805–L818, December 2013.

[OKS+01] Gavin Y. Oudit, Zamaneh Kassiri, Rajan Sah, Rafael J. Ramirez, Carsten Zobel, and Peter H. Backx. The Molecular Physiology of the Cardiac Transient Outward Potassium Current (Ito) in Normal and Diseased Myocardium. *Journal of Molecular and Cellular Cardiology*, 33(5):851–872, May 2001.

[OVVR11] Thomas O'Hara, László Virág, András Varró, and Yoram Rudy. Simulation of the Undiseased Human Cardiac Ventricular Action Potential: Model Formulation and Experimental Validation. *PLOS Computational Biology*, 7(5):e1002061, May 2011.

[Pal53] George E Palade. Fine structure of blood capillaries. *J. Appl. Phys.*, 24:1424–1436, 1953.

[PBN+12] P. Pathmanathan, M. O. Bernabeu, S. A. Niederer, D. J. Gavaghan, and D. Kay. Computational modelling of cardiac electrophysiology: Explanation of the variability of results from different numerical solvers. *Int J Numer Method Biomed Eng*, 28(8):890–903, August 2012.

[PBS93] A. E. Pollard, M. J. Burgess, and K. W. Spitzer. Computer simulations of three-dimensional propagation in ventricular myocardium. Effects of intramural fiber rotation and inhomogeneous conductivity on epicardial activation. *Circ. Res.*, 72(4):744–756, April 1993.

[PC05] Sangita P. Patel and Donald L. Campbell. Transient outward potassium current, 'Ito', phenotypes in the mammalian left ventricle: Underlying molecular, cellular and biophysical mechanisms. *J. Physiol. (Lond.)*, 569(Pt 1):7–39, November 2005.

[PDZI74] L. M. Popescu, I. Diculescu, U. Zelck, and N. Ionescu. Ultrastructural distribution of calcium in smooth muscle cells of guinea-pig taenia coli. *Cell Tissue Res.*, 154(3):357–378, September 1974.

[PE88] A. M. Pertsov and E. A. Ermakova. Mechanism of the Drift of a Spiral Wave in an Inhomogeneous-Medium. *Biofizika+*, 33(2):338–342, March 1988.

[PHE+01] Lioudmila Polontchouk, Jacques-Antoine Haefliger, Berit Ebelt, Thomas Schaefer, Dominik Stuhlmann, Uwe Mehlhorn, Ferdinand Kuhn-Regnier, E Rainer De Vivie, and Stefan Dhein. Effects of chronic atrial fibrillation

on gap junction distribution in human and rat atria. *J Am Coll Cardiol*, 38(3):883–891, 2001.

[PJ13] S. V. Pandit and J. Jalife. Rotors and the dynamics of cardiac fibrillation. *Circulation research*, 112(5):849–62, March 2013.

[PK95] A. Panfilov and J. P. Keener. Re-entry in an anatomical model of the heart. *Chaos, Solitons & Fractals*, 5(3):681–689, March 1995.

[PMG+03] Aimée Paulussen, Gert Matthijs, Marc Gewillig, Peter Verhasselt, Nadine Cohen, and Jeroen Aerssens. Mutation analysis in congenital Long QT Syndrome–a case with missense mutations in KCNQ1 and SCN5A. *Genet Test*, 7(1):57–61, 2003.

[PMI08] Hemal H. Patel, Fiona Murray, and Paul A. Insel. Caveolae as organizers of pharmacologically relevant signal transduction molecules. *Annu. Rev. Pharmacol. Toxicol.*, 48:359–391, 2008.

[PNM+02] Silvia G. Priori, Carlo Napolitano, Mirella Memmi, Barbara Colombi, Fabrizio Drago, Maurizio Gasparini, Luciano DeSimone, Fernando Coltorti, Raffaella Bloise, Roberto Keegan, Fernando E. S. Cruz Filho, Gabriele Vignati, Abraham Benatar, and Angelica DeLogu. Clinical and molecular characterization of patients with catecholaminergic polymorphic ventricular tachycardia. *Circulation*, 106(1):69–74, July 2002.

[PNT+01] Silvia G. Priori, Carlo Napolitano, Natascia Tiso, Mirella Memmi, Gabriele Vignati, Raffaella Bloise, Vincenzo Sorrentino, and Gian Antonio Danieli. Mutations in the Cardiac Ryanodine Receptor Gene (hRyR2) Underlie Catecholaminergic Polymorphic Ventricular Tachycardia. *Circulation*, 103(2):196–200, January 2001.

[PRG+13] Anil Purohit, Adam G. Rokita, Xiaoqun Guan, Biyi Chen, Olha M. Koval, Niels Voigt, Stefan Neef, Thomas Sowa, Zhan Gao, Elizabeth D. Luczak, Hrafnhildur Stefansdottir, Andrew C. Behunin, Na Li, Ramzi N. El-Accaoui, Baoli Yang, Paari Dominic Swaminathan, Robert M. Weiss, Xander H.T Wehrens, Long-Sheng . S. Song, Dobromir Dobrev, Lars S. Maier, and Mark E. Anderson. Oxidized Ca2+/Calmodulin-Dependent Protein Kinase II Triggers Atrial Fibrillation. *Circulation*, 128(16):1748–1757, October 2013.

[PS14] Patricia Pellicena and Howard Schulman. CaMKII inhibitors: From research tools to therapeutic agents. *Front Pharmacol*, 5:21, 2014.

[PTH02] A. Pullan, K. Tomlinson, and P. Hunter. A Finite Element Method for an Eikonal Equation Model of Myocardial Excitation Wavefront Propagation. *SIAM J. Appl. Math.*, 63(1):324–350, January 2002.

[PWE+14] E. R. Pfeiffer, A. T. Wright, A. G. Edwards, J. C. Stowe, K. McNall, J. Tan, I. Niesman, H. H. Patel, D. M. Roth, J. H. Omens, and A. D. McCulloch. Caveolae in ventricular myocytes are required for stretch-dependent conduction slowing. *J. Mol. Cell. Cardiol.*, 76:265–274, November 2014.

[QH92] Y. Qiu and D. J. Hearse. Comparison of ischemic vulnerability and responsiveness to cardioplegic protection in crystalloid-perfused versus blood-perfused hearts. *J. Thorac. Cardiovasc. Surg.*, 103(5):960–968, May 1992.

[Qua09] Alfio Quarteroni. *Numerical Models for Differential Problems*. Springer Milan, Milano, 2009.

[QWG99] Z. Qu, J. N. Weiss, and A. Garfinkel. Cardiac electrical restitution properties and stability of reentrant spiral waves: A simulation study. *Am. J. Physiol.*, 276(1 Pt 2):H269–283, January 1999.

[QXO+13] Zhilin Qu, Lai-Hua H. Xie, Riccardo Olcese, Hrayr S. Karagueuzian, Peng-Sheng S. Chen, Alan Garfinkel, and James N. Weiss. Early afterdepolarizations in cardiac myocytes: Beyond reduced repolarization reserve. *Cardiovasc Res*, 99(1):6–15, July 2013.

[RCM97] J. M. Rogers, M Courtemanch, and A. D. McCulloch. Finite element methods for modelling impulse propagation in the heart. In Alexander V. Panfilov and Arun V. Holden, editors, *Computational Biology of the Heart*, pages 217–233. Wiley, March 1997. Google-Books-ID: q_VFAAAAYAAJ.

[RH73] Michael R. Rosen and Brain F. Hoffman. Mechanisms of Action of Antiarrhythmic Drugs. *Circ. Res.*, 32(1):1–8, January 1973.

[RHK+11] Jarkko J. Ronkainen, Sandra L. Hänninen, Topi Korhonen, Jussi T. Koivumäki, Reka Skoumal, Sini Rautio, Veli-Pekka P. Ronkainen, and Pasi Tavi. Ca2+-calmodulin-dependent protein kinase II represses cardiac transcription of the L-type calcium channel alpha(1C)-subunit gene (Cacna1c) by DREAM translocation. *J Physiol*, 589(Pt 11):2669–86, June 2011.

[RHS79] D. E. Roberts, L. T. Hersh, and A. M. Scher. Influence of cardiac fiber orientation on wavefront voltage, conduction velocity, and tissue resistivity in the dog. *Circ. Res.*, 44(5):701–712, May 1979.

[RM94a] J. M. Rogers and A. D. McCulloch. A collocation–Galerkin finite element model of cardiac action potential propagation. *IEEE Trans Biomed Eng*, 41(8):743–757, August 1994.

[RM94b] J. M. Rogers and A. D. McCulloch. Nonuniform muscle fiber orientation causes spiral wave drift in a finite element model of cardiac action potential propagation. *Journal of cardiovascular electrophysiology*, 5(6):496–509, June 1994.

[RS94] S Rohr and B M Salzberg. Multiple site optical recording of transmembrane voltage (MSORTV) in patterned growth heart cell cultures: Assessing electrical behavior, with microsecond resolution, on a cellular and subcellular scale. *Biophys J*, 67(3):1301–1315, September 1994.

[RS06] Yoram Rudy and Jonathan R. Silva. Computational biology in the study of cardiac ion channels and cell electrophysiology. *Q Rev Biophys*, 39(1):57–116, February 2006.

[RvL+12] Jonathan L. Respress, Ralph J. van Oort, Na Li, Natale Rolim, Sayali S. Dixit, Angela deAlmeida, Niels Voigt, William S. Lawrence, Darlene G. Skapura, Kristine Sk$\aa$rdal, Ulrik Wisløff, Thomas Wieland, Xun Ai, Steven M. Pogwizd, Dobromir Dobrev, and Xander H. T. Wehrens. Role of RyR2 phosphorylation at S2814 during heart failure progression. *Circ Res*, 110(11):1474–83, May 2012.

[RWL02] Babak Razani, Scott E. Woodman, and Michael P. Lisanti. Caveolae: From cell biology to animal physiology. *Pharmacol. Rev.*, 54(3):431–467, September 2002.

[SB01] S. F. Steinberg and L. L. Brunton. Compartmentation of G protein-coupled signaling pathways in cardiac myocytes. *Annu. Rev. Pharmacol. Toxicol.*, 41:751–773, 2001.

[SBEB+03] Eric Schulze-Bahr, Lars Eckardt, Günter Breithardt, Karlheinz Seidl, Thomas Wichter, Christian Wolpert, Martin Borggrefe, and Wilhelm Haverkamp. Sodium channel gene (SCN5A) mutations in 44 index patients with Brugada syndrome: Different incidences in familial and sporadic disease. *Hum. Mutat.*, 21(6):651–652, June 2003.

[SBP+08] M. Said, R. Becerra, J. Palomeque, G. Rinaldi, M. A. Kaetzel, P. L. Diaz-Sylvester, J. A. Copello, J. R. Dedman, C. Mundiña-Weilenmann, L. Vittone, and A. Mattiazzi. Increased intracellular Ca2+ and SR Ca2+ load contribute to arrhythmias after acidosis in rat heart. Role of Ca2+/calmodulin-dependent protein kinase II. *Am J Physiol Heart Circ Physiol*, 295(4):H1669–83, October 2008.

[SBR95] Nikolai M. Soldatov, Alexandre Bouron, and Harald Reuter. Different Voltage-dependent Inhibition by Dihydropyridines of Human Ca Channel Splice Variants. *J. Biol. Chem.*, 270(18):10540–10543, May 1995.

[SBV+11] M. Said, R. Becerra, C. A. Valverde, M. A. Kaetzel, J. R. Dedman, C. Mundiña-Weilenmann, X. H. Wehrens, L. Vittone, and A. Mattiazzi. Calcium-calmodulin dependent protein kinase II (CaMKII): A main signal responsible for early reperfusion arrhythmias. *J Mol Cell Cardiol*, 51(6):936–44, December 2011.

[SBW08] Rainer Schimpf, Martin Borggrefe, and Christian Wolpert. Clinical and molecular genetics of the short QT syndrome. *Curr. Opin. Cardiol.*, 23(3):192–198, May 2008.

[SCI12] Peter J. Schwartz, Lia Crotti, and Roberto Insolia. Long-QT Syndrome. *Circ. Arrhythm. Electrophysiol.*, 5(4):868–877, August 2012.

[SEH+12] Kalyanam Shivkumar, Kenneth A Ellenbogen, John D Hummel, John M Miller, and Jonathan S Steinberg. Acute termination of human atrial fibrillation by identification and catheter ablation of localized rotors and sources: First multicenter experience of focal impulse and rotor modulation (FIRM) ablation. *J Cardiovasc Electrophysiol*, 23(12):1277–1285, 2012.

[SEP+02] Jeroen P. P. Smits, Lars Eckardt, Vincent Probst, Connie R. Bezzina, Jean Jacques Schott, Carol Ann Remme, Wilhelm Haverkamp, Günter Breithardt, Denis Escande, Eric Schulze-Bahr, Hervé LeMarec, and Arthur A. M. Wilde. Genotype-phenotype relationship in Brugada syndrome: Electrocardiographic features differentiate SCN5A-related patients from non-SCN5A-related patients. *J. Am. Coll. Cardiol.*, 40(2):350–356, July 2002.

[SGA13] Diana Shy, Ludovic Gillet, and Hugues Abriel. Cardiac sodium channel NaV1.5 distribution in myocytes via interacting proteins: The multiple pool model. *Biochim. Biophys. Acta*, 1833(4):886–894, April 2013.

[SH05] Rashmi R. Shah and Luc M. Hondeghem. Refining detection of drug-induced proarrhythmia: QT interval and TRIaD. *Heart Rhythm*, 2(7):758–772, July 2005.

[SHB+98] F. Schröder, R. Handrock, D. J. Beuckelmann, S. Hirt, R. Hullin, L. Priebe, R. H. Schwinger, J. Weil, and S. Herzig. Increased availability and open probability of single L-type calcium channels from failing compared with nonfailing human ventricle. *Circulation*, 98(10):969–76, September 1998.

[SHSD04] Laura J. Sampson, Yasunobu Hayabuchi, Nick B. Standen, and Caroline Dart. Caveolae Localize Protein Kinase A Signaling to Arterial ATP-Sensitive Potassium Channels. *Circ. Res.*, 95(10):1012–1018, November 2004.

[SHST+14] Louise E. See Hoe, Jan M. Schilling, Emiri Tarbit, Can J. Kiessling, Anna R. Busija, Ingrid R. Niesman, Eugene Du Toit, Kevin J. Ashton, David M. Roth, John P. Headrick, Hemal H. Patel, and Jason N. Peart. Sarcolemmal cholesterol and caveolin-3 dependence of cardiac function, ischemic tolerance, and opioidergic cardioprotection. *Am. J. Physiol. Heart Circ. Physiol.*, 307(6):H895–903, September 2014.

[SJW+09] M. K. Stiles, B. John, C. X. Wong, P. Kuklik, A. G. Brooks, D. H. Lau, H. Dimitri, K. C. Roberts-Thomson, L. Wilson, P. De Sciscio, G. D. Young, and P. Sanders. Paroxysmal lone atrial fibrillation is associated with an abnormal atrial substrate: Characterizing the "second factor". *Journal of the American College of Cardiology*, 53(14):1182–91, April 2009.

[SKG+94] J. E. Saffitz, H. L. Kanter, K. G. Green, T. K. Tolley, and E. C. Beyer. Tissue-specific determinants of anisotropic conduction velocity in canine atrial and ventricular myocardium. *Circ. Res.*, 74(6):1065–1070, June 1994.

[SKZ+03] Farzad Sarmast, Arun Kolli, Alexey Zaitsev, Keely Parisian, Amit S Dhamoon, Prabal K Guha, Mark Warren, Justus MB Anumonwo, Steven M Taffet, and Omer Berenfeld. Cholinergic atrial fibrillation: IK, ACh gradients determine unequal left/right atrial frequencies and rotor dynamics. *Cardiovasc. Res.*, 59(4):863–873, 2003.

[SLK13] Jürgen Scharhag, Herbert Löllgen, and Wilfried Kindermann. Competitive sports and the heart: Benefit or risk? *Dtsch Arztebl Int*, 110(1-2):14–23; quiz 24; e1–2, January 2013.

[SLNG91] C. F. Starmer, A. A. Lastra, V. V. Nesterenko, and A. O. Grant. Proarrhythmic response to sodium channel blockade. Theoretical model and numerical experiments. *Circulation*, 84(3):1364–1377, September 1991.

[SLT05] Joakim Sundnes, Glenn Terje Lines, and Aslak Tveito. An operator splitting method for solving the bidomain equations coupled to a volume conductor model for the torso. *Math Biosci*, 194(2):233–248, April 2005.

[SM76] Guy Salama and Martin Morad. Merocyanine 540 as an Optical Probe of Transmembrane Electrical Activity in the Heart. *Science*, 191(4226):485–487, 1976.

[SM02] Nicholas Sperelakis and Keith McConnell. Electric field interactions between closely abutting excitable cells. *IEEE Eng Med Biol Mag*, 21(1):77–89, Jan-Feb 2002.

[SMERC16] Marwan Saad, Ahmed Mahmoud, Islam Y Elgendy, and C. Richard Conti. Ranolazine in Cardiac Arrhythmia. *Clin Cardiol*, 39(3):170–178, March 2016.

[SNA+15] Junhui Sun, Tiffany Nguyen, Angel M. Aponte, Sara Menazza, Mark J. Kohr, David M. Roth, Hemal H. Patel, Elizabeth Murphy, and Charles Steenbergen. Ischaemic preconditioning preferentially increases protein S-nitrosylation in subsarcolemmal mitochondria. *Cardiovasc. Res.*, 106(2):227–236, May 2015.

[SNC+01] Dawinder S. Sohal, Mai Nghiem, Michael A. Crackower, Sandra A. Witt, Thomas R. Kimball, Kevin M. Tymitz, Josef M. Penninger, and Jeffery D. Molkentin. Temporally Regulated and Tissue-Specific Gene Manipulations in the Adult and Embryonic Heart Using a Tamoxifen-Inducible Cre Protein. *Circ. Res.*, 89(1):20–25, July 2001.

[SNM+14] Daniel Soetkamp, Tiffany T. Nguyen, Sara Menazza, Christine Hirschhäuser, Ulrike B. Hendgen-Cotta, Tienush Rassaf, Klaus D. Schlüter, Kerstin Boengler, Elizabeth Murphy, and Rainer Schulz. S-nitrosation of mitochondrial connexin 43 regulates mitochondrial function. *Basic Res. Cardiol.*, 109(5):433, 2014.

[SPS+11] Paari Dominic Swaminathan, Anil Purohit, Siddarth Soni, Niels Voigt, Madhu V. Singh, Alexey V. Glukhov, Zhan Gao, B. Julie He, Elizabeth D. Luczak, Mei-ling A. L. Joiner, William Kutschke, Jinying Yang, J. Kevin Donahue, Robert M. Weiss, Isabella M. Grumbach, Masahiro Ogawa, Peng-Sheng S. Chen, Igor Efimov, Dobromir Dobrev, Peter J. Mohler, Thomas J. Hund, and Mark E. Anderson. Oxidized CaMKII causes cardiac sinus node dysfunction in mice. *J Clin Invest*, 121(8):3277–88, August 2011.

[SQAC+02] D. Sanchez-Quintana, R. H. Anderson, J. A. Cabrera, V. Climent, R. Martin, J. Farre, and S. Y. Ho. The terminal crest: Morphological features relevant to electrophysiology. *Heart*, 88(4):406–11, October 2002.

[SS91] G. S. Skinner and H. L. Swinney. Periodic to Quasi-Periodic Transition of Chemical Spiral Rotation. *Physica D*, 48(1):1–16, February 1991.

[SS95] Madison S Spach and C Frank Starmer. Altering the topology of gap junctions a major therapeutic target for atrial fibrillation. *Cardiovasc Res*, 30(3):337–344, 1995.

[SSBH03] Fiona J Sutherland, Michael J Shattock, Kathryn E Baker, and David J Hearse. Mouse isolated perfused heart: Characteristics and cautions. *Clin. Exp. Pharmacol. Physiol.*, 30(11):867–878, November 2003.

[SSH08] Marzio Sala, W. F. Spotz, and M. A. Heroux. PyTrilinos: High-performance distributed-memory solvers for Python. *ACM Trans Math Softw*, 34(2):7:1–7:33, March 2008.

[SSRL94] Bela Szabo, Raed Sweidan, Cadathur V. Rajagopalan, and Ralph Lazzara. Role of Na+:Ca2+ Exchange Current in Cs+-Induced Early Afterdepolarizations in Purkinje Fibers. *J. Cardiovasc. Electrophysiol.*, 5(11):933–944, November 1994.

[SST+96] K. S. Song, P. E. Scherer, Z. Tang, T. Okamoto, S. Li, M. Chafel, C. Chu, D. S. Kohtz, and M. P. Lisanti. Expression of caveolin-3 in skeletal, cardiac, and smooth muscle cells. Caveolin-3 is a component of the sarcolemma and co-fractionates with dystrophin and dystrophin-associated glycoproteins. *J. Biol. Chem.*, 271(25):15160–15165, June 1996.

[STD+05] Igor Splawski, Katherine W. Timothy, Niels Decher, Pradeep Kumar, Frank B. Sachse, Alan H. Beggs, Michael C. Sanguinetti, and Mark T. Keating. Severe arrhythmia disorder caused by cardiac L-type calcium channel mutations. *Proc. Natl. Acad. Sci. U. S. A.*, 102(23):8089–8096, June 2005.

[STS+04] Igor Splawski, Katherine W. Timothy, Leah M. Sharpe, Niels Decher, Pradeep Kumar, Raffaella Bloise, Carlo Napolitano, Peter J. Schwartz, Robert M. Joseph, Karen Condouris, Helen Tager-Flusberg, Silvia G. Priori, Michael C. Sanguinetti, and Mark T. Keating. Ca(V)1.2 calcium channel dysfunction causes a multisystem disorder including arrhythmia and autism. *Cell*, 119(1):19–31, October 2004.

[Sun06] Joakim Sundnes. *Computing the Electrical Activity in the Heart*. Springer, Berlin; New York, 2006.

[SVKG11] U. Schotten, S. Verheule, P. Kirchhof, and A. Goette. Pathophysiological mechanisms of atrial fibrillation: A translational appraisal. *Physiological reviews*, 91(1):265–325, January 2011.

[SW02] J. P. P. Smits and Arthur A. M. Wilde. Brugada syndrome: In search of a genotype-phenotype relationship. *Herzschrittmacherther Elektrophysiol*, 13(3):142–148, September 2002.

[SWK+09] Can M. Sag, Daniel P. Wadsack, Sepideh Khabbazzadeh, Marco Abesser, Clemens Grefe, Kay Neumann, Marie-Kristin . K. Opiela, Johannes Backs, Eric N. Olson, Joan Heller Brown, Stefan Neef, Sebastian K.G Maier, and Lars S. Maier. Calcium/Calmodulin-Dependent Protein Kinase II Contributes to Cardiac Arrhythmogenesis in Heart Failure. *Circ. Heart Fail.*, 2(6):664–675, November 2009.

[SXS+09] Daisuke Sato, Lai-Hua H. Xie, Ali A. Sovari, Diana X. Tran, Norishige Morita, Fagen Xie, Hrayr Karagueuzian, Alan Garfinkel, James N. Weiss, and Zhilin Qu. Synchronization of chaotic early afterdepolarizations in the genesis of cardiac arrhythmias. *Proc Natl Acad Sci U A*, 106(9):2983–8, March 2009.

[TCH+08] William H. Thiel, Biyi Chen, Thomas J. Hund, Olha M. Koval, Anil Purohit, Long-Sheng S. Song, Peter J. Mohler, and Mark E. Anderson. Proarrhythmic defects in Timothy syndrome require calmodulin kinase II. *Circulation*, 118(22):2225–34, November 2008.

[TDI09] P. B. Tabereaux, D. J. Dosdall, and R. E. Ideker. Mechanisms of VF maintenance: Wandering wavelets, mother rotors, or foci. *Heart rhythm : the official journal of the Heart Rhythm Society*, 6(3):405–15, March 2009.

[Thi39] E. W. Thiele. Relation between Catalytic Activity and Size of Particle. *Ind. Eng. Chem.*, 31(7):916–920, July 1939.

[THJ+08] Yasuo M. Tsutsumi, Yousuke T. Horikawa, Michelle M. Jennings, Michael W. Kidd, Ingrid R. Niesman, Utako Yokoyama, Brian P. Head, Yasuko Hagiwara, Yoshihiro Ishikawa, Atsushi Miyanohara, Piyush M. Patel, Paul A. Insel, Hemal H. Patel, and David M. Roth. Cardiac-specific overexpression of caveolin-3 induces endogenous cardiac protection by mimicking ischemic preconditioning. *Circulation*, 118(19):1979–1988, November 2008.

[THW+13] Karl Toischer, Nico Hartmann, Stefan Wagner, Thomas H. Fischer, Jonas Herting, Bernhard C. Danner, Can M. Sag, Thomas J. Hund, Peter J. Mohler, Luiz Belardinelli, Gerd Hasenfuss, Lars S. Maier, and Samuel Sossalla. Role of late sodium current as a potential arrhythmogenic mechanism in the progression of pressure-induced heart disease. *J Mol Cell Cardiol*, 61:111–22, August 2013.

[TJO+12] Liang Tang, Boyoung Joung, Masahiro Ogawa, Peng-Sheng Chen, and Shien-Fong Lin. Intracellular calcium dynamics, shortened action potential duration, and late-phase 3 early afterdepolarization in Langendorff-perfused rabbit ventricles. *J. Cardiovasc. Electrophysiol.*, 23(12):1364–1371, December 2012.

[TKB07] Henk E. D. J. Ter Keurs and Penelope A. Boyden. Calcium and Arrhythmogenesis. *Physiol Rev*, 87(2):457–506, April 2007.

[TKK+99] S. Tessier, P. Karczewski, E. G. Krause, Y. Pansard, C. Acar, M. Lang-Lazdunski, J. J. Mercadier, and S. N. Hatem. Regulation of the transient outward K(+) current by Ca(2+)/calmodulin-dependent protein kinases II in human atrial myocytes. *Circ Res*, 85(9):810–9, October 1999.

[TM99] G. F. Tomaselli and E. Marbán. Electrophysiological remodeling in hypertrophy and heart failure. *Cardiovasc Res*, 42(2):270–83, May 1999.

[tP06] K. H. W. J. ten Tusscher and A. V. Panfilov. Alternans and spiral breakup in a human ventricular tissue model. *Am J Physiol Heart Circ Physiol*, 291(3):H1088–100, September 2006.

[Tra11] Natalia A. Trayanova. Whole-heart modeling: Applications to cardiac electrophysiology and electromechanics. *Circ. Res.*, 108(1):113–128, January 2011.

[Tra14] Natalia A. Trayanova. Mathematical approaches to understanding and imaging atrial fibrillation: Significance for mechanisms and management. *Circ. Res.*, 114(9):1516–1531, April 2014.

[TRVH+13] C. Tobon, C. A. Ruiz-Villa, E. Heidenreich, L. Romero, F. Hornero, and J. Saiz. A three-dimensional human atrial model with fiber orientation. Electrograms and arrhythmic activation patterns relationship. *PloS one*, 8(2):e50883, 2013.

[TTH+14a] Yasuo M. Tsutsumi, Rie Tsutsumi, Yousuke T. Horikawa, Yoko Sakai, Eisuke Hamaguchi, Yoshihiro Ishikawa, Utako Yokoyama, Asuka Kasai, Noriko Kambe, and Katsuya Tanaka. Geranylgeranylacetone protects the heart via caveolae and caveolin-3. *Life Sci.*, 101(1-2):43–48, April 2014.

[TTH+14b] Yasuo M. Tsutsumi, Rie Tsutsumi, Yousuke T. Horikawa, Yoko Sakai, Eisuke Hamaguchi, Hiroshi Kitahata, Asuka Kasai, Noriko Kambe, and Katsuya Tanaka. Geranylgeranylacetone and volatile anesthetic-induced cardiac protection synergism is dependent on caveolae and caveolin-3. *J Anesth*, 28(5):733–739, October 2014.

[Tun78] Leslie Tung. *A Bi-Domain Model for Describing Ischemic Myocardial D-c Potentials.* Thesis, Massachusetts Institute of Technology, 1978.

[TVHK+10] David J. Tester, Carmen Valdivia, Carole Harris-Kerr, Marielle Alders, Benjamin A. Salisbury, Arthur A. M. Wilde, Jonathan C. Makielski, and Michael J. Ackerman. Epidemiologic, molecular, and functional evidence suggest A572D-SCN5A should not be considered an independent LQT3-susceptibility mutation. *Heart Rhythm*, 7(7):912–9, July 2010.

[TWHA05] David J. Tester, Melissa L. Will, Carla M. Haglund, and Michael J. Ackerman. Compendium of cardiac channel mutations in 541 consecutive unrelated patients referred for long QT syndrome genetic testing. *Heart Rhythm*, 2(5):507–17, May 2005.

[TZMSS14] Saeed Torabi Ziaratgahi, Megan E. Marsh, Joakim Sundnes, and Raymond J. Spiteri. Stable time integration suppresses unphysical oscillations in the bidomain model. *Front. Phys*, 2:40, 2014.

[VAY+06] Matteo Vatta, Michael J. Ackerman, Bin Ye, Jonathan C. Makielski, Enoh E. Ughanze, Erica W. Taylor, David J. Tester, Ravi C. Balijepalli, Jason D. Foell, Zhaohui Li, Timothy J. Kamp, and Jeffrey A. Towbin. Mutant caveolin-3 induces persistent late sodium current and is associated with long-QT syndrome. *Circulation*, 114(20):2104–2112, November 2006.

[VCJ08] Miguel Vaquero, David Calvo, and José Jalife. Cardiac fibrillation: From ion channels to rotors in the human heart. *Heart Rhythm*, 5(6):872–879, June 2008.

[VCP+05] Carmen R. Valdivia, William W. Chu, Jielin Pu, Jason D. Foell, Robert A. Haworth, Mathew R. Wolff, Timothy J. Kamp, and Jonathan C. Makielski. Increased late sodium current in myocytes from a canine heart failure model and from failing human heart. *J Mol Cell Cardiol*, 38(3):475–83, March 2005.

[VHA+95] E. Vanoli, S. S. Hull, P. B. Adamson, R. D. Foreman, and P. J. Schwartz. K+ channel blockade in the prevention of ventricular fibrillation in dogs with acute ischemia and enhanced sympathetic activity. *J. Cardiovasc. Pharmacol.*, 26(6):847–854, December 1995.

[VKS+14] Christopher T. Villongco, David E. Krummen, Paul Stark, Jeffrey H. Omens, and Andrew D. McCulloch. Patient-specific modeling of ventricular activation pattern using surface ECG-derived vectorcardiogram in bundle branch block. *Prog. Biophys. Mol. Biol.*, 115(2-3):305–313, August 2014.

[VLH+15] Rengasayee Veeraraghavan, Joyce Lin, Gregory S. Hoeker, James P. Keener, Robert G. Gourdie, and Steven Poelzing. Sodium channels in the Cx43 gap junction perinexus may constitute a cardiac ephapse: An experimental and modeling study. *Pflugers Arch - Eur J Physiol*, 467(10):2093–2105, October 2015.

[VLW+12] Niels Voigt, Na Li, Qiongling Wang, Wei Wang, Andrew W. Trafford, Issam Abu-Taha, Qiang Sun, Thomas Wieland, Ursula Ravens, Stanley Nattel, Xander H. T. Wehrens, and Dobromir Dobrev. Enhanced sarcoplasmic reticulum Ca2+ leak and increased Na+-Ca2+ exchanger function underlie delayed afterdepolarizations in patients with chronic atrial fibrillation. *Circulation*, 125(17):2059–70, May 2012.

[vMD+10] Ralph J. van Oort, Mark D. McCauley, Sayali S. Dixit, Laetitia Pereira, Yi Yang, Jonathan L. Respress, Qiongling Wang, Angela C. De Almeida, Darlene G. Skapura, Mark E. Anderson, Donald M. Bers, and Xander H. T. Wehrens. Ryanodine receptor phosphorylation by calcium/calmodulin-dependent protein kinase II promotes life-threatening ventricular arrhythmias in mice with heart failure. *Circulation*, 122(25):2669–79, December 2010.

[VMSJ99] Dhananjay Vaidya, Gregory E. Morley, Faramarz H. Samie, and José Jalife. Reentry and Fibrillation in the Mouse Heart. *Circ. Res.*, 85(2):174–181, July 1999.

[VVS+13] Ravi Vaidyanathan, Amanda L. Vega, Chunhua Song, Qing Zhou, Bihua Tan, Stuart Berger, Jonathan C. Makielski, and Lee L. Eckhardt. The Interaction of Caveolin 3 Protein with the Potassium Inward Rectifier Channel Kir2.1 PHYSIOLOGY AND PATHOLOGY RELATED TO LONG QT SYNDROME 9 (LQT9). *J. Biol. Chem.*, 288(24):17472–17480, June 2013.

[WA14] Yuejin Wu and Mark E. Anderson. CaMKII in sinoatrial node physiology and dysfunction. *Front Pharmacol*, 5:48, 2014.

[WCd+96] A. L. Waldo, A. J. Camm, H. deRuyter, P. L. Friedman, D. J. MacNeil, J. F. Pauls, B. Pitt, C. M. Pratt, P. J. Schwartz, and E. P. Veltri. Effect of d-sotalol on mortality in patients with left ventricular dysfunction after recent and remote myocardial infarction. The SWORD Investigators. Survival With Oral d-Sotalol. *Lancet*, 348(9019):7–12, July 1996.

[WDR+06] Stefan Wagner, Nataliya Dybkova, Eva C. L. Rasenack, Claudius Jacobshagen, Larissa Fabritz, Paulus Kirchhof, Sebastian K. G. Maier, Tong Zhang, Gerd Hasenfuss, Joan Heller Brown, Donald M. Bers, and Lars S. Maier. Ca2+/calmodulin-dependent protein kinase II regulates cardiac Na+ channels. *J Clin Invest*, 116(12):3127–38, December 2006.

[Web09] John G. Webster. *Medical Instrumentation: Application and Design*. Wiley, Hoboken, NJ, 4 edition edition, February 2009.

[Wei52] Silvio Weidmann. The electrical constants of Purkinje fibres. *J Physiol*, 118(3):348–360, November 1952.

[WGK+10] James N. Weiss, Alan Garfinkel, Hrayr S. Karagueuzian, Peng-Sheng S. Chen, and Zhilin Qu. Early afterdepolarizations and cardiac arrhythmias. *Heart Rhythm*, 7(12):1891–9, December 2010.

[WHG+09] Stefan Wagner, Elena Hacker, Eleonora Grandi, Sarah L. Weber, Nataliya Dybkova, Samuel Sossalla, Thomas Sowa, Larissa Fabritz, Paulus

Kirchhof, Donald M. Bers, and Lars S. Maier. Ca/calmodulin kinase II differentially modulates potassium currents. *Circ Arrhythm Electrophysiol*, 2(3):285–94, June 2009.

[WHM+12] Mathias Wilhelms, Hanne Hettmann, Mary M Maleckar, Jussi T Koivumäki, Olaf Dössel, and Gunnar Seemann. Benchmarking electrophysiological models of human atrial myocytes. *Front. Physiol.*, 3:1–15, 2012.

[Wil06] Ronald Wilders. Dynamic clamp: A powerful tool in cardiac electrophysiology. *J Physiol*, 576(Pt 2):349–359, October 2006.

[Win94] A. T. Winfree. Electrical turbulence in three-dimensional heart muscle. *Science*, 266(5187):1003–1006, November 1994.

[WK11] Hiroshi Watanabe and Björn C. Knollmann. Mechanism underlying catecholaminergic polymorphic ventricular tachycardia and approaches to therapy. *J Electrocardiol*, 44(6):650–5, 2011.

[WKS+91] D. R. Witcher, R. J. Kovacs, H. Schulman, D. C. Cefali, and L. R. Jones. Unique phosphorylation site on the cardiac ryanodine receptor regulates calcium channel activity. *J Biol Chem*, 266(17):11144–52, June 1991.

[WKS+06] James N. Weiss, Alain Karma, Yohannes Shiferaw, Peng-Sheng Chen, Alan Garfinkel, and Zhilin Qu. From Pulsus to Pulseless. *Circ. Res.*, 98(10):1244–1253, May 2006.

[WLRM04] Xander H. T. Wehrens, Stephan E. Lehnart, Steven R. Reiken, and Andrew R. Marks. Ca2+/calmodulin-dependent protein kinase II phosphorylation regulates the cardiac ryanodine receptor. *Circ. Res.*, 94(6):e61–70, April 2004.

[WNGQ11] James N. Weiss, Michael Nivala, Alan Garfinkel, and Zhilin Qu. Alternans and Arrhythmias. *Circ. Res.*, 108(1):98–112, January 2011.

[WPBJ15] B. Cicero Willis, Daniela Ponce-Balbuena, and José Jalife. Protein assemblies of sodium and inward rectifier potassium channels control cardiac excitability and arrhythmogenesis. *Am. J. Physiol. Heart Circ. Physiol.*, 308(12):H1463–1473, June 2015.

[WSS+95] Q. Wang, J. Shen, I. Splawski, D. Atkinson, Z. Li, J. L. Robinson, A. J. Moss, J. A. Towbin, and M. T. Keating. SCN5A mutations associated with an inherited cardiac arrhythmia, long QT syndrome. *Cell*, 80(5):805–811, March 1995.

[WZB+06] Xu Wu, Tong Zhang, Julie Bossuyt, Xiaodong Li, Timothy A. McKinsey, John R. Dedman, Eric N. Olson, Ju Chen, Joan Heller Brown, and

Donald M. Bers. Local InsP3-dependent perinuclear Ca2+ signaling in cardiac myocyte excitation-transcription coupling. *J Clin Invest*, 116(3):675–82, March 2006.

[XGN99] H. Xu, W. Guo, and J. M. Nerbonne. Four kinetically distinct depolarization-activated K+ currents in adult mouse ventricular myocytes. *J. Gen. Physiol.*, 113(5):661–678, May 1999.

[XQG98] Fagen Xie, Zhilin Qu, and Alan Garfinkel. Dynamics of reentry around a circular obstacle in cardiac tissue. *Phys. Rev. E*, 58(5):6355–6358, November 1998.

[XQY+04] Fagen Xie, Zhilin Qu, Junzhong Yang, Ali Baher, James N. Weiss, and Alan Garfinkel. A simulation study of the effects of cardiac anatomy in ventricular fibrillation. *J. Clin. Invest.*, 113(5):686–693, March 2004.

[XSG+10] Yuanfang Xie, Daisuke Sato, Alan Garfinkel, Zhilin Qu, and James N. Weiss. So little source, so much sink: Requirements for afterdepolarizations to propagate in tissue. *Biophys J*, 99(5):1408–15, September 2010.

[Yam55] E. Yamada. The fine structure of the gall bladder epithelium of the mouse. *J Biophys Biochem Cytol*, 1(5):445–458, September 1955.

[YB94] W. Yuan and D. M. Bers. Ca-dependent facilitation of cardiac Ca current is due to Ca-calmodulin-dependent protein kinase. *Am J Physiol*, 267(3 Pt 2):H982–93, September 1994.

[YBF+08] Bin Ye, Ravi C. Balijepalli, Jason D. Foell, Stacie Kroboth, Qi Ye, Yu-Hong Luo, and Nian-Qing Shi. Caveolin-3 associates with and affects the function of hyperpolarization-activated cyclic nucleotide-gated channel 4. *Biochemistry*, 47(47):12312–12318, November 2008.

[YFJ+11] Lina Yao, Peidong Fan, Zhan Jiang, Serge Viatchenko-Karpinski, Yuzhi Wu, Dmytro Kornyeyev, Ryoko Hirakawa, Grant R. Budas, Sridharan Rajamani, John C. Shryock, and Luiz Belardinelli. Nav1.5-dependent persistent Na+ influx activates CaMKII in rat ventricular myocytes and N1325S mice. *Am J Physiol Cell Physiol*, 301(3):C577–86, September 2011.

[YGPE09] Viktor Yarotskyy, Guofeng Gao, Blaise Z. Peterson, and Keith S. Elmslie. The Timothy syndrome mutation of cardiac CaV1.2 (L-type) channels: Multiple altered gating mechanisms and pharmacological restoration of inactivation. *J Physiol*, 587(Pt 3):551–65, February 2009.

[YHJ+11] Masayuki Yazawa, Brian Hsueh, Xiaolin Jia, Anca M. Pasca, Jonathan A. Bernstein, Joachim Hallmayer, and Ricardo E. Dolmetsch. Using induced

pluripotent stem cells to investigate cardiac phenotypes in Timothy syndrome. *Nature*, 471(7337):230–4, March 2011.

[YHP+03] Jian-An Yao, Wajid Hussain, Pravina Patel, Nicholas S Peters, Penelope A Boyden, and Andrew L Wit. Remodeling of gap junctional channel function in epicardial border zone of healing canine infarcts. *Circ. Res.*, 92(4):437–443, 2003.

[YLLS02a] Tracy L. Yarbrough, Tong Lu, Hon-Chi Lee, and Erwin F. Shibata. Localization of Cardiac Sodium Channels in Caveolin-Rich Membrane Domains. *Circ. Res.*, 90(4):443–449, March 2002.

[YLLS02b] Tracy L. Yarbrough, Tong Lu, Hon-Chi Lee, and Erwin F. Shibata. Localization of cardiac sodium channels in caveolin-rich membrane domains: Regulation of sodium current amplitude. *Circ. Res.*, 90(4):443–449, March 2002.

[YMA+01] Nobuhito Yanagi, Toru Maruyama, Makoto Arita, Yoshikazu Kaji, and Yoshiyuki Niho. Alterations in electrical and mechanical activity in Langendorff-perfused guinea pig hearts exposed to decreased external sodium concentration with or without hypotonic insult. *Pathophysiology*, 7(4):251–261, March 2001.

[YRM+14] Kai-Chien Yang, Cody A. Rutledge, Mao Mao, Farnaz R. Bakhshi, An Xie, Hong Liu, Marcelo G. Bonini, Hemal H. Patel, Richard D. Minshall, and Samuel C. Dudley. Caveolin-1 modulates cardiac gap junction homeostasis and arrhythmogenecity by regulating cSrc tyrosine kinase. *Circ Arrhythm Electrophysiol*, 7(4):701–710, August 2014.

[YTW03] Sandro Yong, Xiaoli Tian, and Qing Wang. LQT4 gene: The "missing" ankyrin. *Mol Interv*, 3(3):131–6, May 2003.

[YVSO+07] Junying Yu, Maxim A. Vodyanik, Kim Smuga-Otto, Jessica Antosiewicz-Bourget, Jennifer L. Frane, Shulan Tian, Jeff Nie, Gudrun A. Jonsdottir, Victor Ruotti, Ron Stewart, Igor I. Slukvin, and James A. Thomson. Induced Pluripotent Stem Cell Lines Derived from Human Somatic Cells. *Science*, 318(5858):1917–1920, December 2007.

[ZGZH05] Henggui Zhang, Clifford J Garratt, Jiujiang Zhu, and Arun V Holden. Role of up-regulation of IK1 in action potential shortening associated with atrial fibrillation in humans. *Cardiovasc. Res.*, 66(3):493–502, 2005.

[Zim98] Heinz-Gerd G. Zimmer. The Isolated Perfused Heart and Its Pioneers. *News Physiol Sci*, 13:203–210, August 1998.

[ZLK93] X. Q. Zou, H. Levine, and D. A. Kessler. Interaction between a Drifting Spiral and Defects. *Phys Rev E*, 47(2):R800–R803, February 1993.

[ZLM+12] Yongjie Zhang, Xinghua Liang, Jun Ma, Yiming Jing, Matthew J. Gonzales, Christopher Villongco, Adarsh Krishnamurthy, Lawrence R. Frank, Vishal Nigam, Paul Stark, Sanjiv M. Narayan, and Andrew D. McCulloch. An atlas-based geometry pipeline for cardiac Hermite model construction and diffusion tensor reorientation. *Med Image Anal*, 16(6):1130–1141, August 2012.

[ZMD+03] Tong Zhang, Lars S. Maier, Nancy D. Dalton, Shigeki Miyamoto, John Ross, Donald M. Bers, and Joan Heller Brown. The deltaC isoform of CaMKII is activated in cardiac hypertrophy and induces dilated cardiomyopathy and heart failure. *Circ Res*, 92(8):912–9, May 2003.

[ZWK+14] Yanmin Zhang, JingJing Wu, James H. King, Christopher L.-H. Huang, and James A. Fraser. Measurement and interpretation of electrocardiographic QT intervals in murine hearts. *Am. J. Physiol. Heart Circ. Physiol.*, 306(11):H1553–1557, June 2014.

[ZXW+12] Zhenghang Zhao, Yuanfang Xie, Hairuo Wen, Dandan Xiao, Charelle Allen, Nadezhda Fefelova, Wen Dun, Penelope A. Boyden, Zhilin Qu, and Lai-Hua Xie. Role of the transient outward potassium current in the genesis of early afterdepolarizations in cardiac cells. *Cardiovasc. Res.*, 95(3):308–316, August 2012.

[ZYTW07] Teng Zhang, Sandro L. Yong, Xiao-Li Tian, and Qing K. Wang. Cardiac-specific overexpression of SCN5A gene leads to shorter P wave duration and PR interval in transgenic mice. *Biochem. Biophys. Res. Commun.*, 355(2):444–450, April 2007.